Paulo José Paulino de Souza

Optimization and Application of the Quantum Adiabatic Theorem, and the Quantum Origin of Classical Interference

Brazil

2022

Paulo José Paulino de Souza

Optimization and Application of the Quantum Adiabatic Theorem, and the Quantum Origin of Classical Interference

Dissertação realizada sob orientação do Prof. Dr. Celso Jorge Villas-Boas e co-orientação do Dr. Alan Costa dos Santos, apresentada ao Programa de Posgraduação em Física da Universidade Federal de São Carlos, em complementação aos requisitos para obtenção da titulação de Mestre em Física.

Universidade Federal de São Carlos

Departamento de Física

Programa de Pós-Graduação

Supervisor: Prof. Dr. Celso Jorge Villas-Boas

Co-supervisor: Dr. Alan Costa dos Santos

Brazil

2022

Paulo José Paulino de Souza

Optimization and Application of the Quantum Adiabatic Theorem, and the Quantum Origin of Classical Interference/ Paulo José Paulino de Souza. – Brazil, 2022-

109 p.

Supervisor: Prof. Dr. Celso Jorge Villas-Boas
Co-supervisor: Dr. Alan Costa dos Santos

Dissertação (Mestrado) – Universidade Federal de São Carlos
Departamento de Física
Programa de Pós-Graduação, 2022.

1. Quantum Adiabatic Theorem. 2. Quantum Adiabatic Brachistochrone. 3. Quantum Adiabatic Search. 4. Superconducting Quantum Batteries. 5. Quantum Annealing. 6. Quantum Interference.

Canta-me a Cólera — ó deusa! — funesta de Aquiles Pelida,
causa que foi de os Aquivos sofrerem trabalhos sem conta
e de baixarem para o Hades as almas de heróis numerosos
e esclarecidos, ficando eles próprios aos cães atirados
e como pasto das aves. Cumpriu-se de Zeus o desígnio
desde o princípio em que os dois, em discórdia, ficaram cindidos,
o de Atreu filho, senhor de guerreiros, e Aquiles divino.

Acknowledgements

Tenho absoluta certeza que essa dissertação de mestrado não é um trabalho unicamente meu. Sua existência também é fruto de esforços coletivos de pessoas muito caras a mim.

Agradeço, em primeiro lugar, meu orientador Prof. Dr. Celso que além da ótima orientação acadêmica, me deu valiosos conselhos sobre a vida e sobre o que é ser um cientista. Agradeço ao meu co-orientador Dr. Alan, pela paciência e pela confiança e dedicada orientação. De fato, agradeço ao Grupo de Otimização Quântica por toda a ajuda e aprendizado.

Agradeço meus pais Paulo e Patrícia pelo suporte que recebo e que foi e é fundamental para meu crescimento pessoal e acadêmico. Agradeço minha irmã, Júlia, por todo "elogio", conversa torta, encheção de saco contínua bilateral que é tão boa e engraçada. Agradeço minha vó (pessoa que me ensinou as operações básicas) por tudo seu carinho e dedicação à nossa família. Agradeço aos meus finados avôs e minha finada avó, pelo exemplo de vida e pelas aconchegantes memórias. Agradeço aos meus tios e primos pelos bons momentos juntos.

Vivendo em São Carlos conheci pessoas que são parte fundamental da minha vida. Agradeço à Ana Flávia, minha companheira, com quem compartilho pequenos e grandes momentos, crescimento, batalhas e festas e que há seis anos me apoia nessa vida acadêmica. Agradeço à família da Ana, por terem tão bem me acolhido. Agradeço a República Rep Zeppelin. Em especial, agradeço ao Abominável, que muito contribuiu para minha formação de físico e de pessoa. Agradeço ao Pestana, Bird, Xarli, Clone, Peão, Tamino, Gonzo, Latello, Toru, Ink, Pastel, Doido, os Kraus e agregados. Ao Wilson, eu agradeço, amigo meu, pelas grandes conversas sobre filosofia, literatura, e, mísero eu, Física. Agradeço aos amigos que fiz na UFSCar, que, apesar de serem novos, gosto tanto que considero meus primos (Dani, Dani, Lucas, Caique, Carol, Renan, Marcão, Jaguá, Maju e Jefin).

For fim, agradeço à Capes pelo financiamente e à UFSCar pela estrutura.

Resumo

Nesta dissertação desenvolvemos três tópicos. No primeiro tópico estudamos o método da braquistócrona adiabática quântica (QAB) para otimizar dinâmicas adiabáticas. Na primeira parte desse estudo investigamos o carregamento e o descarregamento de uma bateria quântica supercondutora *transmon* de três níveis. O processo de carga dessa bateria foi acelerado usando o método da QAB, de onde fizemos uma análise sobre a aplicação de vínculos nas funções de interpolação. Completamos o estudo descrevendo o processo de auto-descarga da bateria, que é como ela perde sua carga para o ambiente, e verificamos que ele é não-Ôhmico. Além disso, aplicamos a QAB ao algorítimo de Grover adiabático para quando há limitação de recursos para sua execução, por exemplo quando há limite na potência máxima dos campos externos ou na energia total disponível. A segunda parte da dissertação é sobre a teoria do computador quântico da D-Wave e suas limitações, como a falta de conexões globais entre os qubits. Para avaliar o estado da arte da tecnologia, resolvemos nesse computador o problema do caixeiro viajante. Além disso, fizemos um revisão bibliográfica sobre os problemas que o *annealer* quântico pode resolver e sobre as estratégias para superar suas limitações experimentais. Por último, no terceiro tópico provamos que a descrição da interação entre luz e matéria usando flutuações quânticas leva a ambiguidades para casos com muitos modos de luz. Mostramos que a interferência clássica surge na ótica quântica pelo comportamento coletivo dos modos de luz, de onde emerge os estados *bright* a *dark* da luz. No caso de muitos modos, o critério para um átomo no estado fundamental ser excitado é a existência de projeções em estados não *dark*, e não as flutuações quânticas.

Palavras-chaves: Teorema Adiabático Quântico. Braquistócrona Adiabática Quântica. Busca Adiabática Quântica. Baterias Quânticas Supercondutoras. Recozimento Quântico. Interferência Quântica.

Abstract

In this master's thesis, we developed three different topics. In the first topic, we studied the quantum adiabatic brachistochrone method (QAB) for optimizing adiabatic dynamics. In the first part of this study, we reported the investigation of the charging and discharging processes of a transmon superconducting three-level quantum battery. The charging process was enhanced using the QAB method, in which we analyzed the effect of constraining the interpolation functions. We completed the battery study by showing that its self-discharging process, which is how the device loses its charge to the environment, is non-Ohmic. Furthermore, we considered the application of the QAB method to the adiabatic Grover algorithm for times when there is limited resources for its execution, for instance when there is a limit on the maximum power of the external fields or in the available total energy. The second part is concerned with the theory of the D-Wave's quantum annealer and its limitations, as the lack of global connections between the qubits. For evaluating the state-of-the-art of this quantum simulator, we solved the traveling salesman problem on it. Moreover, we did a literature review about problems this processor can handle and different strategies to avoid its limitations. Finally, in the third topic, we proved that describing light-matter interaction using quantum fluctuations yields ambiguities for multi-modes of light. We showed that classical interference emerges in quantum optics due to collective bright and dark states of light. In a multi-mode case, the criterion for a ground-state atom to be excited is the existence of a projection on non-dark states rather than quantum fluctuations.

Key-words: Quantum Adiabatic Theorem. Quantum Adiabatic Brachistochrone. Quantum Adiabatic Search. Superconducting Quantum Batteries. Quantum Annealing. Quantum Interference.

Contents

1 Introduction

The quantum revolution is commonly based on established technologies, such as batteries, communication channels, and thermal engines [1–6]. However, in the on going revolution not only did we need to build devices on a very small scale, but we need to use genuine quantumness as well. For example, classical computers fail to simulate large quantum systems due to the scaling size of the Hilbert space, but when using quantum bits, this problem vanishes [7, 8]. Nonetheless, we are in the noisy intermediate-scale quantum era (NISQ) [9], meaning that our quantum devices are affected by the measurement apparatus and noise. Although we are far from the quantum supremacy [10], we see a Moore-like law in the increasing of the quantum computational power [11]. The new quantum devices explore a range of different systems, such as trapped ions [12], quantum dots [13], and cavity quantum electrodynamics [14]. A technology that has an increasing interest and usage by the community is the superconducting devices [15, 16]. They have a plethora of applications, for instance, in quantum computing [17] and quantum batteries [1, 18]. Particularly, the experimental setups of Chapters 4 and 5 are built using them.

A relevant quantum control method applicable to different quantum technologies is the quantum adiabatic theorem. Different from adiabaticity in thermodynamics [19], which regards a process without heat exchanging with external environments, adiabaticity in this work is about a *slow* variation of a time-dependent system. This theorem states that if a quantum system evolves adiabatically, the Schrödinger-eigenspaces evolve uncoupled from each other [20–22]. Therefore, the system will be in the same instantaneous state during the entire time evolution. This theorem has a crucial role in quantum annealing [23], digitized quantum computing [24], quantum thermodynamics [25], stimulated Raman adiabatic passage (STIRAP) [26], and in quantum information processing [27]. The adiabaticity is achieved by respecting a quantitative adiabatic condition that imposes a time scale, τ, to the dynamics total time [28–35]. The adiabatic condition can be achieved using different evolution protocols, and, naturally, some of them are better than others. For instance, the adiabatic Grover's algorithm has a quadratic speedup over its classical version, but if this algorithm is executed with a naive protocol, it loses its quantum improvement [36]. Methods have been developed to hasten these processes, some of them are based on machine learning [37], optimal control theory [38], etc [36, 39]. In this dissertation (Chapters 3 and 4), we will focus on the Quantum Adiabatic Brachistochrone (QAB) [40]. This method has a further generalization for quantum open system [41] and it was implemented experimentally [1].

Moreover, the application of adiabatic dynamics to quantum computing gives rise to the Turing complete paradigm of computation called adiabatic quantum computation

(AQC) [42]. Although this paradigm has some qualities, such as robustness against relaxation phenomena, problems with dephasing, thermal effects or engineering limitation bring delays for building this kind of computer. Despite these drawbacks, there is the quantum annealing technique, which is a NISQ version of QAC that uses adiabatic evolutions for solving binary optimization problems [3, 43]. This class of problems is present in areas such as condensed matter systems [44], complex networks, and logistic problems [45, 46]. Quantum annealing technologies are being led by the D-Wave Company [47]. In its first generations of quantum processors, we saw that indeed they were capable of correctly solving problems, notwithstanding their small scale [23, 48, 49]. Now, we see some realist prospectives and problems wherein quantum annealer performs better than classical algorithms [44, 46]. In Chapter 5 we describe how to use this computer and we briefly introduce the related technology.

Moving to fundamentals of physics, we have a description of interference of electromagnetic (EM) waves based on the superposition of EM fields [50], but when light is quantum, this description fails, since there are interfering states with no EM field. The quantum explanation for this phenomenon was based on quantum fluctuations of the EM field [51]. However, there exist some ambiguities when we consider multi-modes of light, where collective behaviour emerges. In Chapter 6, we accurately addressed this problem with a new collective quantum basis of the light modes [52].

Thus, this Master's thesis has three projects in four Chapters and is organized as follows: In Chapter 2, we make a review of the physical and mathematical tools, quantum adiabatic dynamics, we will use in Chapters 3, 4, and 5. Also, Chapter 2 describes the quantum adiabatic brachistochrone optimization method for adiabatic dynamics we use in Chapters 3 and 4. In Chapter 3, we analyse the performance of the adiabatic Grover algorithm for scenarios with limited resources for its execution, which is a characteristic of the NISQ devices. In Chapter 4, we present the theoretical and experimental characterization of a superconducting transmon quantum battery [1]. Chapter 5 concerns the usage and the basic description of the D-Wave's quantum annealer [53]. Additionally, we described the simulated annealing algorithm and we argue that its solutions are good references for the quantum annealing solutions [54]. Finally, in Chapter 6, we integrally reproduce our paper [52] in which it is demonstrated that classical interference of light is accurately modeled using a collective quantum basis of the modes of light and not quantum fluctuations. In this introduction, we made general considerations about the main themes we studied, but every Chapter, with results, has its contextualization and historical details.

2 Basic Tools

2.1 Adiabatic Theorem

2.1.1 Classical Adiabatic Theorem

Before we go to the formalism of adiabatic evolutions in quantum systems, we will review the classical (non-quantum) adiabatic invariants, which are quantities that do not change during adiabatic evolutions. The adiabatic invariants are the classical analog of the quantum adiabatic theorem [20].

Since the property of being integrable is an exception in multidimensional mechanical systems, many approximated methods are being developed to understand, at least, the global behavior of these systems. Further, the theory of adiabatic invariants is a method that is valid when a sufficiently *slow* perturbation is acting on the system, keeping one or more quantities quasi-conserved during the dynamics.

A given Hamiltonian varies slowly if

$$\frac{\partial \mathcal{H}}{\partial t} = \mathrm{O}\left(\frac{1}{\tau}\mathcal{H}\right) \ , \tag{2.1}$$

for a natural time scale τ, for instance the oscillation period of a oscillator. This equation means that if the *slowness* of the perturbation divided by the system characteristic time is nearly zero, we are in the adiabatic regime [20, 55]. Moreover, beyond the dependence on generalized variables, the Hamiltonian might be a function of a set of parameters $\lambda_i(t)$, which are arbitrary functions of time. We say that if $\lambda_i(t)$ adiabatically changes the system, if the variation of the parameter is small compared with a time scale τ of the system. Mathematically, the relation $\dot{\lambda}_i/\lambda_i \ll \tau$ must stand. Therefore, if λ_i obeys the adiabatic condition, it will be possible, without knowing the explicit form of λ_i, to define invariants, from which we find the global behavior of the system. As an example, we will look at a mechanical system, which is under a generalized force [56].

Let us suppose a system described by the Lagrangian $\mathcal{L}$ and by its generalized variables, q_1, q_2, $\dot{q}_1$, $\dot{q}_2$. The Lagrange equations, when a generalized conservative force, Q_1, is acting on the coordinate q_1, are

$$\frac{\mathrm{d}}{\mathrm{d}t}\frac{\partial \mathcal{L}}{\partial \dot{q}_1} - \frac{\partial \mathcal{L}}{\partial q_1} = Q_1, \quad \frac{\mathrm{d}}{\mathrm{d}t}\frac{\partial \mathcal{L}}{\partial \dot{q}_2} - \frac{\partial \mathcal{L}}{\partial q_2} = 0 \ , \tag{2.2}$$

where $\dot{q}_i = \mathrm{d}q_i/\mathrm{d}t$ for $i = 1, 2$. Owing to strong physical interpretation the Hamiltonian formalism, *i.e.* the total energy[1], we will change to this frame by applying a Legendre

[1] If the system is conservative.

transform on $\mathcal{L}$, which consists in defining $p_i = \partial\mathcal{L}/\partial\dot{q}_i$ and $\mathcal{H} = p_i\dot{q}_i - \mathcal{L}$. Thereafter, evaluating the differential of $\mathcal{H}$ and using Eq. (2.2), we find

$$\begin{aligned} \mathrm{d}\mathcal{H} &= \dot{q}_i \mathrm{d}p_i + p_i \mathrm{d}\dot{q}_i - \frac{\partial\mathcal{L}}{\partial q_i}\mathrm{d}q_i - \frac{\partial\mathcal{L}}{\partial\dot{q}_i}\mathrm{d}\dot{q}_i \\ &= \dot{q}_i \mathrm{d}p_i + p_i \mathrm{d}\dot{q}_i - \frac{\partial\mathcal{L}}{\partial q_i}\mathrm{d}q_i - p_i \mathrm{d}\dot{q}_i \\ &= \dot{q}_1 \mathrm{d}p_1 + \dot{q}_2 \mathrm{d}p_2 + (Q_1 - \dot{p}_1)\,\mathrm{d}q_1 - \dot{p}_2 \mathrm{d}q_2 \ , \end{aligned} \tag{2.3}$$

from which we find the Hamilton equations,

$$\frac{\partial\mathcal{H}}{\partial q_1} = -\dot{p}_1 + Q_1, \quad \frac{\partial\mathcal{H}}{\partial p_1} = \dot{q}_1, \quad \frac{\partial\mathcal{H}}{\partial q_2} = -\dot{p}_2, \quad \frac{\partial\mathcal{H}}{\partial p_2} = \dot{q}_2 \ . \tag{2.4}$$

Dividing Eq. (2.3) by $\mathrm{d}t$ and using the Eq. (2.4), we find the time derivative of the total energy

$$\frac{\mathrm{d}\mathcal{H}}{\mathrm{d}t} = Q_1\dot{q}_1 \ , \tag{2.5}$$

which is the generalized work of the force Q_1. However, if the force is time independent, we can write $\mathrm{d}\mathcal{H} = Q_1\mathrm{d}q_1$. Therefore, assuming that the variable q_1 is just slowly varied due to the force Q_1 [56], the derivative of the canonical momentum $\dot{p}_1$ will be negligible against Q_1 and the motion equation will be approximately

$$\frac{\partial\mathcal{H}}{\partial q_1} = -\dot{p}_1 + Q_1 \approx Q_1 \ . \tag{2.6}$$

We can apply this method in the following physical system: *Suppose we have a mass m oscillating in a vertical plane and bounded at the origin by a wire with initial length L. The wire is pulled by the force Q, therefore having its length being shortened.* For this system, we have the Hamiltonian

$$\mathcal{H} = \frac{p_L^2}{2m} + \frac{p_\theta^2}{2mL^2} - mgL\cos(\theta) \ , \tag{2.7}$$

where p_L is the canonical momentum in the direction of the wire, p_θ is the canonical momentum in the angular direction and the rightmost term in the equation is the gravitational energy. Since we know that the parameter that adiabatically changes the system is L, by using the Eq. (2.6) we find

$$Q_L = -p_\theta^2/\left(mL^3\right) - mg\cos(\theta) \tag{2.8}$$

Hence, evaluating the mean values of a oscillation period, we find

$$\begin{aligned} \mathrm{d}\mathcal{H} &= \langle Q_1\rangle \mathrm{d}q_1 \\ &= -\left\langle \frac{p_\theta^2}{mL^2} + mgL\cos(\theta)\right\rangle \frac{\mathrm{d}L}{L} \\ &= -\frac{3E}{2}\frac{\mathrm{d}L}{L} \ , \end{aligned} \tag{2.9}$$

since the variation of L is very small in an oscillation period, we used the mean values for a pendulum with fixed length

$$\left\langle \frac{p_\theta^2}{2mL^2} \right\rangle = \langle mgL\cos(\theta)\rangle = \frac{E}{2} \ . \tag{2.10}$$

So, in this adiabatic approximation we say that the mean energy of a pendulum is equal to a quasi-conserved quantity[2] E, since the external force is very small. Finally, from Eq. (2.9) and considering $\mathrm{d}\mathcal{H} = \mathrm{d}E$ we find the adiabatic invariant,

$$\frac{\mathrm{d}E}{E} = -\frac{3}{2}\frac{\mathrm{d}L}{L} \rightarrow EL^{3/2} = C, \quad C \in \mathbb{R} \ . \tag{2.11}$$

The physical interpretation of this equation is the following: When the wire length decreases, the energy increases by a power of 3/2. Thus, the quantity $EL^{3/2}$ is an adiabatic invariant. In conclusion, the adiabatic treatment has enabled us to find the behaviour of the system energy without solving the Hamilton equations, Eq (2.3).

2.1.2 The quantum adiabatic theorem

We now move to quantum mechanical description of the adiabatic theorem. In this subsection, we will enunciate and prove the quantum adiabatic theorem, which is the foundation of Chapters 3, 4 and 5. There are many versions of the adiabatic theorem, some more formal or general than others, but in this master's thesis we will work with the Max Born and Vladimir Fock formulation and proof given in 1928 [21]. Although we will describe a simple version of the adiabatic theorem, the proof that is concluded with the derivation of the adiabatic condition is sufficient for our applications and many others [28–35, 57]. We hereby will consider $\hbar = 1$ for simplifying the notation.

We start by defining the adiabatic dynamics, through which we state the adiabatic theorem [29].

Definition 1 (Adiabatic Dynamics)**.** *A closed quantum system, whose Hamiltonian is given by $H(t)$, is subjected to an adiabatic dynamics if its Hilbert space can be decoupled into Schrödinger-eigenspaces with distinct, time-continuous, and non-crossing instantaneous eigenvalues of $H(t)$.*

A Schrödinger-eigenspace is a set of orthonormal eigenvectors with the same eigenvalue in the Hilbert space of $H(t)$. In the case where the system is nondegenerate, the Schrödinger-eigenspaces are unidimensional and all the eigenvectors evolve uncoupled to each other. Therefore, a system that evolves according to an adiabatic dynamics definition will remain in its instantaneous state while its eigenvalues evolve continuously. This consequence of the adiabatic dynamics is the adiabatic theorem [21, 58].

[2] This means that the variation in a time period is very small, *i.e.* according to the condition in Eq. (2.1).

Let us begin the proof of the theorem with a time dependent Hamiltonian $H(t)$ with a discrete spectrum. The system spectrum is given by the eigenvalue equation, $H(t)\left|\psi_n(t)\right\rangle = E_n(t)\left|\psi_n(t)\right\rangle$, and its time evolution is given by the Schrödinger equation, $H(t)\left|\Psi(t)\right\rangle = i\partial_t\left|\Psi(t)\right\rangle$. Thus, the general form of an instantaneous state is

$$\left|\Psi(t)\right\rangle = \sum_n c_n(t)e^{i\theta_n(t)}\left|\psi_n(t)\right\rangle \ , \tag{2.12}$$

where $\theta_n(t) \equiv -\int_0^t E_n(t')\mathrm{d}t'$.

The application of the Schrödinger equation on $\left|\Psi(t)\right\rangle$ yields

$$\partial_t\left|\Psi\right\rangle = i\sum_n\left\{\dot{c}_n\left|\psi_n\right\rangle + c_n\left|\dot{\psi}_n\right\rangle - iE_nc_n\left|\psi_n\right\rangle\right\}e^{i\theta_n} = \sum_n c_nE_n\left|\psi_n\right\rangle e^{i\theta_n}. \tag{2.13}$$

We have omitted the time dependence in the former equations and we will specify it just when necessary. The third term of the second equation cancels out the right hand side of the equation, resulting in

$$\sum_n\left\{\dot{c}_n\left|\psi_n\right\rangle + c_n\left|\dot{\psi}_n\right\rangle\right\}e^{i\theta_n} = 0 \ . \tag{2.14}$$

The multiplication of Eq. (2.14) by an arbitrary "bra", $\langle\psi_m|$, yields

$$\begin{aligned}\sum_n\left\{\dot{c}_n\delta_{nm} + c_n\left\langle\psi_m|\dot{\psi}_n\right\rangle\right\}e^{i\theta_n} = 0 \ , \\ \therefore \quad \dot{c}_m = -\sum_{n\neq m} c_n\left\langle\psi_m|\dot{\psi}_n\right\rangle e^{-i\int(E_n-E_m)\mathrm{d}t}.\end{aligned} \tag{2.15}$$

It is possible to evaluate $\left\langle\psi_m|\dot{\psi}_n\right\rangle$, for $m \neq n$, by performing a derivative on the eigenvalue equation,

$$\begin{aligned}\mathrm{d}_t\left(H\left|\psi_n\right\rangle\right) = \mathrm{d}_t\left(E_n\left|\psi_n\right\rangle\right) \ , \\ \left\langle\psi_m\left|\dot{H}\right|\psi_n\right\rangle + E_m\left\langle\psi_m|\dot{\psi}_n\right\rangle = E_n\left\langle\psi_m|\dot{\psi}_n\right\rangle \ ,\end{aligned} \tag{2.16}$$

so

$$\left\langle\psi_m|\dot{\psi}_n\right\rangle = \frac{\left\langle\psi_m\left|\dot{H}\right|\psi_n\right\rangle}{E_n - E_m}, \ \forall\, n \neq m \ . \tag{2.17}$$

Substituting Eq. (2.17) in Eq. (2.14) we obtain the exact equation for the coefficients dynamics,

$$\dot{c}_m = -c_m\left\langle\psi_m|\dot{\psi}_m\right\rangle - \sum_{n\neq m} c_n\frac{\left\langle\psi_m\left|\dot{H}\right|\psi_n\right\rangle}{E_n - E_m}e^{-i\int(E_n-E_m)\mathrm{d}t} \ , \tag{2.18}$$

where the summation is over all pairs of the system eigenstates. This result shows that the coupling between the eigenstate coefficients is given by the second term on the right-hand side of the equation, which means that the population flow between eigenstates is limited by it. Thus, if the rightmost term in Eq. (2.18) can be neglected, the dynamical coefficients will be described purely by the differential equation,

$$\dot{c}_m = -c_m\left\langle\psi_m|\dot{\psi}_m\right\rangle, \tag{2.19}$$

that has a simple solution, $c_m(t) = c_m(0)e^{\gamma_m}$, where $\gamma_m = \int_0^t \left\langle \psi_m(t')|\dot{\psi}_m(t')\right\rangle \mathrm{d}t'$ is the geometric phase [59]. We can find the nature of γ by doing the following procedure,

$$\begin{aligned} \langle\psi_m|\psi_m\rangle &= 1 \ , \\ \frac{\mathrm{d}}{\mathrm{d}t}\langle\psi_m|\psi_m\rangle &= \left\langle\dot{\psi}_m|\psi_m\right\rangle + \left\langle\psi_m|\dot{\psi}_m\right\rangle \\ &= 2\mathrm{Re}\left[\left\langle\psi_m|\dot{\psi}_m\right\rangle\right] \\ &= 0 \ . \end{aligned} \tag{2.20}$$

Hence, we conclude that γ is a purely imaginary number.

Therefore, if the initial state is the superposition of eigenvectors $|\psi_m(0)\rangle$, the adiabatically evolved state will be

$$|\Psi(t)\rangle = \sum_m c_m(0)\,|\psi_m(t)\rangle\, e^{i\theta_m(t)-\gamma_m(t)}. \tag{2.21}$$

The exponentials multiplying the eigenvectors are purely imaginary, thereby keeping its modulus equal to one.

2.1.3 The traditional adiabatic condition

One may ask why or when it is possible to neglect the second term on the right-hand side of the Eq. (2.18). With the aim of understanding this action, we will use Eq. (2.17) to rewrite Eq. (2.18) as

$$e^{-\gamma_m}\frac{\mathrm{d}}{\mathrm{d}t}\left(c_m e^{\gamma_m}\right) = -\sum_{n\neq m} c_n \frac{\left\langle\psi_m\left|\dot{H}\right|\psi_n\right\rangle}{\Delta_{nm}} e^{-i\int_0^t(\Delta_{nm}(t'))\mathrm{d}t'} \ , \tag{2.22}$$

where $\Delta_{nm} = E_n - E_m$, is the energy difference between the eigenstates. Now, to set a time scale to our problem, let us define the parametrized time, $s \equiv t/\tau$, where τ is the total evolution time. In addition, after defining the quantity

$$F_{nm}(s) \equiv c_n(s)\,\langle\psi_m\,|\mathrm{d}_s H|\,\psi_n\rangle\,, \tag{2.23}$$

we find the expression for the dynamical coefficients of a time-dependent Hamiltonian,

$$c_m(s)e^{\gamma_m} = c_m(0) - \sum_{n\neq m}\int_0^s \frac{F_{nm}}{\Delta_{nm}} e^{-i\tau\int_0^{s'}\Delta_{nm}(s'')\mathrm{d}s''}. \tag{2.24}$$

The term in the sum contains our subject, whereby we will derive means to find an adiabatic condition. Specifically, we will find a way to turn the second term in the right-hand side of the former equation negligible.

Let us take the integral

$$I(s) = \int_0^s \frac{F_{nm}}{\Delta_{nm}} e^{-i\tau\int_0^{s'}\Delta_{mn}(s'')\mathrm{d}s''}\mathrm{d}s' \ , \tag{2.25}$$

In order to rewrite the integral, we consider the derivative

$$\begin{aligned}\frac{\mathrm{d}}{\mathrm{d}s'}\left(\frac{F_{nm}}{\Delta_{nm}^2}e^{-i\tau\int_0^{s'}\Delta_{mn}(s'')\mathrm{d}s''}\right) &= \frac{\mathrm{d}}{\mathrm{d}s'}\left(\frac{F_{nm}}{\Delta_{nm}^2}\right)e^{-i\tau\int_0^{s'}\Delta_{mn}(s'')\mathrm{d}s''} \\ &+ \frac{F_{nm}}{\Delta_{nm}^2}e^{-i\tau\int_0^{s'}\Delta_{mn}(s'')\mathrm{d}s''}\left(-i\tau\Delta_{nm}(s)\right) \ , \\ &= \frac{\mathrm{d}}{\mathrm{d}s'}\left(\frac{F_{nm}}{\Delta_{nm}^2}\right)e^{-i\tau\int_0^{s'}\Delta_{mn}(s'')\mathrm{d}s''} - i\tau\frac{F_{nm}}{\Delta_{nm}}e^{-i\tau\int_0^{s'}\Delta_{mn}(s'')\mathrm{d}s''} \ ,\end{aligned} \tag{2.26}$$

thus

$$\begin{aligned}\frac{F_{nm}}{\Delta_{nm}}e^{-i\tau\int_0^{s'}\Delta_{mn}(s'')\mathrm{d}s''} = \frac{-i}{\tau}\Bigg[&\frac{\mathrm{d}}{\mathrm{d}s'}\left(\frac{F_{nm}}{\Delta_{nm}^2}e^{-i\tau\int_0^{s'}\Delta_{mn}(s'')\mathrm{d}s''}\right) \\ &- \frac{\mathrm{d}}{\mathrm{d}s'}\left(\frac{F_{nm}}{\Delta_{nm}^2}\right)e^{-i\tau\int_0^{s'}\Delta_{mn}(s'')\mathrm{d}s''}\Bigg] \ .\end{aligned} \tag{2.27}$$

$I(s)$ then becomes

$$I(s) = -\frac{i}{\tau}\left[\frac{F_{nm}(s)}{\Delta_{nm}^2(s)}e^{-i\tau\int_0^{s}\Delta_{nm}\mathrm{d}s'} - \frac{F_{nm}(0)}{\Delta_{nm}(0)} - \int_0^s\frac{\mathrm{d}}{\mathrm{d}s'}\left(\frac{F_{nm}(s')}{\Delta_{nm}^2(s')}\right)e^{-i\tau\int_0^{s'}\Delta_{nm}\mathrm{d}s''}\mathrm{d}s'\right] . \tag{2.28}$$

In the rightmost term, we can use the Riemann-Lebesgue lemma [60] to say that for a large τ the integrand oscillates in a very high frequency, approaching the integral to zero[3]. Consequently, for an adiabatic evolution we must have,

$$\tau \gg \max_{n,m}\left[\max_{0<s<1}\left|\frac{\langle\psi_m(s)\left|\mathrm{d}_sH(s)\right|\psi_n(s)\rangle}{\Delta_{nm}^2(s)}\right|\right] \ , \tag{2.29}$$

where $\mathrm{d}_s \equiv \mathrm{d}/\mathrm{d}s$. Also, as we can also find in the literature,

$$\max_{n,m}\left[\max_{0<s<1}\left|\frac{1}{\tau}\frac{\langle\psi_m(s)\left|\mathrm{d}_sH(s)\right|\psi_n(s)\rangle}{\Delta_{nm}^2(s)}\right|\right] \leq \epsilon \ , \tag{2.30}$$

where $\epsilon \ll 1$ is an arbitrary small real constant. The traditional adiabatic condition states that the total time of evolution is inversely proportional to the square of the energy difference between the considered eigenvalues. Therefore, if the condition is satisfied, the Eq. (2.19) is valid.

The global adiabatic condition we found can be used to derive a local adiabatic condition. However, we first need to define the concept of *interpolation speed*. Let $s(t)$ now be a curve parametrized by the time variable, t, such that

$$s(t) : \{t \in [0,\tau] \longmapsto [0,1] \in \mathbb{R}, s(0) = 0, s(\tau) = 1\} \ . \tag{2.31}$$

[3] We can not use the Riemann-Lebesgue lemma in Eq. (2.25) because we will not have a time scale τ for adiabaticity.

The interpolation speed is

$$v(t) \equiv \frac{\mathrm{d}s}{\mathrm{d}t} \ , \tag{2.32}$$

so, this quantity represents how fast the curve $s(t)$ changes as a function of time t.

With this concept in mind together with Eq. (2.30) we can define the local adiabatic condition,

$$v(s)\frac{|F_{mn}(s)|}{\Delta_{mn}^2(s)} \leq \epsilon, \quad \forall\ s \in [0,1] \ . \tag{2.33}$$

This means that the interpolation velocity can increase (decrease) when the quantity $|F_{nm}(s)|/\left(\epsilon\Delta_{nm}(s)^2\right)$ decrease (increase) for keeping the global adiabatic condition valid.

It is noteworthy that the adiabatic theorem is exactly satisfied for a time-dependent system only if the total evolution time goes to infinity. Thus, for finite evolution times, the final state will always deviate from the desired one. To account for the overlap between the evolved state, $|\phi(\tau)\rangle$, and the actual instantaneous state, $|\Psi(\tau)\rangle$, both in time τ, it is convenient to define the Fidelity between them

$$\mathcal{F} = |\langle\phi(\tau)|\Psi(\tau)\rangle| \ . \tag{2.34}$$

Hence, $\mathcal{F}$ is equal one if, and only if, the total time of evolution goes to infinity. Nonetheless, it is possible to find very good approximations to adiabaticity, $\mathcal{F} \approx 1$, in a finite and reasonable total dynamics time [61].

2.1.3.1 The adiabatic theorem as a infinite series

The adiabatic approximation can be thought of as a perturbation series in $1/\tau$ and in the former subsection we found just the first term of the series. Although the adiabatic condition we calculated up to first order is sufficient for ensuring adiabaticity [28–35, 57], we can go further and repeat the procedure for finding higher orders of the expansion. To calculate the next term, let us consider the integral

$$\int_0^s \frac{\mathrm{d}}{\mathrm{d}s'}\left(\frac{F_{nm}}{\Delta_{nm}^2}\right) e^{-i\tau\int_0^{s'}\Delta_{nm}\mathrm{d}s''}\mathrm{d}s' \ . \tag{2.35}$$

The integrand can be rewritten as

$$\begin{aligned}
&\frac{\mathrm{d}}{\mathrm{d}s'}\left[\frac{\mathrm{d}}{\mathrm{d}s'}\left(\frac{F_{mn}}{\Delta_{mn}^3}\right)e^{-i\tau\int_0^{s'}\Delta_{mn}ds''}\right]\\
&=\left\{\frac{\mathrm{d}^2}{\mathrm{d}s'^2}\left(\frac{F_{mn}}{\Delta_{mn}^3}\right)-(i\tau\Delta_{mn})\frac{\mathrm{d}}{\mathrm{d}s'}\left(\frac{F_{mn}}{\Delta_{mn}^3}\right)\right\}e^{-i\tau\int_0^{s'}\Delta_{mn}ds''}\\
&=\left\{\frac{\mathrm{d}^2}{\mathrm{d}s'^2}\left(\frac{F_{mn}}{\Delta_{mn}^3}\right)+(-i\tau\Delta_{mn})\left[\frac{F'_{mn}}{\Delta_{mn}^3}-3\frac{F_{mn}\Delta'_{mn}}{\Delta_{mn}^4}\right]\right\}e^{-i\tau\int_0^{s'}\Delta_{mn}ds''}\\
&=\left\{\frac{\mathrm{d}^2}{\mathrm{d}s'^2}\left(\frac{F_{mn}}{\Delta_{mn}^3}\right)-i\tau\left(\frac{F'_{mn}}{\Delta_{mn}^2}-3\frac{F_{mn}\Delta'_{mn}}{\Delta_{mn}^3}\right)-i\tau\left(\frac{F_{mn}\Delta'_{mn}}{\Delta_{mn}^3}-\frac{F_{mn}\Delta'_{mn}}{\Delta_{mn}^3}\right)\right\}e^{-i\tau\int_0^{s'}\Delta_{mn}ds''}\\
&=\left\{\frac{\mathrm{d}^2}{\mathrm{d}s'^2}\left(\frac{F_{mn}}{\Delta_{mn}^3}\right)-i\tau\left(\frac{F'_{mn}}{\Delta_{mn}^2}-2\frac{F_{mn}\Delta'_{mn}}{\Delta_{mn}^3}\right)+i\tau\frac{F_{mn}\Delta'_{mn}}{\Delta_{mn}^3}\right\}e^{-i\tau\int_0^{s'}\Delta_{mn}ds''}\\
&=\left\{\frac{\mathrm{d}^2}{\mathrm{d}s'^2}\left(\frac{F_{mn}}{\Delta_{mn}^3}\right)-i\tau\frac{\mathrm{d}}{\mathrm{d}s'}\left(\frac{F_{mn}}{\Delta_{mn}^2}\right)+i\tau\frac{F_{mn}\Delta'_{mn}}{\Delta_{mn}^3}\right\}e^{-i\tau\int_0^{s'}\Delta_{mn}ds''}\ .
\end{aligned}\tag{2.36}$$

Therefore, Eq. (2.35) becomes

$$\begin{aligned}
&\int_0^s\frac{\mathrm{d}}{\mathrm{d}s'}\left(\frac{F_{nm}}{\Delta_{nm}^2}\right)e^{-i\tau\int_0^{s'}\Delta_{nm}\mathrm{d}s''}\mathrm{d}s'\\
&=\frac{i}{\tau}\left[\frac{\mathrm{d}}{\mathrm{d}s'}\left(\frac{F_{mn}}{\Delta_{mn}^3}\right)e^{-i\tau\int_0^{s'}\Delta ds''}\right]\Bigg|_0^s-\frac{i}{\tau}\int_0^s e^{-i\tau\int_0^{s'}\Delta ds''}\left[\frac{\mathrm{d}^2}{\mathrm{d}s'^2}\left(\frac{F_{mn}}{\Delta_{mn}^3}\right)-i\tau\frac{F_{mn}\Delta'_{mn}}{\Delta_{mn}^3}\right]\mathrm{d}s'\ .
\end{aligned}\tag{2.37}$$

After the application of the Riemann-Lebesgue lemma, the integral in Eq. (2.25) is expanded in a series of the total dynamics time

$$\begin{aligned}
\int_0^s\frac{F_{nm}}{\Delta_{nm}}e^{-i\tau\int_0^{s'}\Delta_{mn}(s'')\mathrm{d}s''}\mathrm{d}s' &= \frac{-i}{\tau}\frac{F_{nm}(s)}{\Delta_{nm}^2(s)}e^{-i\tau\int_0^{s}\Delta_{nm}\mathrm{d}s'}\Bigg|_0^s\\
&\quad-\frac{1}{\tau^2}\left[\frac{\mathrm{d}}{\mathrm{d}s'}\left(\frac{F_{mn}}{\Delta_{mn}^3}\right)e^{-i\tau\int_0^{s'}\Delta ds''}\right]\Bigg|_0^s+\mathrm{O}(\tau^{-3})\ ,
\end{aligned}\tag{2.38}$$

and the adiabatic condition will now be a maximization over the terms

$$\tau\gg\max_{n,m}\left\{\max_{0<s<1}\left[\frac{F_{mn}(s)}{\Delta_{mn}^2(s)},\frac{1}{\tau}\frac{\mathrm{d}}{\mathrm{d}s}\left(\frac{F_{mn}(s)}{\Delta_{mn}^3(s)}\right)\right]\right\}\ .\tag{2.39}$$

2.2 Calculus of variations: The Brachistochrone

In the following, we will formulate the quantum adiabatic brachistochrone. For this purpose, we will start with a resume of the history of the brachistochrone problem. Further, we will review the basis of calculus of variations, which will be applied to the classical brachistochrone problem. Finally, in the following section, the quantum adiabatic brachistochrone will be defined using an analogy with the classical brachistochrone curve.

Let us suppose that there are two fixed points, A and B, in distinct vertical positions. If a mass m slides without friction from A to B, the trajectory time will depend on the shape of the curve connecting the two points. Finding the curve that leads to the shortest time is know as the Brachistochrone problem. This term, Brachistochrone, comes from old Greek and it is an agglutination of two words, "brákhistos" and "khrónos", meaning "shortest" and "time", respectively.

This problem was first formulated by Galileo Galilei who guessed that this curve would be an arch of a circle. Although it was a very good guess, as represented in Fig. 1(b), it was wrong [62]. Moreover, the modern formulation and the first solution were given by Johann Bernoulli in 1696. In his proof, he identified one symmetry in this problem that also occurs when light propagates through a media with a variable refraction index. Hence, he used Fermat's principle, saying if the particle was a light ray it would go through the shortest time curve, the brachistochrone. During his development, he realized that this was a challenging task and he decided to send letters inviting the best mathematicians of his time to face this problem. As expected, due to its difficult, just five letters were respond: Newton, Jakob Bernoulli (Johann's brother), Gottfried Leibniz, Ehrenfried Walther von Tschirnhaus, and Guillaume de l'Hôpital. In spite of the fact that all solutions were remarkable, the one provided by Jakob Bernoulli was refined by Leonhard Euler and becomes the foundation of the calculus of variations [63].

The problem of finding the Brachistochrone curve was not the first that opened the road for the creation of the Calculus of Variation theory, which was Newton's minimal resistance problem. However, due to the importance of the Brachistochrone curve and the impact it had on the scientific community, this problem is a landmark for the calculus of variations.

2.2.1 Calculus of Variations

The Calculus of Variations concerns finding the extrema of a functional, which can be a minimum, a maximum of a saddle point. Differently from a function that receives a point or a vector as input, a functional receives a function as input and returns a real value. As examples of functionals, we have inner products or definite integrals. Here we will study definite integrals as functionals using a simplified formulation [64], even though adequate for our purposes.

Definition 2 (Functional)**.** *Let* $\{f(q(s), q'(s), s) : \mathbb{R}^3 \mapsto \mathbb{R}\}$ *be a sufficiently differentiable known function and* $q(s)$ *be a function such that*

$$\left\{q : s \in [a, b] \mapsto \mathbb{R}, q \in C^2, q(a) = q_a, q(b) = q_b\right\} . \tag{2.40}$$

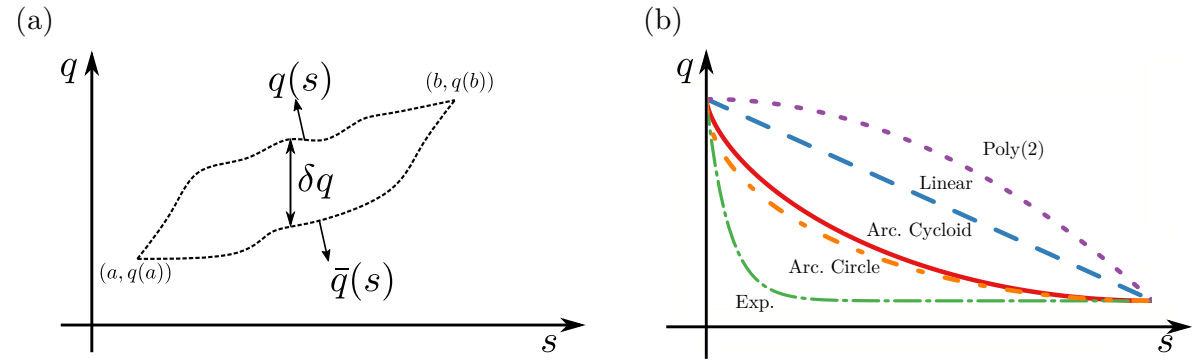

Figure 1 – (a) An illustration showing the variation of a curve, $\delta q = q - \bar{q} = \epsilon\eta$. (b) Representation of different curves that obeys the boundary conditions, thereby being solution of the functional T. Source: Made by the author.

A functional is defined,

$$A\left[q\right] = \int_a^b f(q, q', s)\mathrm{d}s \ . \tag{2.41}$$

In order to minimize a functional, let us define a variation of the function q, as represented in Fig. 1(a),

Definition 3 (Variation)**.** *If $\eta(s)$ is a twice differential function and obeys the boundary condition $\eta(a) = \eta(b) = 0$, a neighboring curve of q is*

$$\bar{q}(s) = q(s) + \epsilon\eta(s) \ , \tag{2.42}$$

where ϵ is a real constant. The boundary conditions for η are necessary to ensure that the neighboring curves also pass through the endpoints, $(a, q(a)), (b, q(b))$.

Additionally, if $q(s)$ is a known function and an extremum of $A[\bullet]$, then $A[\bar{q}]$ becomes a function of ϵ ,

$$\xi(\epsilon) = A\left[\bar{q}\right] = \int_a^b f(\bar{q}(s), \bar{q}'(s), s)\mathrm{d}s \ . \tag{2.43}$$

Thus, by construction, the function $\xi(\epsilon)$ must have an extremum in $\epsilon = 0$. Hence, a necessary condition for $\bar{q}$ be an extremum of $A[\bullet]$, is

$$\left.\frac{\mathrm{d}\xi}{\mathrm{d}\epsilon}\right|_{\epsilon=0} = \int_a^b \left(\frac{\partial f}{\partial q}\frac{\partial \bar{q}}{\partial \epsilon} + \frac{\partial f}{\partial q'}\frac{\partial \bar{q}'}{\partial \epsilon}\right)_{\epsilon=0} \mathrm{d}s = 0 \ , \tag{2.44}$$

where we used that $q(s) = \bar{q}(s)$ when $\epsilon = 0$. Although this result is correct it can be simplified. Firstly, by using the definition of neighboring curves, Eq. (2.42), one finds that $\partial\bar{q}/\partial\epsilon = \eta$ and $\partial\bar{q}'/\partial\epsilon = \eta'$. Thus

$$\left.\frac{\mathrm{d}\xi}{\mathrm{d}\epsilon}\right|_{\epsilon=0} = \int_a^b \left(\frac{\partial f}{\partial \bar{q}}\eta + \frac{\partial f}{\partial \bar{q}'}\eta'\right)\mathrm{d}s = 0 \ . \tag{2.45}$$

Secondly, we can perform an integration by part of the second term inside the integral to remove η',

$$\int_a^b \eta' \frac{\partial f}{\partial q'} \mathrm{d}s = \frac{\partial f}{\mathrm{d}q'} \eta \Big|_a^b - \int_a^b \eta \frac{\mathrm{d}}{\mathrm{d}s} \left(\frac{\partial f}{\partial q'} \right) \mathrm{d}s = - \int_a^b \eta \frac{\mathrm{d}}{\mathrm{d}s} \left(\frac{\partial f}{\partial q'} \right) \mathrm{d}s \ , \tag{2.46}$$

where the left term after the first equality signal is zero due to the boundary conditions that η is subjected. Thus, Eq (2.44) reads

$$\begin{aligned} \int_a^b \left[\frac{\partial f}{\partial q} - \frac{\mathrm{d}}{\mathrm{d}s} \left(\frac{\partial f}{\partial q'} \right) \right] \eta \mathrm{d}s = 0 \ , \\ \therefore \quad \frac{\partial f}{\partial q} - \frac{\mathrm{d}}{\mathrm{d}s} \left(\frac{\partial f}{\partial q'} \right) = 0 \ , \end{aligned} \tag{2.47}$$

where the second expression, the Euler-Lagrange equation (ELE), was found after the application of the fundamental Lemma of the Calculus of Variations. When considering functions, the first derivative test yields the stationary points, but it does not provide information whether this point is a maximum, a minimum, or a saddle point. This characteristic can be found using the second derivative test. To determine if the solution of the ELE is a local minimum, a maximum or a saddle point, one has to apply the second derivative test [65], (see Appendix A for more details).

The method we used to derive the Euler-Lagrange equation is analog to using the Gateaux derivative concept [65], but the method we used, as present in analytical mechanics text books [64], is more intuitive and easy to comprehend for the purpose of this master's thesis.

2.2.2 The Classical Brachistochrone Curve

Now, our goal is to understand the meaning of a time functional, which will be achieved by the formulation and solving the problem of finding the Brachistochrone curve in a classical mechanics system.

The problem is described as follows: *There are two points, A and B, in different heights, but not in the same vertical line. Then, for a particle that is subjected just to the gravitational force, what is the curve wherein the moving body travel time is smaller?*

This problem requires the minimization of the time, then we can write the total travel time as an integral,

$$T = \int_0^T \mathrm{d}t = \int_A^B \frac{\mathrm{d}s}{v(s)} \ . \tag{2.48}$$

Since we are considering no dissipation, we can evoke the conservation of energy law, $mgy = \frac{mv^2}{2}$, thus $v = \sqrt{2gy}$. Moreover, rewriting the space differential as $\mathrm{d}s = \sqrt{1 - x'^2}\mathrm{d}y$,

where $x' = \mathrm{d}x/\mathrm{d}y$, the integral reads

$$T = \int_A^B \frac{\mathrm{d}s}{v(s)} = \frac{1}{\sqrt{2g}} \int_0^{y_0} \sqrt{\frac{1+x'^2}{y}} \mathrm{d}y \ . \tag{2.49}$$

Here we indeed have a functional, because we can choose distinct curves to evaluate this integral, as Fig 1(b) shows. For instance, we can choose the straight line, a polynomial, the arc of a circle, etc.

In this problem we have $f(x, x', y) = \sqrt{(1+x'^2)/y}$, thus the ELE yields

$$\begin{aligned} \frac{\partial f}{\partial x} - \frac{\mathrm{d}}{\mathrm{d}y'}\left(\frac{\partial f}{\partial x'}\right) = 0, \\ \frac{\mathrm{d}}{\mathrm{d}y'}\left(\frac{\partial \sqrt{(1+x'^2)/y}}{\partial x'}\right) = \frac{\mathrm{d}}{\mathrm{d}y'}\left(\frac{x'}{\sqrt{y\,(1+x'^2)}}\right) = 0, \\ \therefore \frac{x'}{\sqrt{y\,(1+x'^2)}} = C, \quad C \in \mathbb{R}. \end{aligned} \tag{2.50}$$

This differential equation can be approached by introducing a parameter α, $x' = \tan(\alpha)$. Hence,

$$y = \frac{1}{C^2} \frac{\tan(\alpha)^2}{1+\tan(\alpha)^2} = \frac{1}{C^2} \sin(\alpha)^2 = \frac{1}{2C^2} \left[1 - \cos(2\alpha)\right]. \tag{2.51}$$

In addiction, since $x' = \mathrm{d}x/\mathrm{d}y$,

$$\begin{aligned} \mathrm{d}x &= \tan(\alpha)\,\mathrm{d}y \\ &= \frac{2}{C^2} \tan(\alpha) \sin(\alpha) \cos(\alpha)\,\mathrm{d}\alpha \\ &= \frac{1}{C^2} \left[1 - \cos(2\alpha)\right] \mathrm{d}\alpha \\ \therefore \quad x &= \frac{1}{2C^2} \left[2\alpha - \sin(2\alpha)\right] + D, \quad D \in \mathbb{R}. \end{aligned} \tag{2.52}$$

Finally, noting that $D = 0$ since $y = 0$ for $x = 0$ and rewriting α as $\theta = 2\alpha$ we find the equation of the curve that connects the point A to the point B,

$$x(\theta) = \frac{1}{2C^2} \left[\theta - \sin(\theta)\right], \quad y(\theta) = \frac{1}{2C^2} \left[1 - \cos(\theta)\right]. \tag{2.53}$$

Therefore, the Brachistochrone we found is an arc of a cycloid. Curiously, the arc of a cycloid is also the Tautochrone, which is a curve wherein the travel time is invariable by moving the initial position along it.

2.3 Adiabatic Quantum Brachistochrone

When we proved the quantum adiabatic theorem, we saw that the fidelity between the evolved state and the target one is 1 if, and only if, the total dynamics time, τ, goes

to infinity. However, there are no information about τ for when we want to reach fidelities nearly equal to one. On the other hand, some interpolation functions will fit better to the adiabatic condition, as the local adiabatic condition shows, thus indicating that τ might be a function of $\{q_i(s)\}$. For searching the optimal way, regarding τ, to adiabatically evolve a quantum system, the authors in the Ref. [40] proposed a method based on the calculus of variations, on the local adiabatic condition, and on the classical Brachistochrone curve, the "Quantum Adiabatic Brachistochrone" (QAB).

The time functional for the quantum adiabatic brachistochrone method is defined with the same arguments used for finding the classical Brachistochrone curve, Sec. 2.2.2. Thus, we write a time functional based on a speed

$$\tau = \int_0^\tau \mathrm{d}t = \int_0^1 \frac{\mathrm{d}s}{v(s)}. \tag{2.54}$$

where s will be a curve parametrized by time, Eq. (2.31). Differently from the classical problem, here we do not have an expression for $v(s)$, nevertheless we can give an *ansatz* for it. Using the expression of the local adiabatic condition, Eq. (2.33), we can define the adiabatic speed as $v^{\mathrm{ad}}(s) = \epsilon\Delta^2/|F_{nm}|$. Hence, for a quantum system described by the time dependent Hamiltonian $H(s) = \sum_i q_i(s)H_i$, where the set $\{q_i(s)\}$ is the set of interpolation functions and H_i are static Hamiltonians, the QAB functional reads

$$\tau\left[\mathbf{q}(s), \mathbf{q}'(s)\right] = \int_0^\tau \frac{\mathrm{d}s}{v^{\mathrm{ad}}(s)} = \int_0^1 \frac{F_{mn}}{\epsilon\Delta^2}\mathrm{d}s = \frac{1}{\epsilon}\int_0^1 \mathcal{L}'\left(\mathbf{q}, \mathbf{q}'\right)\mathrm{d}s\ . \tag{2.55}$$

where $\mathcal{L}'\left(\mathbf{q}, \mathbf{q}'\right)$ is the Lagrangian defined by the equation,

$$\mathcal{L}'\left(\mathbf{q}, \mathbf{q}'\right) = \frac{||\mathrm{d}_s H(s)||}{\Delta^2(s)}. \tag{2.56}$$

Within the Lagrangian, we changed $|\left\langle\psi_m(s)\right|\mathrm{d}_s H(s)\left|\psi_n(s)\right\rangle|$ by the Frobenius norm $||A|| = \sqrt{\mathrm{Tr}(A^\dagger A)}$ as to enable a geometric treatment, which investigation is beyond the scope of this text, though. Additionally, It is noteworthy that the inclusion of the Frobenius norm does not change the physical meaning of the Lagrangian. To show this, in Appendix D we prove the identity $\mathrm{Tr}\left[A^\dagger A\right] = \sum_{ij}|a_{ij}|^2$, where $(A)_{ij} = a_{ij}$. Additionally, we can write the eigenstates of H using the eigenstates of $\mathrm{d}_s H$

$$\left|\psi_j\right\rangle = \sum_i a_i \left|\phi_i\right\rangle\ , \tag{2.57}$$

where $(\mathrm{d}_s H)\left|\phi_i\right\rangle = \lambda_i\left|\phi_i\right\rangle$ and λ_i is the eigenvalue of the Hamiltonian derivative. Thus,

$$\begin{aligned}\left\langle\psi_m\right|d_s H\left|\psi_n\right\rangle &= \left\langle\psi_m\right|\sum_{i,j}(\mathrm{d}_s H)_{i,j}\left|\phi_i\right\rangle\left\langle\phi_j\right|\left|\psi_n\right\rangle \\ &= \sum_{i,j} a_i^* b_j (\mathrm{d}_s H)_{i,j}\ .\end{aligned} \tag{2.58}$$

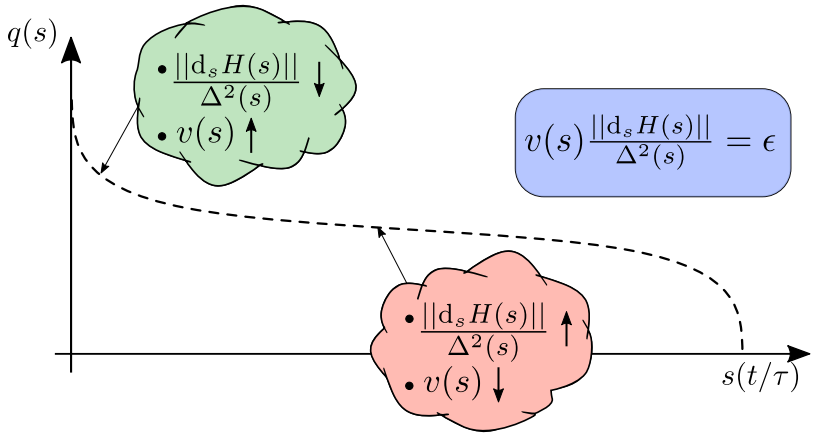

Figure 2 – Scheme for the quantum adiabatic brachistochrone interpretation, where $q(s)$ is derived from the optimization of the time functional through the Euler-Lagrange equations. The speed to the interpolation $v(s)$ yielded by the Euler-Lagrange equation will adapt itself to the local adiabatic condition used in the ansatz, Eq. (2.60). Since the Lagrangian is not explicitly time-dependent, it will be a constant resulting the relation on the blue box. Source: Made by the author.

Since the coefficients a and b are normalized, we have

$$|\sum_{i,j} a_i^* b_j (\mathrm{d}_s H)_{i,j}| \leq \sqrt{\sum_{ij} |(\mathrm{d}_s H(s))_{ij}|^2}\ , \tag{2.59}$$

that is triangular-like inequality. Therefore, when we extremize the Lagrangian with the Frobenious, we find interpolation functions that also extremize the matrix elements $(\mathrm{d}_s H(s))_{ij}$, thereby optimizing a Lagrangian with the norm $|\langle\psi_n|\mathrm{d}_s H|\psi_m\rangle|$.

For avoiding the square-root of the Frobenius norm, we can square the Lagrangian, because it is not explicitly time-dependent (see Appendix C). Therefore, the quantum adiabatic Lagrangian is given by the equation

$$\mathcal{L}(\mathbf{q}, \mathbf{q}') = \frac{||\mathrm{d}_s H(s)||^2}{\Delta^4(s)}\ . \tag{2.60}$$

Since the constant ϵ is arbitrarily small and does not contribute to the Euler-Lagrange equations, the integration of the functional in Eq. (2.55) will not yield the exact total time of the dynamics, which is found after integrating the Schrödinger equation. Therefore, we can physically interpret $\tau[\mathrm{q}, \mathrm{q}']$ as a functional, whose extremization yields the functions that will better fit to the adiabatic condition used in the *ansatz* $v^{\mathrm{ad}}(s)$. Fig. 2 illustrates this interpretation. The population flow from the instantaneous eigenstate to the closest one, concerning the lowest energy gap, is proportional to the adiabatic coefficient

$$\gamma = \frac{||\mathrm{d}_s H(s)||}{\Delta^2(s)}\ , \tag{2.61}$$

and when it increases (decreases), the dynamics, given by $v(s)$, slowdown (speed up). With this interpretation, the QAB method allows us to define different Lagrangians by

using others adiabatic conditions, thereby being a heuristic-like method for finding optimal interpolation functions.

3 Adiabatic Grover algorithm with resources limitations

Quantum computing uses quantum systems to perform computation [66–68]. The digital logic gates paradigm [69–72] executes algorithms by applying a sequence of quantum gates. This Turing complete computation method can be implemented using superconducting qubits [17], trapped ions [73], photonics systems [74], etc [13, 75]. Two benchmark algorithms of this method that paved the way for quantum computing were the Shor algorithm [76], that factors numbers in polynomial time, and the Grover algorithm [77], that provides a quadratic speed up over the classical unstructured search. Similarly, the adiabatic quantum computing (AQC) [78] is an analog quantum computation paradigm [78–80] that explores adiabatic evolutions [22, 81] to implement a Turing complete formalism of computation. This model of quantum computation has been implemented in quantum annealers for optimization tasks, allowing, in the same cases, for speeding up the information processing over its classical counterpart [3, 43, 82, 83].

In AQC, an algorithm is formulated by choosing a set of time-dependent functions, $\{q_n(t)\}$, used to define a driver Hamiltonian, $H(t) = q_0(t)H_0 + q_1(t)H_1$, where H_0 has a trivial ground state and H_1 encodes the problem solution in its ground state. Although the AQC can explore quantum advantages to speed up computational tasks, they demand an adequate choice of the set $\{q_n(t)\}$. For example, the adiabatic Grover algorithm [84] is as efficient counterpart by logic gates, but if non adequate interpolation functions are chosen, the algorithm loses its quantum advantage [36]. Furthermore, concerning the experimental implementation of this algorithm, we see that it also has some potential problems to achieve it in large scales. The main drawback is to build a scalable oracle-like projector for which it is necessary a system with an infinite dimension [85]. In spite of that, some implementations were made [86, 87]

Here, we addressed the Quantum Adiabatic Brachistochrone (QAB) for optimizing the adiabatic Grover algorithm [84][1]. This algorithm has being studied for the last two decades [36, 84, 88, 89], nonetheless the QAB for a general set of interpolation functions has not been found yet and analysis concerning executions of the algorithm with limited resources are missing. The purpose of this Chapter is to perform a numerical analysis of the QAB method applied to the adiabatic Grover algorithm. We imposed constraints to the functions based on experimental constraints. Also, we considered all the interpolation functions expanding the same energy during the Grover's execution. This Chapter is organized as follows: We first review the mathematical formulation of the Grover algorithm.

[1] Preliminary results.

In Sec. II, we demonstrate the correspondence between the method for finding $\{q_n(t)\}$ using a local evolution and the QAB. Additionally, we define a Lagrangian for a general polynomial and find the Hamilton equations for the non-constrained Lagrangian. In section III we analyse the energy efficiency of the interpolation functions and their efficiency when energy is a limited resource.

3.1 Adiabatic Grover algorithm

The Grover algorithm in the adiabatic quantum computation assumes the form of the time-dependent Hamiltonian,

$$H(s) = q_0(s)\left(I - |\psi\rangle\langle\psi|\right) + q_1(s)\left(I - |m\rangle\langle m|\right) \ , \tag{3.1}$$

where we used $\hbar = 1$, $|\psi\rangle = 1/\sqrt{N}\sum_i |i\rangle$ is the superposition of all eigenstates of the identity operator, $|m\rangle$ is the target eigenstate, and s is the parametrized time, Eq. (2.31). We also have the function that performs the interpolation, thereby having the boundary conditions $q_0(0) = q_1(1) = 1$ and $q_0(1) = q_1(0) = 0$.

The eigenvalues of this Hamiltonian can be found by defining a state $|m^\perp\rangle$, that is perpendicular to $|m\rangle$, such that $|\psi\rangle$ is given by

$$|\psi\rangle = \alpha|m^\perp\rangle + \beta\,|m\rangle \ . \tag{3.2}$$

The coefficients are then calculated by exploring the internal product between the target state, $|m\rangle$, and $|\psi\rangle$

$$\langle m|\psi\rangle = \langle m|\sum_{i=1}^{N}\frac{1}{\sqrt{N}}|i\rangle = \frac{1}{\sqrt{N}}\sum_{i=1}^{N}\langle m|i\rangle = \frac{1}{\sqrt{N}} \ . \tag{3.3}$$

The other coefficient is $\beta = \sqrt{(N-1)/N}$ due to the normalization condition. Now, it is possible to define a subspace of the Hamiltonian using these two orthogonal states,

$$H_{|m^\perp\rangle,|m\rangle} = \begin{pmatrix} \langle m\,|H|\,m\rangle & \langle m|H|m^\perp\rangle \\ \langle m^\perp|H|m\rangle & \langle m^\perp|H|m^\perp\rangle \end{pmatrix} \ . \tag{3.4}$$

The first matrix element is,

$$\begin{aligned} \langle m\,|H|\,m\rangle &= \langle m|\left[q_0(s)\left(1 - |\psi\rangle\langle\psi|\right) + q_1(s)\left(1 - |m\rangle\langle m|\right)\right]|m\rangle \\ &= q_0(s)\left(1 - \frac{1}{N}\right) \ . \end{aligned} \tag{3.5}$$

The off-diagonal elements are equal due to the Hamiltonian hermicity and they are

$$\begin{aligned} \langle m|H|m^\perp\rangle &= \langle m|\left[q_0(s)\left(1 - |\psi\rangle\langle\psi|\right) + q_1(s)\left(1 - |m\rangle\langle m|\right)\right]|m^\perp\rangle \\ &= q_0(s)\left(\sqrt{\frac{N-1}{N^2}}\right) \end{aligned} \tag{3.6}$$

Finally, the last element is

$$\begin{aligned}\left\langle m^{\perp}\left|H\right|m^{\perp}\right\rangle &= \left\langle m^{\perp}\right|\left[q_0(s)\left(1-\left|\psi\right\rangle\left\langle\psi\right|\right)+q_1(s)\left(1-\left|m\right\rangle\left\langle m\right|\right)\right]\left|m^{\perp}\right\rangle \\ &= q_0(s)\left(1-\frac{N-1}{N}+q_1(s)\right) \\ &= q_1(s)+\frac{q_0(s)}{N}\ .\end{aligned} \tag{3.7}$$

The diagonalization of the subspace of the Hamiltonian, Eq. (3.4), yields the energies,

$$E_{\pm}=\frac{q_0(s)+q_1(s)\pm\sqrt{\left(q_0(s)-q_1(s)\right)^2-4q_0(s)q_1(s)/N}}{2}\ . \tag{3.8}$$

The other eigenvalues of the Grover's Hamiltonian are found by considering an eigenvector, $|u\rangle$ out of the subspace formed by $|m\rangle$ and $|m^{\perp}\rangle$, which means that $\langle u|m\rangle=\langle u|m^{\perp}\rangle=0$. Therefore,

$$\left\langle u\left|H\right|u\right\rangle = q_0(s)+q_1(s)\ . \tag{3.9}$$

Since the Hamiltonian has N eigenstates, we will have $N-2$ eigenvectors with energy equal to $q_0(s)+q_1(s)$. In summary, the energies of the Grover Hamiltonian are

$$\begin{aligned}E_{\pm} &= \frac{q_0(s)+q_1(s)\pm\sqrt{\left(q_0(s)-q_1(s)\right)^2-4q_0(s)q_1(s)/N}}{2}, \\ E_{N-2} &= q_0(s)+q_1(s)\ .\end{aligned} \tag{3.10}$$

From the energy gap, $\Delta(s)=E_+-E_-$, and the set of eigenstates of $H(s)$, it is possible to estimate the adiabatic time $T_{\rm ad}$ from the standard condition to adiabaticity given by [29, 30]

$$\tau\gg T_{\rm ad}=\max_{n,m}\left[\max_{s\in[0,1]}\left(\frac{\left|\left\langle E_n(s)\right|H'(s)\left|E_m(s)\right\rangle\right|}{\Delta^2_{nm}(s)}\right)\right], \tag{3.11}$$

where $|E_m(s)\rangle$ are the eigenstates of $H(s)$ and $\Delta_{nm}(s)=E_n(s)-E_m(s)$ is the energy gap between $|E_n(s)\rangle$ and $|E_m(s)\rangle$. Here, the parameter $s=t/\tau$ is the normalized time and we denote $f'(s)=\mathrm{d}f(s)/\mathrm{d}s$. From the above equation, we obtain the adiabatic constraint over the total evolution time τ, in which the adiabatic evolution is expected to be achieved only when $\tau\gg T_{\rm ad}$. Because $T_{\rm ad}$ is obtained from an maximization in time, it is clear the role of a good choice of the functions $q_n(s)$.

Moreover, we can find that $\langle E_+\left|d_sH(s)\right|E_-\rangle\leq 1$, meaning that this term does not scale with the number of elements in the database. Now, using the global adiabatic condition, Eq. (3.11), and the linear 'ramp' interpolation ($q_0(t)=1-t/\tau$ and $q_1(t)=t/\tau$) we find $T_{\rm ad}=N$, which is a loss of the quantum speed up over the classical unstructured search [36].

Alternatively, we can derive a better parametrization if we idealize a curve that can adapt to the system eigenspectrum, which is done by using the local adiabatic condition,

Eq. (2.33). Let us consider $q_0(s) = 1 - s(t)$ and $q_1(s) = s(t)$. Further, from the local adiabatic condition, we give a ansatz for a interpolation speed

$$v(s)\frac{1}{\epsilon\Delta(s)^2} \leq \epsilon \quad \rightarrow \quad v^{\text{ad}}(s) = \epsilon\Delta(s)^2 \ . \tag{3.12}$$

Hence, we have the ordinary differential equation

$$\frac{\mathrm{d}s}{\mathrm{d}t} = \epsilon\Delta(s)^2 = \epsilon\left[1 - 4s\,(1-s)\,\frac{N-1}{N}\right] \ , \tag{3.13}$$

that, when integrated from 0 to t, yields

$$t = \frac{1}{2\epsilon}\frac{N}{\sqrt{N-1}}\left\{\arctan\left[\sqrt{N-1}\,(s-1)\right] + \arctan\left(\sqrt{N-1}\right)\right\} \ . \tag{3.14}$$

Evaluating Eq. (3.14) in $s(\tau) = 1$ and expanding it for $N \gg 1$ we find

$$\tau \gg \mathcal{O}\left(\sqrt{N}\right) \ , \tag{3.15}$$

where, by construction, we considered $\epsilon \ll 1$. This result means that it is possible to find an interpolation process that improves the algorithm order of complexity to $\mathcal{O}(\sqrt{N})$, showing, as expected, that the adiabatic quantum computing and the quantum logic gates paradigm are equivalent. In addition, the inversion of Eq. (3.14) becomes

$$\begin{aligned} t/\tau &= \frac{1}{2}\frac{\arctan\left[\sqrt{N-1}\,(2s-1)\right]}{\arctan\left[\sqrt{N-1}\right]} + \frac{1}{2}, \\ \therefore \quad s(t) &= \frac{1}{2} + \frac{\tan\left[(2t/\tau - 1)\arctan\left(\sqrt{N-1}\right)\right]}{2\sqrt{N-1}} \ . \end{aligned} \tag{3.16}$$

The method we used in this section to optimize the adiabatic interpolation does not comprehend all features of the physical system, since we had to set a linear constraint to the interpolation functions, $q_0(s) = 1 - q_1(s)$, for finding the optimization. In the next section, we will use the quantum adiabatic brachistochrone, Sec. 2.3, for generalizing this procedure.

3.2 Grover brachistochrone

A more general method for finding interpolation functions is the quantum adiabatic brachristochrone [40], as we described in Sec. 2.3. In the former section, we find an optimization for the Grover algorithm by defining a differential equation from the interpolation speed and solving it. For the QAB, the interpolation functions are found by solving the Euler-Lagrange equations of the QAB time functional. The Lagrangian of the adiabatic Grover algorithm reads

$$\mathcal{L} = \frac{(q_0' + q_1')^2 - \frac{2}{N}q_0'q_1'}{\left[(q_0 - q_1)^2 + \frac{4}{N}q_0q_1\right]^2} \ , \tag{3.17}$$

where we omitted the dependence of s in the interpolation functions q_0 and q_1, for simplicity. Again, the energy gap $\Delta(s)$ between the instantaneous ground state and first excited one is

$$\Delta(s) = E_+(s) - E_-(s) = \sqrt{\left(q_0(s) - q_1(s)\right)^2 + \frac{4}{N} q_0(s) q_1(s)} \ . \tag{3.18}$$

3.2.1 Constraints

The Euler-Lagrange equations of the Lagrangian as it is in Eq. (3.17), as far as we know, do not have an analytical solution. Nonetheless, we can impose constraints to the functions for finding analytical solutions and then study their physics. These constraints are, in general, mathematical tricks without any physical interpretation, but they can be determined based on physical characteristics of the problem, as we will see in the next subsection.

For a general polynomial constraint, $q_0^\alpha + q_1^\alpha = 1$, where α is a real constant, the Lagrangian is expressed as

$$\mathcal{L} = q_0' 2 \frac{\left[1 - (1 - q_0^\alpha)^{\frac{1}{\alpha}-1} q^{\alpha-1}\right]^2 + \frac{2}{N}(1 - q_0^\alpha)^{\frac{1}{\alpha}-1} q_0^{\alpha-1}}{\left[(q_0 - (1 - q_0^\alpha)^{\frac{1}{\alpha}})^2 + \frac{4}{N} q_0 (1 - q_0^\alpha)^{\frac{1}{\alpha}}\right]^2} \ . \tag{3.19}$$

Using that the Lagrangian is not explicitly time-dependent and the Beltrami's identity (see Appendix B)

$$\mathcal{L} - q_0' \frac{\partial \mathcal{L}}{\partial q_0} = C \ . \tag{3.20}$$

Then, we can use $C = -1$, since the Euler-Lagrange equations are invariant by multiplicative factors. Therefore, the new Euler-Lagrange equation reads

$$1 = q_0'^2 \frac{\left[1 - (1 - q_0^\alpha)^{\frac{1}{\alpha}-1} q_0^{\alpha-1}\right]^2 + \frac{2}{N}(1 - q_0^\alpha)^{\frac{1}{\alpha}-1} q_0^{\alpha-1}}{\left[(q_0 - (1 - q_0^\alpha)^{\frac{1}{\alpha}})^2 + \frac{4}{N} q_0 (1 - q_0^\alpha)^{\frac{1}{\alpha}}\right]^2} \ , \tag{3.21}$$

from which it is derived the expression

$$s(q) = \int_0^q \sqrt{g} dq \ , \tag{3.22}$$

where

$$g = \frac{\left[1 - (1 - q_0^\alpha)^{\frac{1}{\alpha}-1} q_0^{\alpha-1}\right]^2 + \frac{2}{N}(1 - q_0^\alpha)^{\frac{1}{\alpha}-1} q_0^{\alpha-1}}{\left[(q_0 - (1 - q_0^\alpha)^{\frac{1}{\alpha}})^2 + \frac{4}{N} q_0 (1 - q_0^\alpha)^{\frac{1}{\alpha}}\right]^2} \ . \tag{3.23}$$

To find $q_0(t)$, it is necessary to solve the integral in Eq. (3.22) and then invert the function $s(q_0)$. We solved it numerically using the SciPy library [90].

The linear constraint, $\alpha = 1$, yields the same interpolation function given in Eq. (3.16), showing that ignoring the term $|\langle \psi_n | \mathrm{d}_s H(s) | \psi_m \rangle|$ is equivalent to considering

the Lagrangian formalism. Thus, we conclude that the QAB is a generalization of the optimization proposed in the Ref. [36]. For the quadratic constraint, $\alpha = 2$, it is possible to find the interpolation function numerically. We also can solve this problem by performing the change of variables $q_0 = \cos(\omega(s))$ and solve numerically the Euler-Lagrange equation for the new canonical variable $\omega(s) \in \{0, \pi/2\}$ [89].

3.2.2 The unconstrained case

For the general Lagrangian, Eq. (3.17), the Euler Lagrange equations are not separable, which makes the numerical treatment non straightforward. In order to simplify the equations and the numerical method, we do a Legendre transform on $\mathcal{L}$ with respect to q_0' and q_1', which yields the Hamiltonian

$$\begin{aligned}\mathcal{H} &= \sum_{i=0}^{1} q_i' p_i - \mathcal{L} \\ &= \Delta^4 \left[\beta \left(p_0 + p_1\right)^2 + \eta p_0 p_1\right] \\ &= \mathcal{L}(q_0, q_1, q_0', q_1')|_{p_i = \partial\mathcal{L}/\partial q'} \ ,\end{aligned} \tag{3.24}$$

where $p_i = \partial L/\partial q_i'$, $\beta = N^2/(4(N-1)(2N-1))$, and $\eta = -N/(2(N-1))$. Let us note that $\mathcal{H}$ is equal to $\mathcal{L}$, implying that $\mathrm{d}H/\mathrm{d}s = \mathrm{d}\mathcal{L}/\mathrm{d}s = 0$. Then, the Euler-Lagrange equations derived from the Lagrangian $\mathcal{L}' = \frac{||H'(s)||}{\Delta^2(s)}$ and $\mathcal{L} = \mathcal{L}'^2$ will have the same motion equations (see Appendix C). For $\mathcal{L}$, the Hamilton canonical equations read

$$\begin{aligned} p_0' &= 4\left[\eta p_0 p_1 + \beta(p_0 + p_1)^2\right]\left(q_1 - q_0 - \frac{2}{N} q_1\right)\Delta^3 \ , \\ p_1' &= 4\left[\eta p_0 p_1 + \beta(p_0 + p_1)^2\right]\left(q_0 - q_1 - \frac{2}{N} q_0\right)\Delta^3 \ , \\ q_0' &= \Delta^4\left[\eta p_1 + 2\beta(p_0 + p_1)\right] \ , \\ q_1' &= \Delta^4\left[\eta p_0 + 2\beta(p_0 + p_1)\right] \ , \end{aligned} \tag{3.25}$$

and can be approached by standard numerical methods. In this master's thesis, we solved this boundary value problem using the SciPy python library [90].

3.2.3 Fixed power constraint

In laboratories, there can be physical limitations, such as a limitation of resources available for a temporal evolution, that reflect in the experiment results. For instance, in the Ref. [1] the interpolation functions were constrained by power limitation by the arbitrary-wave generator (see Sec. 4.4 for more details). By considering this restriction on the instantaneous energy variation, one can impose a constant power constraint (CPC), which will fix the instantaneous power consumption during all the evolution. The mean energy cost to drive the Hamiltonian from 0 to τ [91–93] is given by

$$\Sigma_\tau = \frac{1}{\tau}\int_0^\tau ||H(t)||\mathrm{d}t = \int_0^1 ||H(s)||\mathrm{d}s \ . \tag{3.26}$$

The power required to move the system from t to $t + \mathrm{d}t$ is the energy variation

$$\begin{aligned} \mathcal{P}(t) &= \frac{\mathrm{d}}{\mathrm{d}t}\left(\Sigma_\tau\right) \\ &\propto ||H(t)|| \ , \end{aligned} \tag{3.27}$$

but since we will equal this quantity to a constant, we will consider, without loss of generalization,

$$|H(s)||^2 = (q_0(s) + q_1(s))^2 - \frac{2q_0(s)q_1(s)}{N} = 1 \ . \tag{3.28}$$

After fixing $||H(s)||^2$, thus fixing $\mathcal{P}(t) =$ 'constant', the function $q_1(s)$ becomes

$$q_1(s) = -q_0(s)\left(1 - \frac{1}{N}\right) \pm \sqrt{1 + q_0^2(s)\frac{1-2N}{N^2}} \ . \tag{3.29}$$

To establish a relationship with the linear constraint, one can take just the *plus* sign before the square root, since in the limit $N \gg 1$ the fixed power constraint is approximated to the linear constraint. The Lagrangian for the CPC reads,

$$\begin{aligned} \mathcal{L}_{\mathrm{CPC}} = &\frac{q_0'^2}{\left[N - q_0^2\left(2 - \frac{1}{N}\right)\right]} \\ &\times \frac{1}{\left[N - 2q_0\left(2 - \frac{3}{N}\right)\left(q_0\left(1 - \frac{1}{N}\right) + \sqrt{1 + q_0^2\frac{1-2N}{N^2}}\right)\right]^2} \ , \end{aligned} \tag{3.30}$$

which was solved numerically using the Beltrami's identity scheme presented in Sec. 3.2.1.

3.2.4 Results

The Fig. 3(a) shows the dynamics total time for a fixed fidelity, $\mathcal{F} = 0.99$, between the evolved state and the target one $|m\rangle$, as a function of $\sqrt{N}$ for different interpolation functions. In this graph we consider the same boundary conditions, $q_0(0) = q_1(\tau) = 1$ and $q_0(\tau) = q_1(0) = 0$, for all protocols. The unconstrained brachistochrone yielded a greater efficiency, while the linear function, $q_0 = 1 - s = 1 - q_1$ the worst. Additionally, the quadratically constrained brachistochrone yielded an algorithm time complexity equal to $\mathcal{O}(N^{0.64})$, Fig. 3(c), thereby increasing the algorithm time complexity in almost 50%. This behaviour may be due to the non-linearity this constraint introduces in the motion equations. The physical interpretation of these results is supported by Fig. 3(b), which shows the adiabatic time T_{ad}, Eq. (3.11), as a function of the square-root of the numbers of items in the database. The curves in the Fig. 3(b) have the same inclination for the scaling time of the algorithm, indicating that evaluating the quantity $\tau_{\mathrm{ad.}}$ is a possible and efficient method for comparing different sets of functions $\{q_0, q_1\}$ without solving the dynamics, consequently saving computational resources.

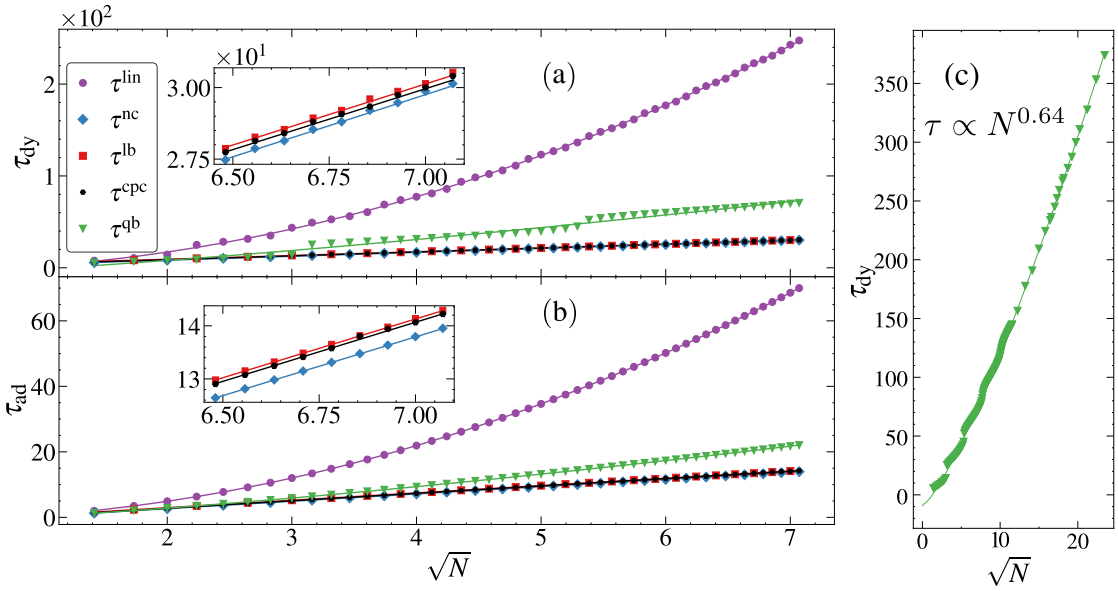

Figure 3 – (a) and (b) dynamics time for reaching the fidelity between the target state and the evolved state fixed in 0.99 and the adiabatic time, respectively, as functions of $\sqrt{N}$ for different interpolation functions. The purple circles represent the linear interpolation, the blue diamonds represent the unconstrained brachistochrone, the red squares the brachistochrone with the linear constraint, the black hexagons the brachistochrone with the constant power constraint, and green inverted triangle quadratically constrained brachistochrone. (c) the partial simulations for the quadratic brachistochrone for the fidelity between the target state and the envolved state fixed in 0.99 as function of $\sqrt{N}$ for N scaling up to 550, wherein we find that $\tau^{\text{qb}} \propto N^{0.64\pm0.1}$. Source: Made by the author.

3.3 Energetic and power cost of quantum evolutions

Another resource that must be taken into account is the mean energy cost for executing the algorithm. For example, when the energy is not a limited resource, it is possible to reach a constant time complexity, O(1), by exchanging time for energy expenditure by using short-cuts to adiabaticity [91]. For measuring this resource usage, we will consider the mean energy cost as defined in Eq (3.26),

$$\Sigma_\tau = \int_0^1 \sqrt{||H(s)||}\mathrm{d}s = \int_0^1 \sqrt{E_+^2(s) + E_-^2(s) + (N-2)E_d^2(s)}\mathrm{d}s \ . \tag{3.31}$$

The quantity Σ_τ of the linear interpolation, $q_0 = (1-s)$ and $q_1 = s$, has an analytical solution

$$\Sigma_\tau^{\text{linear}} = \frac{1}{4}\sqrt{\frac{N-1}{N}}\left[2\sqrt{N} + \sqrt{2}\,(2N-1)\,\text{arctanh}\left(\frac{1}{\sqrt{2N}}\right)\right] \ , \tag{3.32}$$

which, for $N \gg 1$ is $\Sigma_\tau^{\text{linear}} \propto \sqrt{N}$. For all interpolation functions, the mean energies were computed, as Fig. 4(b) shows. All of them scale with $\sqrt{N}$, but with different inclinations.

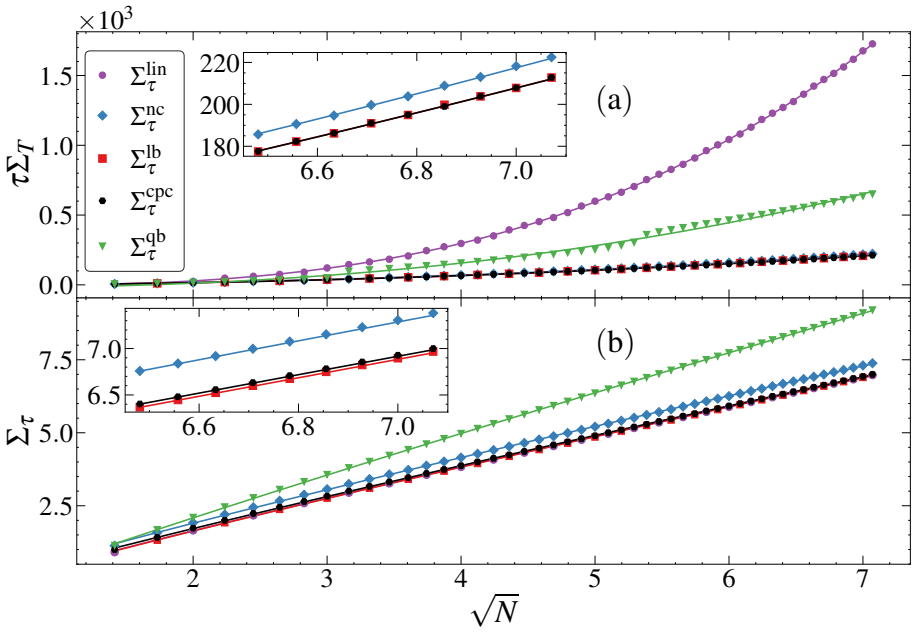

Figure 4 – (a) τ for reaching a fixed fidelity equal to 0.99 times Σ_τ as a function of the square root of the number of items in the database. (b) Σ_τ for different interpolation functions as a function of $\sqrt{N}$. The purple circles represent the linear interpolation, the diamonds the unconstrained brachistochrone, the squares the brachistochrone with the linear constraint, the black hexagons the brachistochrone with the cpc, and the green inverted triangles the quadratically constrained brachistochrone. Source: made by the author.

The unconstrained brachistochrone has almost the same energy expenditure of the linear, but the quadratically constrained brachistochrone shows higher values for Σ_τ. The Fig. 4(a), shows that the curves for the mean energy times the total dynamics time do not diverge from the curves in Fig. 3(a), indicating that resource $\tau\Sigma_\tau$, in the scenario where all the interpolation functions have the same boundary conditions, is not a good parameter to evaluate the efficiency of the algorithm, since it does not give further information regarding the scaling. Also, Fig. 4(b) shows that the quadratically brachistochrone curve spends more energy for the evolution, although having the same scaling, $\Sigma_{\text{qc}} \propto \sqrt{N}$. This indicates that there is not a clear relation between the energy the process demands and its time efficiency.

3.3.1 Fixed Σ_τ scenario

For establishing a reference, we set to all adiabatic processes the energy expenditure of the linear function. The Fig. 5(a) shows the total dynamics time, τ for a fixed process fidelity, as a function of the number of items in the database when all the interpolation functions have the same mean energy, $\Sigma_\tau^{\text{linear}}$. The results show that the protocols with the linear constrained and the CPC Brachistochrones become faster than the others functions.

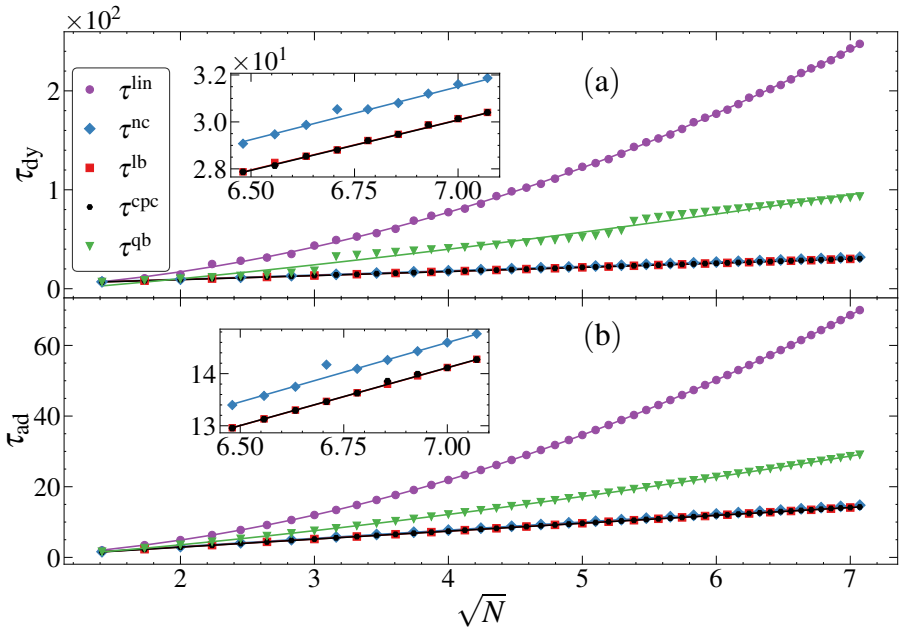

Figure 5 – (a) Total dynamics time for reaching the fidelity between the target state and the evolved state fixed in 0.99 and (b) the adiabatic time in function of $\sqrt{N}$ for different interpolation functions with the same energy cost. The purple circles represent the linear interpolation, the diamonds represent the unconstrained brachistochrone, the squares the brachistochrone with the linear constraint, the black hexagons the brachistochrone with the constant power constraint, and green inverted triangle quadratically constrained brachistochrone. Source: Made by the Author.

This result demonstrates that the linear constrained and the CPC brachistochrones have a greater energy efficiency among all the others functions considered here. In other words, the curves of these constraints fit better to the adiabatic condition without spending as much energy as the non-constrained brachistochrone.

3.4 Conclusion of this Chapter

We analyzed the application of the quantum adiabatic brachistochrone to the adiabatic Grover algorithm for testing mathematical and physical constraints and also the performance of the algorithm for when the mean energy cost and instantaneous power consumption are limited. Through the Beltrami's identity, we showed that the procedure carried out in the Ref. [36] for optimizing the evolution is equivalent to consider the QAB method with the linear constraint. Since finding the scaling of the algorithm by solving the Schrödinger equation is a computationally expensive task, we demonstrated that one can use the adiabatic time for satisfactorily finding this property. This means that it is necessary just to find the interpolation functions. We found the unconstrained brachistochrone numerically, which has yielded the smaller algorithm time execution, as our simulations indicates for the scale of N we tested, although no qualitative gain over

the linear and constant power constraints was observed. Concerning the analysis with mean energy limitation, we showed that the simple linear function, the linear constrained and the CPC brachistochrone curves present almost the same mean energy, while the unconstrained brachistochrone is slightly higher. When we impose the same energies for all interpolation functions, the linear brachistochrone and the one with fixed power become the most efficient functions, despite being qualitatively the same as the brachistochrone with no constraints.

4 Superconducting quantum battery

Mastering industrial processes for building smaller transistors powered up the development of computer sciences, from which modern science relies on. Now, the development and expansion of quantum information and quantum thermodynamics as general areas have been instigating the engineering of quantum devices, which have been yielding new theoretical findings and applications [94]. These new quantum technologies are showing to be relevant in many areas. For example, in quantum metrology [95] these devices were crucial in measuring the gravitational waves [96]. In quantum cryptography, it was established a secure communication channel between two locations 1000 km apart [97]. Furthermore, quantum computing has a promising role in solving physics, chemical, and logistic problems that are untreatable by classical computers [98].

Moreover, in classical circuits there are components storing energy, like capacitors. Similarly, this class of device will also have an important role in quantum engines. However, in quantum apparatus, the device that stores energy must store energy in a quantum way for preserving the desired characteristic of this regime, such as coherence and correlation. Many quantum system were proposed for storing extractable energy, some of them use as resource quantum coherence [99, 100], entanglement [101] or atomic excitation [18, 100]. Differently for classical devices, quantum devices are sensible to the charging process, which means that it must be done according to some rules. For instance, quantum batteries that use adiabatic dynamics in their charging process, must respect the adiabatic condition and, for ensuring time efficiency, it is necessary to optimize the charging protocols. Additionally, as same as classical batteries, quantum batteries lose charge to the environment, but due to decoherence. Since the capacity to a system retains its charge will be a threshold for potential applications, it is necessary to characterize its self-discharging behavior.

In this Chapter, we theoretically describe the experiment about the charging process of a quantum battery and its self-discharging process we reported in collaboration with Prof. Dapeng Yu's research group [1]. Our quantum battery is a superconducting transmon qubit, that simulates a three-level atom. Therefore, the charging process means to drive the atom population that is initially on the ground state to the second excited one. This dynamics can explore the dark-state of the system, allowing a stable charging process or it can explore the unstable charging process, which populates the first excited state during the time evolution. For optimizing this process, we used the quantum adiabatic brachistochrone, described in Sec. 2.3. We finish this Chapter by showing that the self-discharging process of our quantum battery has a super-capacitive behaviour.

4.1 Three-level quantum battery

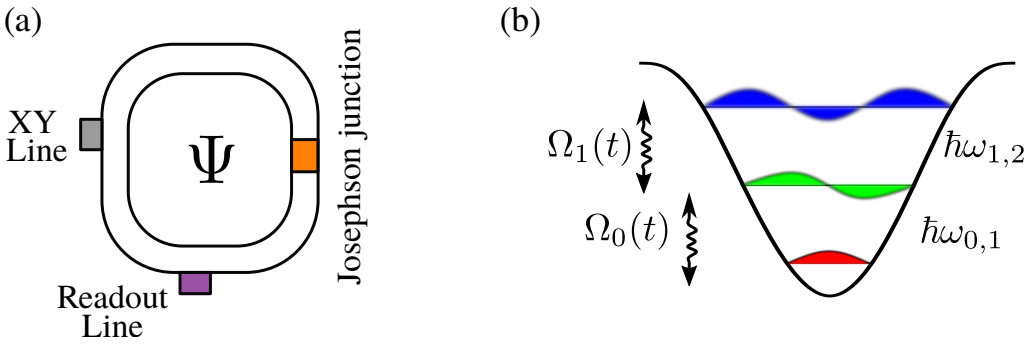

Figure 6 – (a) Illustration of the transmon superconducting that can be used, indeed it was what we used to implement our system. The device is composed by a superconductor, a Josephson junction that introduces an anharmonicity, the readout line and the XY line that connects classical microwave fields that will couple the eigenstates. Source: Made by the author.

In a superconductor [15, 16], the Cooper's pairs move freely and, when one couples a resonant field to this system, the electrons start to behave as harmonic oscillators, where we have the same energy energy gap between all the transitions. Thus, when a field couples with a transition level, it couples with all transition levels, therefore it is not possible to select the atomic levels we want. In the transmon superconducting device, Fig. 6(a), there is a Josepheson Junction, that imposes a potential barrier to the electrons. This effect will make part of the wave function transmit through this barrier and part of the electrons will be reflected, thereby introducing an anharmonicity to the system. In the new Hamiltonian, the transition frequencies between eigenstates will be different and a field coupling the transition from the group state to the first excited one will not see the other transitions in the system. Therefore, with two fields we implemented the charging process of the three-level quantum battery.

The Hamiltonian that describes the quantum battery and the time-dependent system that will inject energy in the system is

$$H(t) = H_0 + H_c(t) \ , \tag{4.1}$$

for

$$\begin{aligned} H_0 &= \sum_{n=1}^{2} \hbar\omega_{n-1,n} \left|\epsilon_n\right\rangle \left\langle\epsilon_n\right| , \\ H_c(t) &= \hbar\Omega_0(t) e^{-i\omega_1 t/\hbar} \left|\epsilon_0\right\rangle \left\langle\epsilon_1\right| + \hbar e^{-i\omega_2 t/\hbar} \Omega_1(t) \left|\epsilon_1\right\rangle \left\langle\epsilon_2\right| + \text{h.c.} \ . \end{aligned} \tag{4.2}$$

H_0 represents the Hamiltonian of a three level system with a ladder-like energy level configuration, $\epsilon_0 < \epsilon_1 < \epsilon_2$, $|\epsilon_n\rangle$ is the state of the n-th energy level, $\hbar\omega_{n-1,n} = \epsilon_n$, and we consider $\epsilon_0 = 0$. The time-dependent Hamiltonian, $H_c(t)$, is responsible for charging the battery. Also, we note that the omegas ω_i are the field frequency, which are in resonance

with the respectively atomic transitions, $\omega_1 = \omega_{0,1}$ and $\omega_2 = \omega_{1,2}$, and the $\Omega_i(t)$ is the Rabi frequency. Since we are interested in charging the battery, we can study the dynamic process due to the charging Hamiltonian, which can be done in the rotation frame

$$\begin{aligned} H_{\mathrm{rf}} &= e^{iH_0t/\hbar}\left[H_0 + H_c(t)\right]e^{-iH_0t/\hbar} + i\hbar\frac{\mathrm{d}}{\mathrm{d}t}\left(e^{iH_0t/\hbar}\right)e^{-iH_0t/\hbar} \\ &= e^{iH_0t/\hbar}H_c(t)e^{-iH_0t/\hbar} \\ &= \hbar\Omega_0(t)\left|\epsilon_0\right\rangle\left\langle\epsilon_1\right| + \hbar\Omega_1(t)\left|\epsilon_1\right\rangle\left\langle\epsilon_2\right| + \mathrm{h.c.} \end{aligned} \tag{4.3}$$

Expressed as a matrix, we have

$$H_{\mathrm{rf}} = \hbar\begin{pmatrix} 0 & \Omega_0(t) & 0 \\ \Omega_0(t) & 0 & \Omega_1(t) \\ 0 & \Omega_1(t) & 0 \end{pmatrix}, \tag{4.4}$$

which has the eigenvalues

$$E_\pm(t) = \pm\Delta(t), \quad E_0 = 0\ , \tag{4.5}$$

where $\Delta(t) = \hbar\sqrt{\Omega_0^2(t) + \Omega_1^2(t)}$ is the energy gap between subsequent eigenvectors. Also, the eigenstates of H_{rf} are

$$\left|E_\pm\right\rangle = \frac{1}{\sqrt{2}}\left[\frac{\Omega_0(t)}{\Delta(t)}\left|\epsilon_0\right\rangle \pm \left|\epsilon_1\right\rangle + \frac{\Omega_1(t)}{\Delta(t)}\left|\epsilon_2\right\rangle\right], \quad \left|E_0\right\rangle = \frac{\Omega_1(t)}{\Delta(t)}\left|\epsilon_0\right\rangle - \frac{\Omega_0(t)}{\Delta(t)}\left|\epsilon_2\right\rangle\ . \tag{4.6}$$

The results in the equation above show that it is possible to charge the battery in two distinct ways. The first protocol is using the superposition of the states with non-zero energy, which is the bright state and it reads

$$\left|\psi^{\mathrm{bright}}(t)\right\rangle = \frac{1}{\sqrt{2}}\left(\left|E_+(t)\right\rangle + \left|E_-(t)\right\rangle\right)\ . \tag{4.7}$$

For completeness, we emphasize that $\left|\psi^{\mathrm{bright}}(0)\right\rangle = \left|\epsilon_0\right\rangle$ and $\left|\psi^{\mathrm{bright}}(\tau)\right\rangle = \left|\epsilon_2\right\rangle$. The dark state protocol uses the zero-energy state,

$$\left|\psi^{\mathrm{dark}}\right\rangle = \left|E_0(t)\right\rangle\ . \tag{4.8}$$

Experimentally, for implementing the bright or dark states the boundary conditions

$$\text{“bright passage”}, \begin{cases} \Omega_0(0) = \Omega_1(\tau) = 1 \\ \Omega_0(\tau) = \Omega_1(0) = 0 \end{cases}, \text{“dark passage”} \begin{cases} \Omega_0(0) = \Omega_1(\tau) = 0 \\ \Omega_0(\tau) = \Omega_1(0) = 1 \end{cases}\ . \tag{4.9}$$

Therefore, using both boundary condition one can drive the population of the battery from the ground state to the second excited state.

So far we have described the battery charging process. Now, for measure the amount of extractable work in the battery we will use the ergotropy [102]

$$\mathcal{E}(t) = \mathrm{Tr}\left[\rho(t)H_0\right] - \min_{U\in\mathcal{U}}\left\{\mathrm{Tr}\left[U\rho(t)U^\dagger H_0\right]\right\}\ , \tag{4.10}$$

where the second term in the right-handed side of the equation is a minimization over all the unitary operators acting on the system. Since the battery population is initially on the ground state and the charging, the ergotropy after the charging is over is

$$\begin{aligned}\mathcal{E}(t) &= \mathrm{Tr}\left[\rho(t)H_0\right] - \mathrm{Tr}\left[\rho_0 H_0\right] \\ &= \mathrm{Tr}\left[\rho(t)H_0\right] - \epsilon_0 \ .\end{aligned} \tag{4.11}$$

The maximum value that the ergotropy can assume is $\mathcal{E}_{\max} = \epsilon_2 - \epsilon_0$, which is achieved when the battery is fully charged.

Suppose we perform a Schrödinger adiabatic evolution using the bright charging protocol, the evolved states will be

$$\begin{aligned}\left|\psi^{\text{bright}}(t)\right\rangle &= \frac{1}{\sqrt{2}}\left\{e^{-(i/\hbar)\int_0^t E_+(t')\mathrm{d}t'}\left|E_+(t)\right\rangle + e^{-(i/\hbar)\int_0^t E_-(t')\mathrm{d}t'}\left|E_-(t)\right\rangle\right\} \\ &= \frac{e^{-(i/\hbar)\int_0^t E_+(t')\mathrm{d}t'}}{\sqrt{2}}\left[\frac{\Omega_0(t)}{\Delta(t)}\left|\epsilon_0\right\rangle + \left|\epsilon_1\right\rangle + \frac{\Omega_1(t)}{\Delta(t)}\left|\epsilon_2\right\rangle\right] \\ &+ \frac{e^{-(i/\hbar)\int_0^t E_-(t')\mathrm{d}t'}}{\sqrt{2}}\left[\frac{\Omega_0(t)}{\Delta(t)}\left|\epsilon_0\right\rangle - \left|\epsilon_1\right\rangle + \frac{\Omega_1(t)}{\Delta(t)}\left|\epsilon_2\right\rangle\right] \ ,\end{aligned} \tag{4.12}$$

and, regrouping the terms

$$\left|\psi^{\text{bright}}(t)\right\rangle = \frac{\cos\left(\tilde{\theta}(t)\right)}{\Delta(t)}\left[\Omega_0(t)\left|\epsilon_0\right\rangle + \Omega_1(t)\left|\epsilon_2\right\rangle\right] - i\sin\left(\tilde{\theta}(t)\right)\left|\epsilon_1\right\rangle \ , \tag{4.13}$$

where $\tilde{\theta}(t) = \int_0^t \Delta(t')\mathrm{d}t'$. Evaluating the system ergotropy for this initial state, we find that

$$\begin{aligned}\mathcal{E}^{\text{bright}}(t) &= \left\langle\psi^{\text{bright}}(t)\left|H_0\right|\psi^{\text{bright}}(t)\right\rangle - \left\langle\epsilon_0\left|H_0\right|\epsilon_0\right\rangle \\ &= \epsilon_2\frac{\cos^2\left(\tilde{\theta}(t)\right)}{\Delta^2(t)}\Omega_1^2(t) + \epsilon_1\sin^2\left(\tilde{\theta}(t)\right) \ .\end{aligned} \tag{4.14}$$

where we used $\epsilon_0 = 0$, as we defined in Eq. (4.2). In the quantity $\mathcal{E}^{\text{bright}}$ we see harmonic terms (sin and cos), which have a defined period τ_c. Therefore, if the total charging time, τ, is exactly τ_c, the battery will be fully charged. However, if $\tau > \tau_c$ then $\mathcal{E}^{\text{bright}}(\tau) < \mathcal{E}_{\max}$. The *unstable* behaviour of the ergotropy for the bight-state charging protocol is due destructive and constructive interference processes that happens during the evolution of the complex phases, which can both enhance and diminish the injection of ergotropy in the battery.

Furthermore, the dark state adiabatic evolution yields the very same dark state

$$\begin{aligned}\left|\psi^{\text{dark}}(t)\right\rangle &= e^{-(i/\hbar)\int_0^t E_0(t')\mathrm{d}t'}\left|\psi^{\text{dark}}(0)\right\rangle \\ &= \left|E_0(t)\right\rangle \ ,\end{aligned} \tag{4.15}$$

since $E_0 = 0$. Thus, an adiabatic evolution stating with the dark state leads to the ergotropy

$$\begin{aligned}\mathcal{E}^{\text{dark}}(t) &= \left\langle \psi^{\text{dark}}(t) \left| H_0 \right| \psi^{\text{dark}}(t) \right\rangle - \left\langle \epsilon_0 \left| H_0 \right| \epsilon_0 \right\rangle \\ &= \frac{\epsilon_2 \Omega_0^2(t) + \epsilon_0 \Omega_1^2(t)}{\Delta^2(t)} \\ &= \frac{\epsilon_2 \Omega_0^2(t)}{\Delta^2(t)} \ .\end{aligned} \tag{4.16}$$

From the ergotropy analysis, we note the different natures of the charging protocols and how they change the behaviour of the charging process. In the bright passage, the ergotropy exhibit the oscillatory behavior, but, if the battery is already characterized, one can fully charge it and then turn of the fields, thereby keeping the maximum stored energy until decoherence acts on the system. On the other hand, the dark state charging allows the to keep the fields on, increasing the robustness of the battery against relaxation process.

4.2 The Brachistrochrone

As we saw in the former section, the charging protocol we want demands the initial state, $|\epsilon_1\rangle$ therefore, our interpolation functions are the fields that couple the system states, Ω_0 and Ω_1. Additionally, the energy gap is $\Delta(s)^2 = \Omega_0^2(s) + \Omega_1^2(s)$. With this information, we can derive the Lagrangian for the quantum battery charging process. The Lagrangian numerator, for $f' = \mathrm{d}f/\mathrm{d}s$, is

$$\mathrm{d}_s H_{\text{int}}(s) = \hbar \Omega_0'(s) \left| \epsilon_1 \right\rangle \left\langle \epsilon_2 \right| + \hbar \Omega_1'(s) \left| \epsilon_2 \right\rangle \left\langle \epsilon_3 \right| + \text{h.c.} \ , \tag{4.17}$$

which, multiplied by its conjugated yields the quantity

$$\begin{aligned}\mathrm{d}_s H_{\text{int}}^\dagger \mathrm{d}_s H_{\text{int}} &= 2\hbar^2 \left({\Omega_1'}^2 + {\Omega_0'}^2 \right) \left| \epsilon_2 \right\rangle \left\langle \epsilon_2 \right| + \hbar^2 \Omega_0^{\dagger\prime} \Omega_1^{\dagger\prime} \left| \epsilon_3 \right\rangle \left\langle \epsilon_1 \right| + \hbar^2 \Omega_0' \Omega_1' \left| \epsilon_1 \right\rangle \left\langle \epsilon_3 \right| \ , \\ \therefore \quad \text{Tr} \left[\mathrm{d}s H_{\text{int}}^\dagger(s) \mathrm{d}s H_{\text{int}}(s) \right] &= 2\hbar^2 \left({\Omega_0'}^2 + {\Omega_1'}^2 \right) \ ,\end{aligned} \tag{4.18}$$

where we omitted the s dependence for simplicity. Thus, the Lagrangian for this system is

$$\mathcal{L} = \frac{{\Omega_0'}^2(s) + {\Omega_1'}^2(s)}{\left[\Omega_0^2(s) + \Omega_1^2(s) \right]^2} \ , \tag{4.19}$$

where we removed the multiplicative constant $2/\hbar^2$, since the Euler-Lagrange equations are invariant to them. The Euler-Lagrange equations applied to Eq. (4.19) yield the system of coupled second-order differential equations

$$\begin{aligned}(\Omega_1^2 + \Omega_2^2)\ddot{\Omega}_1 - 2\left(2\Omega_2 \dot{\Omega}_1 \dot{\Omega}_2 + \Omega_1 (\dot{\Omega}_1^2 - \dot{\Omega}_2^2) \right) = 0, \\ (\Omega_1^2 + \Omega_2^2)\ddot{\Omega}_2 - 2\left(2\Omega_2 \dot{\Omega}_1 \dot{\Omega}_2 - \Omega_2 (\dot{\Omega}_1^2 - \dot{\Omega}_2^2) \right) = 0 \ ,\end{aligned} \tag{4.20}$$

which, as far as we know, do not have an analytical solution, but it is possible to solve it using the standard numerical methods, as it is in Fig. (7).

Now, for solving the Euler-Lagrange equations, we can use the linear constraint, $\tilde{\Omega}_0(s) + \tilde{\Omega}_1(s) = 1$, for $\tilde{\Omega}_i = \Omega_i/\Omega_{\max}$. The Lagrangian now reads

$$\mathcal{L} = 2\frac{\tilde{\Omega}_0'^2}{\left[\left(1-\tilde{\Omega}_0\right)^2 + \tilde{\Omega}_0^2\right]^2} \ , \tag{4.21}$$

and its Euler-Lagrange equation, using the Beltrami's identity, is

$$\tilde{\Omega}_0'(s) = C\left[\left(1-\tilde{\Omega}_0\right)^2 + \tilde{\Omega}_0^2\right] \ . \tag{4.22}$$

After integrating this equation and adjusting the integration constants to the boundary value problem, we find the interpolation

$$\Omega_0 = \frac{\Omega_{\max}}{2} + \frac{\Omega_{\max}}{2}\tan\left[\frac{\pi\,(1-2s)}{4}\right] \ , \tag{4.23}$$

for finding Ω_1 one has to substitute Ω_0 is the constraint. Let us note that Ω_0, as is the former equation, concerns the charging process using the bright passage. In the dark passage, since we turn on $\Omega_1(s)$ first, we have $\Omega_1^{\text{dark}}(s) = \Omega_0^{\text{bright}}(s)$, where the superscript regards the type one the charging process. The motivation for applying the linear constraint does not come from a physical interpretation, but it is a mathematical tool, that allows us to solve the Euler-Lagrange equation analytically without introduce any additional non-linearity to the problem. Moreover, we can evoke some physical characteristic for this system for defining constraints. One important resource in the charging, is the instantaneous power need to move the system from s to $s + \mathrm{d}s$ [91–93]

$$\begin{aligned}\mathcal{P}(s) &= ||H(s)||^2 \\ &= \hbar^2\left[\Omega_0^2(s) + \Omega_1^2(s)\right] \ .\end{aligned} \tag{4.24}$$

Therefore, if we want to invert the system populating adiabatically using the same power in every time interval, we need to use the quadratic constraint, $\Omega_0^2(s) + \Omega_1^2(s) = \Omega_{\max}^2$. Again, we define $\tilde{\Omega}_i = \Omega_i/\Omega_{\max}$ to write the Lagrangian with the quadratic constraint as

$$\mathcal{L} = \frac{\tilde{\Omega}_0'(s)}{1-\tilde{\Omega}_0^2(s)} \ . \tag{4.25}$$

The Euler-Lagrange equation is then

$$\tilde{\Omega}_0'(s) = C\sqrt{1-\tilde{\Omega}_0^2(s)} \ , \tag{4.26}$$

from which we find the solution for the bright passage

$$\Omega_0(s) = \Omega_{\max}\sin\left(\frac{s\pi}{2}\right) \ . \tag{4.27}$$

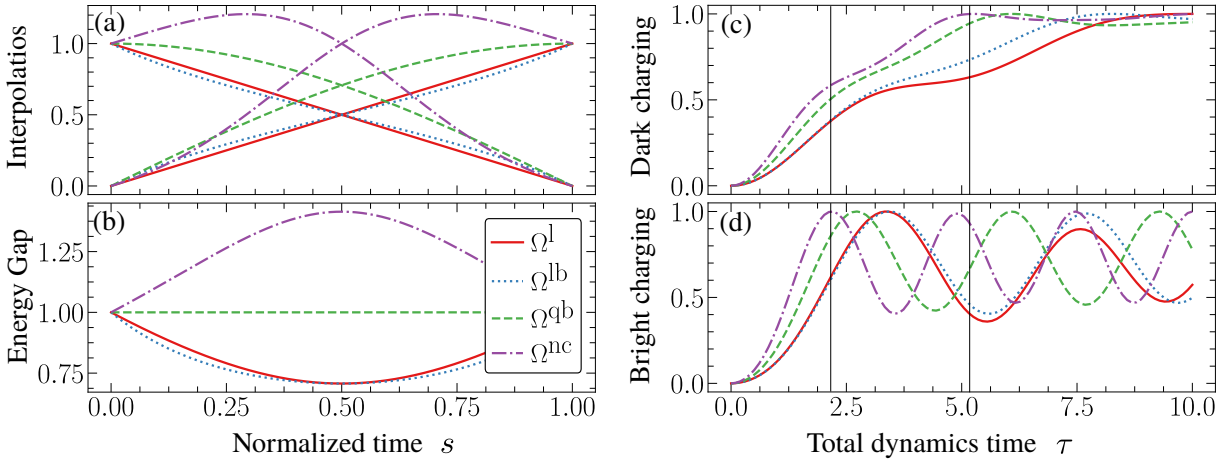

Figure 7 – The parametrization curves (a), and the energy gap (b) as a function of the normalized time s for the interpolation functions: linear, Ω^{l} (linear), brachistochrone with the linear constraint, Ω^{lb} , brachistochrone with the quadratic constraint, Ω^{qb}, and the brachistochrone with no constraints Ω^{nc}. (c) and (d) show the normalized ergotropy as a function of the total dynamics times, τ for the stable and unstable charging protocols, respectively. Parameters: $\epsilon_0 = 1$, $\epsilon_1 = 0.5$, and $\epsilon_2 = 1.05$. Source: Made by the author.

Fig. 7(a) shows the interpolation functions when considering the same initial conditions. In this scenario, the power consumption will vary in each protocol, also the energy expending. Further, Fig. 7(b) shows the energy gap in function of the normalized time s, in which we see that the non-monotonicity of the brachistochrone with no constraints increase the energy gap, thus decreasing the population flow to others eigenstates. Also, as expected by the quadratic constrain, the energy gap is a constant. The other notable behavior is the similarity between the energy gap of the linear interpolation and the linear brachistochrone. Furthermore, Fig. 7(c) and (d) show the normalized ergotropy for the stable and unstable charging process, respectively. The first thing we note is that for small τ, before the black horizontal line, the adiabatic regime is not achieved, since the ergotropy is not in its maximum. The unstable protocol reaches the maximum ergotropy using nearly half of time that the stable uses. Additionally, in the conditions we simulated the system, *i.e* using the same initial conditions for every interpolation function, the brachistochrone with no constraint speedup the adiabatic process. We physically understand this results through the growth of the energy gap during the dynamics.

4.3 Self-discharging process

As we have already discussed in the introduction, every battery exhibits a self-discharging process. Quantum batteries lose their charge due to decoherence. The equation

that will describe these process is the Lindbladian master equation [103]

$$\dot{\rho}(t) = -\frac{i}{\hbar}\left[H_0, \rho(t)\right] + \sum_{n,m} \frac{\Gamma_{nm}}{2}\left[2\sigma_{nm}\rho(t)\sigma_{mn} - \{\sigma_{nn}, \rho(t)\}\right] \ , \tag{4.28}$$

where the first term in the right-handed side of the equation is the Liouvillian that describes an unitary evolution and the other term a non-unitary one. This equation can be solved numerically if we consider all non-unitary effects, such as $|\epsilon_2\rangle \to |\epsilon_0\rangle$ and relation events. However, in the system we will study the time scales for these former process are greater than the adiabatic time scale [1, 18]. Also, dephasing do not take a role in this process, since the population is all initially in the second excited state and we see not coherence in the self-discharging process [1, 18]. Hence, for solving the master equation we will consider just the cascade-like process, $|\epsilon_2\rangle \to |\epsilon_1\rangle \to |\epsilon_0\rangle$. Furthermore, since we will evaluate the stored amount of extractable work through the decaying process, we have the instantaneous ergotropy , Eq. (4.11),

$$\mathcal{E}(t) = \begin{cases} \epsilon_1(\rho_1 - \rho_0) + \epsilon_2(\rho_2 - \rho_1) & \text{if } \rho_2 > \rho_1 > \rho_0 \\ (\rho_2 - \rho_1)(\epsilon_2 - \epsilon_1) & \text{if } \rho_2 > \rho_0 \geq \rho_1 \\ \epsilon_2(\rho_2 - \rho_0) & \text{if } \rho_0 > \rho_2 > \rho_1 \\ 0 & \text{if } \rho_0 > \rho_1 > \rho_2 \end{cases} , \tag{4.29}$$

where $\rho_i = \rho_i(t)$ is the population of the state i in time t. Analysing the ergotropy equation, we see that the only relevant terms to calculate in the master equation are the diagonal ones. Considering the collapses operators $|0\rangle\langle 1|$ and $|1\rangle\langle 2|$, after some math, we find the system of coupled differential equations

$$\dot{\rho}_1(t) = -\Gamma_{10}\rho_1(t) + \Gamma_{21}\rho_2(t) \ , \tag{4.30}$$

$$\dot{\rho}_2(t) = -\Gamma_{21}\rho_2(t) \ . \tag{4.31}$$

Using a simple integration we find that $\rho_2(t) = e^{-t\Gamma_{21}}$. The solution of the equation for $\rho_1(t)$ can be approached by considering the homogeneous part, that yields the solution $\rho_1^{\mathrm{h}}(t) = Ae^{-\Gamma_{10}t}$. The form of the solution will be a linear combination of the homogeneous solution and the non-homogeneity

$$\rho_1(t) = Ae^{-t\Gamma_{10}} + Be^{-t\Gamma_{21}} \ , \tag{4.32}$$

but, since we must have the final condition condition $\rho_1(0) = 0$, $A = -B$. For finding A we have to substitute the partial solution, Eq. (4.32) in the differential equation, Eq. (4.30), and apply the initial condition again. This procedure will ensure that we will find the general solution of the problem. Thereafter, the population of each eigenstate, during the self-discharging process, will be described by the functions

$$\begin{aligned} \rho_2(t) &= e^{-t\Gamma_{21}} \\ \rho_1(t) &= \frac{\Gamma_{10}}{\Gamma_{10} - \Gamma_{21}}\left(e^{-t\Gamma_{21}} - e^{-t\Gamma_{10}}\right) \\ \rho_0(t) &= 1 - (\rho_1 + \rho_2) \ . \end{aligned} \tag{4.33}$$

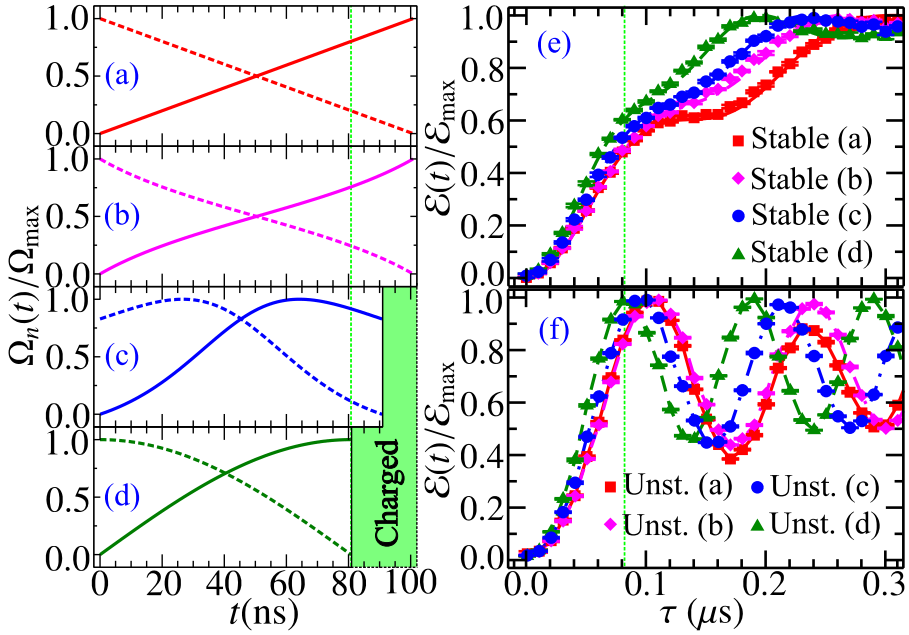

Figure 8 – Interpolation functions, Ω_0 (continuum line) and Ω_1 (dashed line) as a function of the normalized time for (a) a linear ramp, brachistochrone with (b) linear and (c) no constraint, and the brachistochrone with the quadratic constraint (d). (e–f) Experimental result for the ergotropy as a function of the total evolution time τ (as a multiple of $\mathcal{E}_{\max} \approx 51\mu eV$) for (e) stable and (f) unstable charging processes. In the experiment we have set $\Omega_{\max} = 2\pi \times 10$MH. Other parameters: $\Gamma_{10} \approx 51.5$KHz, $\Gamma_{21} \approx 79.7$KHz, $\omega_{0,1} = 2\pi \times 6.26$GHz, and $\omega_{2,1} = 2\pi \times 6.011$GHz. Source: Ref [1].

4.4 The experimental results

In the former section, we talked about the charging process when considering a theoretical scenario where all the interpolation functions have the same initial conditions. In this section, we will describe the physical details of the experiment we reported in Ref. [1] and its results. Further details concerning the experimental setup can be found in [1].

Previously, we simulate the system dynamics considering the same initial conditions for every interpolation function. However, in the experiment we implemented the charging process, the quantities Ω were generated by an arbitrary-wave generator, which had an experimental limitation. The same equipment generates both $\Omega_0(t)$ and $\Omega_1(t)$, and it can only work with a limited instantaneous power, thus the charging process in the experiment had the constraint

$$\Omega_0^2(t) + \Omega_1^2(t) \leq \Omega_{\max}^2 \ . \tag{4.34}$$

This means that we have to change the initial conditions of all functions. It is noteworthy that the brachistochrone with the quadratic constraint uses the full capacity of the arbitrary-wave generator throughout the evolution.

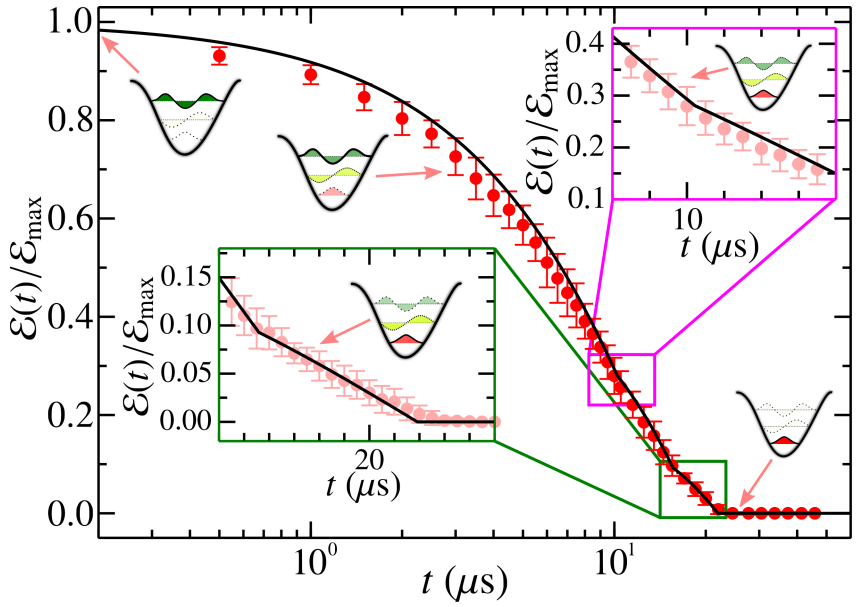

Figure 9 – Instantaneous ergotropy (as a multiple of $\mathcal{E}_{\max}$) in the self-discharging process. The change of population is sketched in each step of the discharging. Inset we highlight the time interval in which the ergotropy changes due to the population inversion, as predicted from Eq. (4.33). The decay rates are $\Gamma_{21} \approx 51.4$KHz and $\Gamma_{32} \approx 79.7$KHz. Source: Ref [1].

In the Figs 8(a)-(d) we have the interpolation function and we see that the initial condition of the non-constrained brachistochrone are smaller than one. Further, in Figs 8(e)-(f) there are the charging process. We note that the experimental results, represented by the circles, are in accordance with the numerical simulations, represented by the lines. In the experiment, the charging process using the brachistochrone with the quadratic constraints is faster, approximately 10%, than the non constrained brachistochrone, followed by the other functions. Physically, we understand this change of performance of the non-constrained brachistochrone as due to the constraint of the experimental apparatus. More specifically, this functions uses more power to adjust itself to the adiabatic condition in a trade off, while the trigonometric functions use less power but they are less fitted to the adiabatic condition. Thus, in the scenario where power is a limited resource, the sine and cosine execute the population inversion faster.

Following to the self-discharge process, the battery is fully charged and then the fields, Ω_0 and Ω_1, are turned off. Then we measure the ergotropy as a function of time, t, as indicated in Fig. 9. The insets highlight the changing of the curve inclination that are consequences of the sum of the exponential decays. This particular characteristic classifies the transmon quantum battery to have a super-capacitive behaviour, which is due to the multi-level nature of the atom and to the asymmetric decaying rates, $\Gamma_{21} \neq \Gamma_{10}$.

4.5 Conclusion of this Chapter

In this Chapter, we presented the joint work with Professor Dapeng Yu's group wherein we fully characterized a three-level superconducting transmon quantum battery. We began by exploring the charging process, performed by coupling the transmon three-level system with external classic fields. Through the charging Hamiltonian, we derive the two different ways to invert the population from the ground state to the second excited one (charging process). We showed that there are the dark and bright charging process and both allows the battery to attain to its maximum charge. From the comparison of the charging protocols, we find out that the dark one is stable, concerning the ergotropy, and it is approximately two times slower than the other charging protocol. The ergotropy injection was enhanced by means of the quantum adiabatic brachistochrone optimization method. In the analysis wherein we setted the same initial values for the fields Ω, the non-constrained brachistochrone was the most efficient, nonetheless due to physical constraints in the experiment, the quadratically constrained brachistochrone was the most efficient in the laboratory. In addition, since our experiment has a good controllability, we can use the unstable population inversion with the quadratically constrained brachistochrone to hasten charging process. We completed the battery characterization when we described its self-discharging process. By solving the master equation with some approximations, we find a effective non-Ohmic discharging, from which we can understand a three-level quantum battery, regarding its loss of energy to the environment, as a supercapacitor.

5 Solving the traveling salesman problem using quantum computing: the quantum annealer

Optimization problems consist in finding the extrema of a function. They can be found in many areas of knowledge, ranging from fundamental physics [104], passing through biology [105], to operations research [106] . For example, all dynamical processes in physics emerge from the extremization of the action functional [64]. Furthermore, logistic problems like inventory organization [107] and the traveling salesman problem [108] also are in the optimization problem category. For doing a complete study of optimization algorithms, we have to take into account the computational complexity theory [69]. A main open problem in this field is to answer if or whether a non-deterministic polynomial-time problem (NP) can be reduced to a polynomial one, which will open paths to new and revolutionary technologies in many fields [109]. Furthermore, there is the class of NP problems that can be formulated as a binary combinatorial problems [45], which are the kind of problem we will work with in this Chapter.

The studies we did in this chapter served as a basis for applications that are currently being developed in our research group, in particular those directly linked to the extension project of our group in partnership with the Center for Advanced Research Wernher von Braun., whose goal is to study quantum computation applied to industrial problems, with a focus on the D-Wave's quantum annealer. In this new field of quantum computing, there are some bias in the actual stage of quantum computation. For instance, algorithms that just solve one part of the problem, but says that it has speedup over the classical computers [110]. Also, in quantum annealing we do not see an improvement in the algorithm complexity. So, for a fair comparison between classical and quantum paradigms of computation, it is necessary to evaluate as many aspects as possible of the algorithms.

This Chapter is based on a paper that we publish on the *Revista Brasileira de ensino de Física* [53] and in a preprint [54]. This part of this Thesis is organized as following: We start by giving an introduction to the D-Wave's quantum processor, giving some details and references concerning its experimental aspects. Then, we define the kind of problem that the D-Wave's quantum processor can solve, which are Ising-like problems. Further, we formulate an optimization problem in a spin Hamiltonian and we give the path (and the codes [111]) to solve it using the Amazon Braket platform [112]. Additionally, we describe the simulated annealing meta-heuristic [113, 114], a classical analog of quantum annealing. This technique is a good strategy to validate the quantum solutions, since it has a well

defined physical behavior and its physical interpretation is based on fluctuations, as the quantum annealing.

5.1 Quantum annealing and the D-Wave Co.

Adiabatic quantum computing is Turing complete paradigm [115], however, as we mentioned in the Chapter 3, it has some experimental limitations such as the demand for system with quasi-infinite dimensions. On the other hand, quantum annealing [116] can be understood as a NISQ [9] version of the adiabatic quantum computing, since it works with Hamiltonian with low dimension connections and there is the presence of noise. This technique was first proposed as a meta-heuristic algorithm that makes use of classical simulation of quantum systems to solve combinatory optimization problems [117, 118], but due the intrinsic difficulty to simulate quantum systems, this class of algorithm has limitations in classical computers. However, the D-Wave company developed a quantum annealing experiment in which one implements a dynamical transverse Ising field [119–121] that can be used to solve binary combinatory optimization problems. The D-Wave's qubits are build using compound-compound Josephson-junction radio frequency superconducting quantum interferences devices (CCJJ rf-SQUIDs), that are micro superconducting circuits that work in the radio-frequency regime and these qubits are connected by other superconducting devices [120, 122]. Due to engineering limitations, it is not possible to build a full connected network of qubits, but we have topologies as Fig. 10 shows. Particularly, it is a problem when we try to solve realistic problems in this processor, because they demand a system wherein every qubit is connected to everyone. To surpass this problem, it is possible to perform a technique called minor embedding [123] that takes a full connected graph and embed it on another graph that does not have all connections. This procedure it-self is NP, but the there are heuristics that find approximate solutions for it. A full connected graph with N vertices will be embedded in another graph with at maximum N^2 connections. Also, the embedding process increases the annealing time by polynomial factors [124]. In spite of these drawbacks, it is possible to solve problems in this computer as the references show [48, 49, 125, 126]. Additionally, we find realistic speedups over classical algorithms [46, 83]. Furthermore, there are other advantages such as the generation of pure random numbers [127] and energy saving [128]. One can access the D-Wave computer using the Amazon Braket platform [112] and the Leap [129], by D-Wave itself.

Speaking about mathematical details, the Hamiltonian that is implemented by the D-Wave reads

$$H(s) = A(s)\sum_i \sigma_i^x + B(s)\left(\sum_{i,j} J_{ij}\sigma_i^z\sigma_j^z + \sum_i h_i\sigma_i^z\right), \tag{5.1}$$

where σ_i^α are the Pauli matrices $\alpha = x, y, z$ for the i-th site, J_{ij} is the coupling between the spin i and j, and h_i is a local field applied to the spin in the i-th site. $A(s)$ and $B(s)$

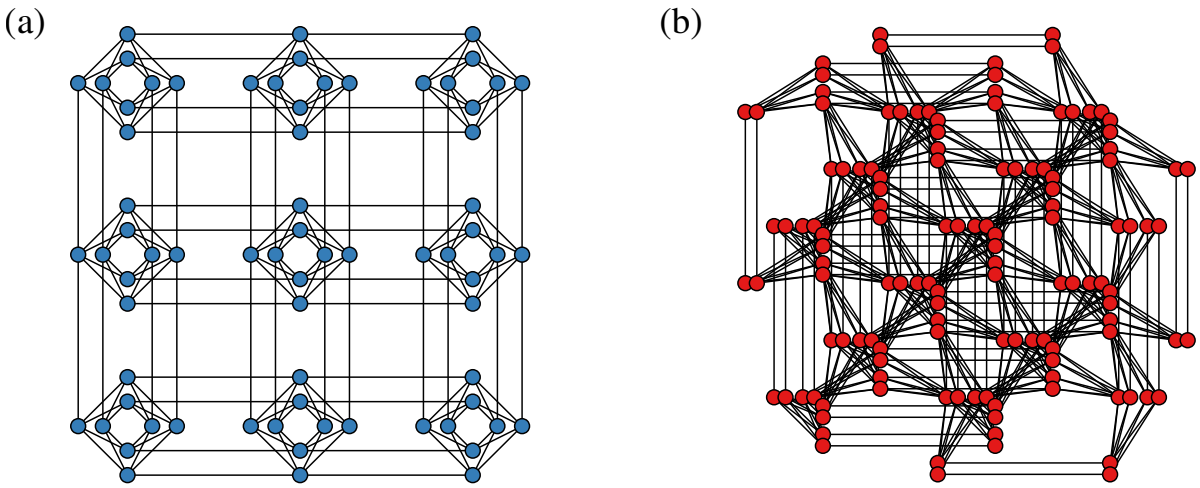

Figure 10 – (a) Topology of the D-Wave's quantum processor *2000Q*, that has 2048 q-bits connected 6 to 6 by the Chimera topology. In (b) we have the D-Wave's next generation, the Advantage processor, that has over 5000 qubits connected 15 to 15 by the topology *Pegasus*. Source: [53]

are the interpolation function, that obey the boundary conditions $A(0) \propto B(1) \neq 0$ and $A(1) = B(0) = 0$, and s is the normalized time. Experimentally, the function $A(s)$ is generated by a magnetic field in the x-direction that fades with time, while $B(s)$ is a global increasing in the coupling J_{ij}. This Hamiltonian is a Ising-like Hamiltonian, or a quadratic unconstrained binary optimization (QUBO) problem if we replace σ^z to $x_i = (1 - \sigma_i^z)/2$, which has binaries eigenvalues, zero or one.

5.1.1 The Traveling Salesman Problem

In this subsection, we will study how one can formulate a optimization problem as a Ising or a QUBO problem, and we will use the NP-hard traveling salesman problem as an example [130]. We used the Ref. [45] for this study, which describes in details how one can formulate some NP-hard and NP-complete problems, including the Karp's 21 NP-complete problems.

Let us first define the traveling salesman problem (TSP). *For a given set of cities and the distance between them, what is the shortest route that a traveling salesperson visits every city just once and return to the initial city?*

Using a classical computer, it is possible to solve the TSP using exact and approximated methods. An efficient approach for exact solution, in relation to the naive solution, is a dynamical programming algorithm [131] that reduces the time complexity from O($N!$) to $N^2 2^N$ and the memory usage to $N2^N$, where N is the number of cities. Using this algorithm, researchers found the optimal solution of instance with 85900 cities [132], using a supercomputer, which toked 139 CPU-years[1]. The approximated algorithms can find

[1] One CPU second is the time to execute one million of floating points operations

solutions with 5% of error for problems with 3×10^6 cities in few hours of CPU time [133]. In the quantum domain, we have some algorithms, for example there is one that has a quadratic speedup over classical dynamical programming, if the graph is sparse [134].

For formulating this problem as a QUBO one [126] we can define the binary variable $x_{i,l}$, which assumes 1 when the salesman is in the city i in the time instant l, and 0 otherwise. Thus, the problem Hamiltonian reads

$$H_{\text{Ising}} = \sum_{i,j \in E} J_{ij} \sum_{l}^{N} x_{i,l} x_{j,l+1} \ , \tag{5.2}$$

where J_{ij} is the distance between city i and city j and E is the set of the connections between the cities. This formulation demands N spins for the cities and N spins for the time instants, thereby requiring N^2 spins in total. We note that $J_{ij} \geq 0, \ \forall \{i,j\} \in E$, then ground state of H_{Ising} is when all the spins are zero, considering the spins collapsed in classical states, which is wrong according to the TSP conditions. For adding the restrictions of the TSP, we need to use Hamiltonians that introduce energy penalties for these solutions. Thus, we have

$$\begin{aligned} H_{\text{penal}} = \lambda \Bigg[& \sum_{l=1}^{N} \left(1 - \sum_{i=1}^{N} x_{i,l} \right)^2 + \sum_{i=1}^{N} \left(1 - \sum_{l=1}^{N} x_{i,l} \right)^2 \\ & + \sum_{(i,j) \notin E} \sum_{l=1}^{N} x_{i,l} x_{j,l+1} \Bigg] \ , \end{aligned} \tag{5.3}$$

where the first term in the right-hand side of the equation increases the energy of solutions in which the salesperson is in more than one city at same time (or in none), the second one increases the energy for trips wherein the agent remains in the same city or never passes there, and the last one raise the energy of trajectories that passes through connections that does not exist. Also, λ, called Lagrange parameter, will give the scale of $\hat{H}_{\text{penal}}$. We note that if λ is too big, the ground state of H_{penal} will be the actual solution of the annealing. Actually, finding a good λ is another problem and it can be approached using classical methods like the one presented in Ref. [46]. Then, the total Hamiltonian for the Traveling salesman problem as a QUBO of Ising is

$$\hat{H}(s) = A(s) \sum_{i,l} x_{i,l} + B(s) \left(\hat{H}_{\text{ising}} + \hat{H}_{\text{penal}} \right) \ . \tag{5.4}$$

Since this problem itself requires N^2 qubits and more, at most, N^2 qubits for the embedding, it is not possible to solve a problem with more than 10 cities on the D-Wave advantage. However, it is possible to develop a heuristic strategy based on the divide and conquer technique, which divides the TSP into smaller TSP instances, solves the smaller problems and then connects the solution as they were cities [126, 135].

We solved a traveling salesman problem, with six randomly distributed cities as Fig. 11 shows. The codes we used can be found in the online repository [111]. In this

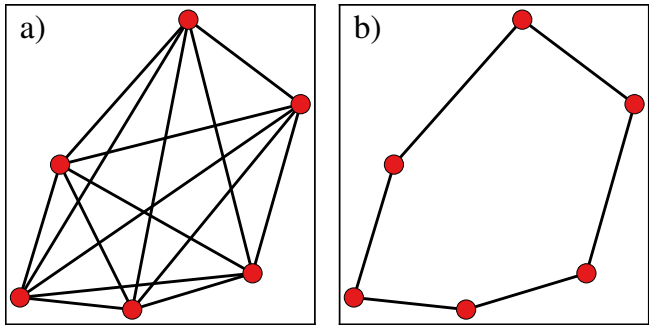

Figure 11 – Six cities distributed randomly in the space. (a) shows the nodes with all possible connections and (b) shows the solution yielded by the D-Wave, which is the optimum solution. Source: [53]

task, we execute the algorithm 500 times, with annealing time of 20 microseconds. The Lagrange factor, λ was chosen based on the average value of tour length [136], given by the equation

$$\lambda_0 = \frac{N \sum J_{ij}}{N_c}, \tag{5.5}$$

where N_c is the number of connections in the problem. This equation does not yield the best λ, but the company recommends to use a λ in the set $\{0.75\lambda_0, 1.5\lambda_0\}$. In our problem, the solution was found using $\lambda = 1.05$.

5.2 Simulated annealing

In the past section, we studied the D-Wave systems and how to formulate problems to solve on it. However, this quantum processor does not guarantee that the solution is the optimum one, since it is a NISQ device [9]. Also, dynamical programming algorithms do not allow to solve problems with many items, due to the exponential scaling times.

There are many strategies for approximately find 'good' solutions for binary combinatory problems, for instance we have genetic algorithms [137], greed algorithms [138], and methods of cross-entropy [139]. Also, there is the simulated annealing meta-heuristic [54, 140, 141] that can be understood as a classical analog of the quantum annealing, since it uses thermal fluctuations and a cooling process to drive an objective function to its lowest energy configuration. It can handle with the scale of problems that the D-Wave solves [142], also it compose more sophisticate algorithms [143]. Due to these properties, we will use the classical solutions of the simulated annealing algorithm as a comparison for the quantum solutions of the D-Wave quantum annealing.

In this section, we will formalize this technique using non-equilibrium stochastic processes and markov chains to prove its convergence to the optimal solution [140, 144, 145]. Also, we will apply it for a TSP to verify its performance and precision.

5.2.1 Markov chains

A stochastic process is defined as a set of random variables, $\{x_t,\, t \in T = \mathbb{R}^*\}$, that evolve with time. When the variables are discrete, $\{x(t_i) = n_i,\ i \in \{1, 2, \cdots, l\}\}$, the stochastic process is defined by the joint probability distribution

$$p_l\left(n_1, n_2, \cdots, n_l\right) \ , \tag{5.6}$$

where l is the number of time intervals. The conditional distribution,

$$p_l\left(n_l | n_1, n_2, \cdots, n_{l-1}\right), \tag{5.7}$$

gives the probability of x assume the value n_l given that it assumed the sequence of events $n_0, n_1, \cdots, n_{l-1}$. A Markovian process is defined by the property

$$p_l\left(n_l | n_1, n_2, \cdots, n_{l-1}\right) = p_l\left(n_l | n_{l-1}\right) \ , \tag{5.8}$$

which says that the probability of the next event depends on the present one only, and we can understand $p_l(n_l|n_{l-1})$ as the transition probability from the state n_{l-1} to the state n_l. Using Eq. (5.8) we write

$$p_l(n_l) = \sum_{n_{l-1}} p_l\left(n_l | n_{l-1}\right) p_{l-1}\left(n_{l-1}\right) \ . \tag{5.9}$$

In terms of matrices, the former equation reduces to

$$|P_l\rangle = T\,|P_{l-1}\rangle \ , \tag{5.10}$$

for $T(m, n)$ being the transition probabilities $p(m|n)$ and $|P_l\rangle$ is a column vector where the element p_i gives the probability of the event i in time l. More specifically, T is stochastic matrix that has the properties

$$\begin{aligned} &(1)\ T(n, m) \geq 0,\ \forall\ m, n \in \mathcal{E}\ , \\ &(2)\ \sum_n T(n, m) = 1\ , \end{aligned} \tag{5.11}$$

which are the axiomatic conditions for probabilities and $\mathcal{E}$ is the set of states in the system. Using the properties of T and the Perron-Frobenius theorem [146] we have

$$|P\rangle = \hat{T}\,|P\rangle\,, \tag{5.12}$$

where $|P\rangle$ is the stationary probability vector of the system, which satisfy the equation

$$\begin{aligned} p(n) &= \sum_m T(n, m) p(m) \\ \therefore \quad &\sum_m \{T(n, m)p(m) - T(m, n)p(n)\} = 0, \end{aligned} \tag{5.13}$$

since $\sum_m T(m,n) = 1$. Therefore, we say that $|P\rangle$ satisfy the detailed balance principle [147, 148],

$$T(n,m)p(m) - T(m,n)p(n) = 0 \ . \tag{5.14}$$

Yet, we described an arbitrary stochastic process, now we will connect it to thermodynamics.

Let us consider Eq. (5.10) with Eq. (5.14)

$$\begin{aligned} p_{l+1}(n) &= \sum_m T(m,n)\frac{p(n)}{p(m)}p_l(m), \\ \frac{p_{l+1}(n)}{p(n)} &= \sum_m T(m,n)\frac{p_l(m)}{p(m)}. \end{aligned} \tag{5.15}$$

Furthermore, a convex function $f(x)$ has the property

$$f\left(\sum_{m=0} x_m p_m\right) \leq \sum_{m=0}^{N} p_m f_m(x_m) \ , \tag{5.16}$$

where p_m is a probability. Thus, if $p_m = T(m,n)$ and $x_m = p_l(m)/p(m)$, we get

$$f\left(\frac{p_{l+1}(n)}{p(n)}\right) \leq \sum_m T(m,n) f\left(\frac{p_l(m)}{p(m)}\right) \ . \tag{5.17}$$

Finally, multiplying it by $p(n)$ and summing in n, we find

$$\begin{aligned} \sum_n p(n) f\left(\frac{p_{l+1}(n)}{p(n)}\right) &\leq \sum_n \sum_m p(n)T(m,n) f\left(\frac{p_l(m)}{p(m)}\right) \\ &= \sum_m f\left(\frac{p_l(m)}{p(m)}\right) \sum_n p(n)T(m,n) \\ &= \sum_m p(m) f\left(\frac{p_l(m)}{p(m)}\right). \end{aligned} \tag{5.18}$$

Finally, if $f(x) = x\ln x$, then

$$\begin{aligned} \sum_n p_{l+1}(n) \ln \frac{p_{l+1}(n)}{p(n)} &\leq \sum_m p_l(m) \ln \frac{p_l(m)}{p(m)} \\ \therefore \quad S_{l+1} &\geq S_l, \end{aligned} \tag{5.19}$$

where $S_l = -k\sum_n p_l(n)\ln p_l(n) + C$ is the Shannon entropy, for k and C constants. We note that when the system reaches the stationary regime, $S_{l+1} = S_l$, we say that the system is thermalized. Also, this equation says that a Markovian process drives the system to the configuration of maximum entropy, and thus to the thermal equilibrium, as the second law of thermodynamics dictates. It is also indicates the proof of convergence of the Metropolis algorithm [149], which is an intermediate part of the simulated annealing. Although this equations proves the convergence of a Markovian process, it gives no information about how far the system is from the equilibrium, which is a characteristic of heuristic algorithms.

5.2.2 The algorithm

Monte Carlo methods are a set of computational techniques that make use of probabilistic simulations to solve numeric problems [150]. Particularly, simulated annealing algorithms are efficient because they use a Monte Carlo strategy over the possible states of a system to calculate expected values of thermodynamic systems, therefore increasing the possibility to reach the maximum entropy level of our system.

For concluding our algorithm formulation, we need to find a rule for sampling and for generating the stochastic process. Let us consider the probability

$$p(s) = \frac{1}{Z} e^{-\beta H(s)}, \tag{5.20}$$

where $H(s)$ is the energy of the of system for the configuration s, $Z = \sum_s e^{-\beta H(s)}$ is the partition function and $\beta = 1/T$ is the inverse temperature in natural unities (Boltzmann constant equal to one). Now, using Eq. (5.20), as we find in statistical mechanics [151], in Eq. (5.10) we find T solving the equation

$$T(s, s') = e^{-\beta(H(s) - H(s'))} \ . \tag{5.21}$$

Nonetheless, if $H(s') > H(s)$, the transition probability is greater than one. One can define the *ad hoc* strategy and redefine T as

$$T(s, s') \equiv \begin{cases} \frac{1}{Z} e^{-\beta[H(s) - H(s')]}, \text{ for } H(s) > H(s') \ , \\ \frac{1}{Z} \text{ otherwise} \ . \end{cases} \tag{5.22}$$

We note that T as defined in Eq. (5.22) obeys the properties defined in Eq. (5.14).

The parameter β will impose an energy scale to the system, which physically dictates the range of the transitions between the system states. Thus, if β is big, the fluctuations are small and the probability to long walks through the system configurational space is low, and if β is small all the states are equally likely to be accessed. The Fig. 12 illustrates the configurational space, in which we see that the system configuration jumps through the states and, if the thermal fluctuations are small, it shall not pass the energy barriers.

This strategy has some problems that will give to it the heuristic characteristic. Firstly, it is not possible to continuously and smoothly drive the system to absolute zero and we have to consider that during the cooling process the system can be arrested in a local minimum. However, it is possible to perform the cooling process *slowly enough* to reach sufficiently lower temperatures, thus the system will have a chance to be in its thermal equilibrium. Also, we must lower the temperature of the system only when it has thermalized, but during the execution of the algorithm there is no way to know when this condition is reached. So, we have to do it approximately.

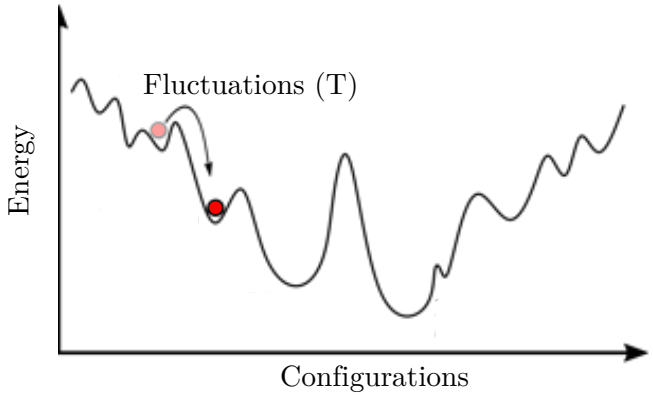

Figure 12 – A scheme to represent the simulated annealing algorithm. The horizontal axis represents the 'configurations' of the system and the vertical one represents the correspondent energies. The red circle is the configuration of the system in time t and the blurred circle is the previously configuration of the system. The arrow connecting the circles represents the thermal fluctuation that moves the system from the configuration to configuration. Source: [54].

We defined and gave arguments about all parts of the simulated annealing. Now, let us summarize the algorithm for a Ising-like Hamiltonian,

$$H = \sum_i h_i x_i + \sum_{<i,j>} J_{ij} x_i x_j \ , \tag{5.23}$$

where x_i is a binary variable, h_i is an anisotropy in the site i and J_{ij} is the coupling between the sites i and j. In the simulated annealing, the fluctuations change the value of x_i from 0 to 1 or vice versa, as Eq. (5.22) says. Thus, the algorithm follows the steps:

1. Define an initial state randomly, s, and a initial temperature T_0;
2. Chose a site randomly and change the value of x_i, thus finding a new state s';
3. If $H(s') < H(s)$: accept the new state;
4. Else: sample a random number, η, between 0 and 1.
   - If $\eta < T(s', s)$ accept the state s',
   - otherwise, keep the state s;
5. For n_i steps given, decrease the temperature, $T_{i+1} = \tau T_i$, for τ being the cooling coefficient and $\tau \in \{0 < y < 1,\ y \in \mathrm{R}\}$;
6. Set a stopping condition, for instance the total number of steps N_t.

5.3 Simulations and results

To analyse the performance of the simulated annealing we will use the traveling salesman problem, as we did for the quantum annealing. First, we have to study the

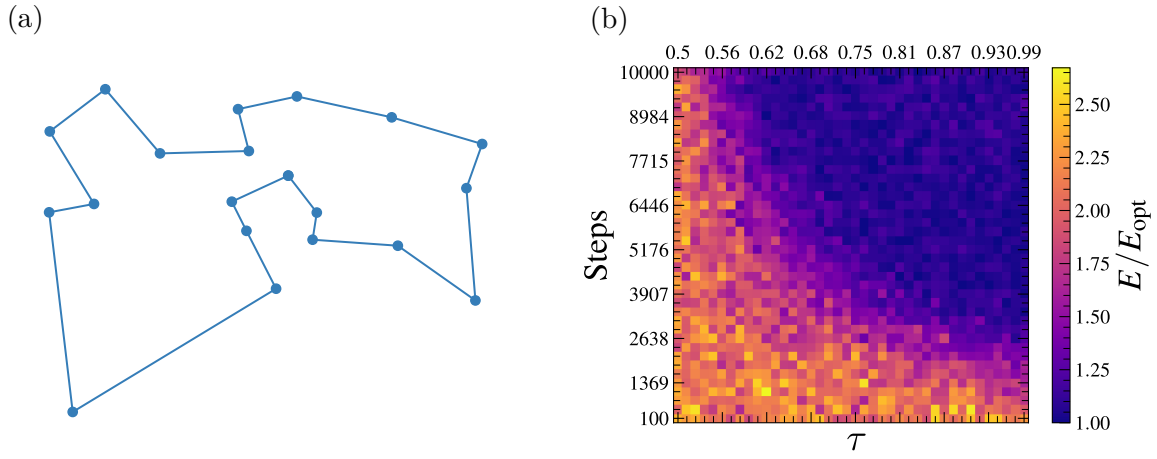

Figure 13 – (a) 20 cities distributed in a 1×1 square and the optimal solution that we found using a dynamical programming algorithm. (b) Heat map of the normalized solution by the optimal one in function of τ and n_t. Parameters used: $T_0 = 1$ and $N_t = 10^5$.

parameters for finding a guideline for the algorithm. We note that the algorithm, as we defined in this dissertation, asks for five parameters: the initial configuration (S_0), initial temperature (T_0), cooling ratio (τ), iterations in the same temperature (n_i), and total number of iterations (N_t). The initial configuration can be any and it is not a good option using a faster optimization algorithm, for example the greedy algorithm, to find a 'good' first guess since it can be in a local minimum. Also, in high temperature this guess will be lost since the states are effectively equiprobables. Thus we can use a random initial configuration. The initial temperature can be chosen based on the scale of the system energy, which can be evaluated by finding the average trajectory length using Eq. (5.5). Further, the cooling coefficient τ is the percentage of temperature decreasing. The interactions with the same temperature is the number of markovian iterations in the same temperature that will lead the system to the thermal equilibrium and the total number of iterations is the total number of steps of the optimization process.

We note that finding the best set of parameters for one instance of the travelling salesman problem will be a computational expensive task. However, we can fix some parameters and work with some others. The Fig. 13(a) shows the best route of a 20 cities traveling salesman problem and Fig 13(b) shows a heat map where we fixed the all the parameters, but τ and n_t. This fist analysis shows that there are a good region of parameters that yielded the optimal solution and, in the right bottom region we see that using $\tau \approx 1$ we can reduce the number of steps given by the algorithm, therefore decreasing the execution time. To test this method in a more realistic scenario, concerning the number of cities, we can place the cities in a regular square grid.

Fig. 14(a) shows the optimal tour that we get from Ref. [152] and, Fig. 14(b) shows the result of a simulated annealing algorithm. The approximated solution we get

(a) Optimal tour: Distance = 10 (b) SA tour: Distance = 10.43

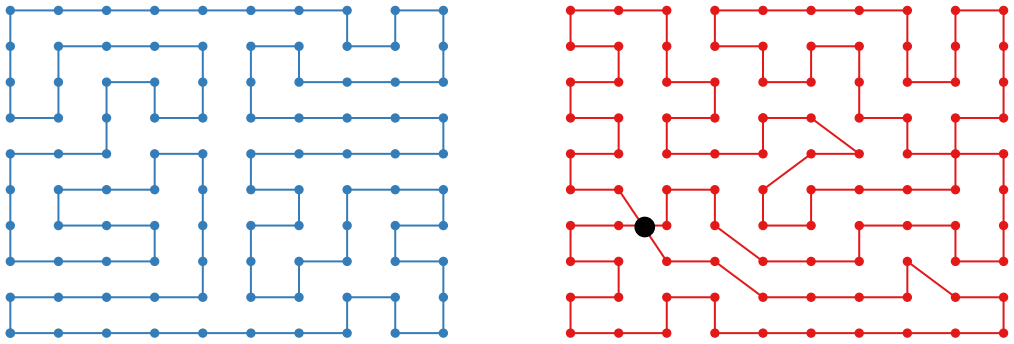

Figure 14 – Two solutions of a instance of the traveling salesman problem with the cities regularly setted in a grid. (a) the optimal solution and (b) the approximated solution from the simulated annealing algorithm. The black circle in Fig (b) highlights a crossing in the tour, which indicates that the solution is not the optimal one. Parameters used: $T_0 = 1$, $\tau = 0.995$, $N_t = 10^6$, and $n_i = 500$.

is nearly four percent longer than the optimal tour. We call attention for the detail that the simulated annealing took the order of 10^6 iterations, while the optimal solution via dynamical programming would take 10^{32} iterations. We observe that the simulated annealing algorithm can found theses suboptimal tours with less resources since they are more abundant and, for finding the optimal solution the number of interaction will also increase exponentially.

Concerning the D-Wave quantum computer, the state-of-the-art processor, the Advantage can only support instances of the travelling salesman problem with 12 cities and it can solve find satisfactory solutions with 9 cities.

5.4 Conclusion of the Chapter

In this Chapter, we reviewed the D-wave's new quantum technology for solving binary combinatory optimization problems that is already working and have been showing a fast development. Although there is no evidence of quantum speedup over the classical solver, it has been paving the way to adiabatic quantum computing technologies. Also, it demands less resources than the classical supercomputers, and it is instigating the research for new physics, as superconducting atoms and cryogenics. Here we showed how to use the D-Wave supercomputer, we gave details and references of its engineering and we presented an efficient heuristic method for making a comparison between quantum and classical solutions.

Concerning this part of this thesis, we published an educational paper in the *Revista Brasileira de Ensino de Física* [53] and we are preparing another manuscript to the same journal about the simulated annealing [54].

6 Bright and Dark States of Light: The Quantum Origin of Classical Interference

The former Chapters are correlated to optimization and adiabatic evolutions, thus they share the same mathematical tools and physics background. However, this Chapter of this thesis concerns a study on the relation between quantum and classical interference of light. As a results of this project, we posted on ArXiv a theoretical paper wherein we show that classical interference of light emerges due to a collective phenomena of light modes interacting with an atom. Therefore, in the following, we will integrally reproduce our paper [52].

6.1 Introduction

Interference phenomena are fundamental to understanding how electromagnetic waves combine in our environment to eventually interact with matter. If one considers two electromagnetic waves with the same polarization, with complex electric fields E_1 and $e^{i\delta\phi}E_1$ at the position of an atom with an electric dipole moment, the resulting total field reads $(1 + e^{i\delta\phi})E_1$. Consequently, interference is said to be constructive for in-phase fields and destructive for out-of-phase fields (see Fig. 15(a)). This reflects the importance of the relative phase of the electric field $\delta\phi$ for the atom-light coupling, since the atom can experience an amplified, or diminished, total field due to this interference pattern.

The advent of quantum optics brought new fundamental insights on how light interacts with matter. According to this theory, the picture of a dipole moment generated by an average electric field $\langle E\rangle$ is incomplete, when not completely wrong. Indeed, even when one considers a single light mode coupled to the particle, a Fock state $|N\rangle$ yields $\langle E\rangle = 0$ for any number of photons N, but it does generate non-trivial light-atom dynamics. The most accepted solution to this conundrum comes from the work developed by Glauber in the Ref. [153], which gave the mathematical framework to determine the probability of existing light and matter interaction. However, the physical interpretation supported by quantum optics textbooks [51, 154–156], argues that Fock states possess an electric field variance $\langle \delta E^2\rangle = \langle E^2\rangle - \langle E\rangle^2 \propto 2N + 1$, which is nonzero, even for the vacuum state ($N = 0$). This sounds reasonable since, as any observable in quantum mechanics, the electric field is fully described only when considering all of its moments $\langle E^n\rangle$. Classical optics addresses the lowest moment ($n = 1$), with all higher moments which are intrinsically given by $\langle E^n\rangle = \langle E\rangle^n$. Quantum-mechanically, this corresponds to a coherent state in the limit of large photon numbers [157].

In this context, the concept of interference which describes the summation of fields in classical optics has little relevance; if classical optics fails to describe the coupling of a particle to a single-mode Fock state, how could it properly describe the combination of several such modes? This highlights an important gap in the classical understanding for the summation of fields, and their joint interaction with matter. While the concept of interference presents a rather intuitive picture in the classical world, no clear equivalent exists to describe the summation of quantum fields.

In this work, we bridge this gap by showing that a decomposition of the total state of the radiation field on a collective Dicke-like bosonic basis offers a natural interpretation of constructive and destructive interferences, in terms of bright (or superradiant) and dark (or subradiant) states. Using this framework, we prove that quantum fluctuations are not the key ingredient to explain the light-atom coupling. The necessary and sufficient condition instead is the existence of at least one finite projection on a non-dark state. Such a criterion justifies why even a single Fock state couples to an atom without invoking quantum fluctuations. Furthermore, the collective basis for bosonic modes predicts a vast class of entangled states which couple to the atom with intermediate superradiant transition rates, with no counterpart in classical theory.

The manuscript is organized as follows: In Sec. 6.2, we introduce the collective basis, with a particular attention to perfectly dark and maximally superradiant states. In Sec. 6.3, we discuss how these states relate to destructive and constructive interference in classical theory. We also discuss why classical interference is unable to properly describe the excitation of an atom, whereas our approach provides a natural explanation. In Sec. 6.4, we revisit the double-slit experiment using the collective basis. Then, in Sec. 6.5, we discuss the different interference patterns obtained in a Mach-Zehnder interferometer when employing quantum and classical fields, interpreting the results in terms of collective states. In Sec. 6.6, we extend our formalism to M modes and, in Sec. 6.7, we discuss how our predictions could be observed using trapped ions or cavity QED setups. Application of dark and bright states in quantum information processing is presented in Sec. 6.8. The conclusions and perspectives are presented in Sec. 6.9, and a detailed derivation of the analytical expressions presented in the main text can be found in the Appendices.

6.2 Two-mode collective basis

Let us consider two light modes A and B, with annihilation (creation) operators a ($a^\dagger$) and b ($b^\dagger$), coupled resonantly to a two-level atom. The raising (lowering) atomic operator σ^+ (σ^-) realizes transitions between ground $|g\rangle$ and excited $|e\rangle$ states, and the coupling constant g is assumed identical for both modes, for simplicity. Such an atom-modes

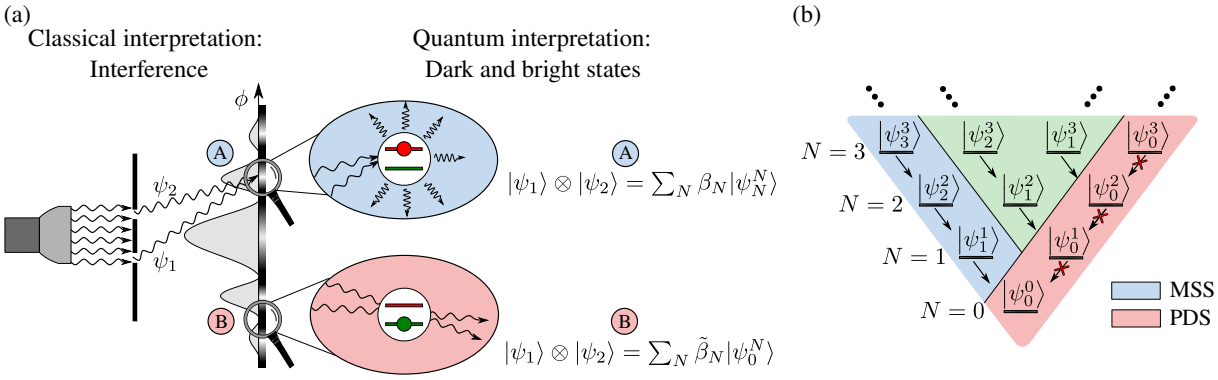

Figure 15 – (a) Double slit experiment: Two waves $\psi_1(\phi_1 = kr_1)$ and $\psi_2(\phi_2 = kr_2)$ meet to form fringes which can be interpreted in terms of interference in the classical theory, and of dark and bright states in our approach. (b) Dicke-like ladder for two light modes with the left side containing the maximally superradiant states (MSS, in blue), and the right one with the perfectly dark states (PDS, in red). Differently from the atomic case, the number of excitations is not bounded ($N \to \infty$).

system is described by the following Hamiltonian in the interaction picture:

$$H = g(a + b)\sigma^+ + g(a^\dagger + b^\dagger)\sigma^-. \tag{6.1}$$

The dimensionless total electric field operator at the atom position is given by the superposition of the two fields:

$$E = (a + b) + \left(a^\dagger + b^\dagger\right). \tag{6.2}$$

The atom acts as a probe for the field resulting from the combination of the fields at its position. Yet, as we shall see later, the particle may not be excited even by a nontrivial field, in which case other ways are required to detect the state of the fields (see Sec. 6.7). From a classical point of view, all operators in (6.2) must be replaced by complex amplitudes, and the atom is not excited only if the total electric field is zero. Quantum mechanically, as discussed in the introduction, the atom can be excited by light modes with zero electric field expectation value (such as Fock states), a phenomenon attributed to the quantum fluctuations of the field. Yet, it turns out that there exist two-mode fields with nonzero quantum fluctuations, other than the vacuum, which do not excite the atom. Hence, quantum fluctuations cannot be the only explanation of why the emitter is excited by a superposition of light modes

Let us illustrate the apparent inconsistency between the coupling of combined fields with matter in the classical and quantum pictures. To this end we first consider the coherent states $|\alpha\rangle$ and $|-\alpha\rangle$ in the modes A and B. Using the eigenvalue relations $a\,|\alpha, -\alpha\rangle = \alpha\,|\alpha, -\alpha\rangle$ and $b\,|\alpha, -\alpha\rangle = -\alpha\,|\alpha, -\alpha\rangle$, we obtain

$$H\,|\alpha, -\alpha\rangle\,|g\rangle = g\,(\alpha - \alpha)\,|\alpha, -\alpha\rangle\,|e\rangle = 0, \tag{6.3}$$

making clear that the state $|\alpha, -\alpha\rangle$ is unable to excite the atom[1]. This can be explained invoking classical interference, since the sum of the nonzero expectation values of the electric field from each mode actually cancels out:

$$\begin{aligned}\langle E\rangle &= \langle a + a^\dagger\rangle + \langle b + b^\dagger\rangle, \\ &= (\alpha + \alpha^*) + (-\alpha - \alpha^*) = 0.\end{aligned} \tag{6.4}$$

However, such an explanation fails for the state

$$|\Upsilon\rangle = \frac{1}{2}\left(|0\rangle + |1\rangle\right)_A \left(|0\rangle - |1\rangle\right)_B, \tag{6.5}$$

which also has a zero total electric field expectation value, but survives the action of the Hamiltonian: $H|\Upsilon\rangle|g\rangle \neq 0$. Therefore, the atom-field coupling does not cancel for state $|\Upsilon\rangle$.

As pointed out in the introduction, quantum fluctuations would be the next natural candidate to explain why two different states with $\langle E\rangle = 0$ affect the atom in such disparate ways. However, the scenario becomes even more puzzling when we compute the variance of E for the states $|\alpha, -\alpha\rangle$ and $|\Upsilon\rangle$: it gives $\langle \Delta E^2\rangle = 2$ for both cases, which is the same as the two-mode vacuum state. Therefore, the two states here presented with $\langle E\rangle = 0$ exhibit nonzero quantum fluctuation, yet only $|\Upsilon\rangle$ is able to excite the atom. These simple examples naturally lead us to the following question: Why do some states of the radiation field couple to matter, and others do not? If the explanation is not the average field and fluctuations, then what is the proper criterion for such a coupling to occur?

To address this question, we introduce the following set of two-mode N-photon states:

$$\left|\psi_n^N\right\rangle = \sum_{m=0}^{N} C_{m,n}^N \left|m, N-m\right\rangle, \tag{6.6}$$

where $|n_A, n_B\rangle$ refers to the product Fock state with n_A photons in mode A and n_B in mode B. The coefficients $C_{m,n}^N$ of these collective states are given by (see Appendix F.1)

$$\begin{aligned}C_{m,n}^N &= \sqrt{\frac{n!(N-n)!}{2^N}} \\ &\times \sum_{q=q_{\min}}^{q_{\max}} \frac{(-1)^{m-q}\sqrt{m!\,(N-m)!}}{q!(n-q)!\,(m-q)!(N-n-m+q)!},\end{aligned} \tag{6.7}$$

with $q_{\min} = \max(0, n+m-N)$ and $q_{\max} = \min(m, n)$. States (6.6) are derived from the symmetric $(a+b)/\sqrt{2}$ and antisymmetric $(-a+b)/\sqrt{2}$ collective operators [158, 159], and constitute a complete basis which satisfies the following coupling relation:

$$H\left|\psi_n^N\right\rangle|g\rangle = g\sqrt{2n}\left|\psi_{n-1}^{N-1}\right\rangle|e\rangle. \tag{6.8}$$

[1] We note that this condition we use $H|\psi\rangle = 0$ for the absence of light-matter interaction is equivalent to what is defined in the Ref. [153].

The physical process described by (6.8) corresponds to the excitation of the atom through the transition from state $\left|\psi_n^N\right\rangle$ to $\left|\psi_{n-1}^{N-1}\right\rangle$, see Fig. 15(b).

The collective basis (6.6) presents a strong analogy to the N-excitation Dicke basis for multi-atom systems [160, 161]. In analogy to the "cooperation number" for Dicke states, the $\sqrt{2n}$ factor represents the cooperativity of the emission, where the $\sqrt{2}$ factor comes from the fact that there are two modes interacting with the atom. In particular, the $n = 0$ case corresponds to the perfectly dark state (PDS) for the subspace of N photons

$$\left|\Psi_0^N\right\rangle = \sqrt{\frac{N!}{2^N}} \sum_{m=0}^{N} \frac{(-1)^m}{\sqrt{m!\,(N-m)!}} \left|m, N-m\right\rangle, \tag{6.9}$$

which does not couple to the atom. It was coined subradiant by Dicke since $H\left|\psi_0^N\right\rangle|g\rangle = 0$. Oppositely, the $n = N$ state

$$\left|\Psi_N^N\right\rangle = \sqrt{\frac{N!}{2^N}} \sum_{m=0}^{N} \frac{1}{\sqrt{m!\,(N-m)!}} \left|m, N-m\right\rangle \tag{6.10}$$

presents a transition rate $g\sqrt{2N}$, which is $\sqrt{2}$ times that of the single-mode result: $H_{JC}\left|g\right\rangle\left|N\right\rangle = g\sqrt{N}\left|e\right\rangle\left|N-1\right\rangle$ [162], with H_{JC} the Jaynes-Cummings Hamiltonian. State (6.10) is the analogue of the symmetric superradiant mode, studied by Dicke in the decay cascade [160, 163], and represents the most superradiant of the states with N photons. We here refer to this state as the maximally superradiant state (MSS). Finally, states within the range $0 < n < N$ present intermediate transition rates. As opposed to the two-level atom case, the present Hilbert space is unbounded, even for a finite number of field modes, since each one can support an arbitrary number of photons [161], see Fig.15(b).

6.3 Connection with classical interference

Let us now discuss how this basis articulates with the concept of interference, starting with two-mode coherent states. When considering in-phase coherent states, one obtains a state that decomposes exclusively on the MSS subspace:

$$\left|\alpha, \alpha\right\rangle = e^{-|\alpha|^2} \sum_{N=0}^{\infty} \sqrt{\frac{2^N}{N!}} \alpha^N \left|\psi_N^N\right\rangle. \tag{6.11}$$

This implies that the emission is enhanced by a factor 2 as compared to a single coherent state: $H\left|\alpha, \alpha\right\rangle\left|g\right\rangle = 2\alpha g\left|\alpha, \alpha\right\rangle\left|e\right\rangle$ against $H\left|\alpha, 0\right\rangle\left|g\right\rangle = g\alpha\left|\alpha, 0\right\rangle\left|e\right\rangle$, respectively. This result is here interpreted as the signature of a state which projects on the MSS subspace only, but from a classical perspective, it corresponds to a constructive interference for in-phase fields. As for the state describing two coherent fields with opposite phases, it decomposes in terms of PDSs only:

$$\left|\alpha, -\alpha\right\rangle = e^{-|\alpha|^2} \sum_{N=0}^{\infty} \sqrt{\frac{2^N}{N!}} \alpha^N \left|\psi_0^N\right\rangle. \tag{6.12}$$

This state presents a suppressed interaction $H\left|\alpha,-\alpha\right\rangle\left|g\right\rangle=0$, which can be interpreted either as belonging to the PDS subspace or, classically, as a destructive interference for two fields with the same amplitude, but opposite phases.

Less intuitively, the introduced basis provides an explanation for the coupling of state $|\Upsilon\rangle$ from Eq. (6.5) to the atom, despite it having zero average electric field (a destructive interference from the classical perspective) and the same electric field variance as state $|\alpha,-\alpha\rangle$. Indeed, it decomposes along MSS and PDS subspaces as

$$|\Upsilon\rangle=\frac{1}{2}\left[\left|\psi_0^0\right\rangle-\sqrt{2}\left|\psi_0^1\right\rangle+\frac{1}{\sqrt{2}}\left(\left|\psi_0^2\right\rangle-\left|\psi_2^2\right\rangle\right)\right], \tag{6.13}$$

so the finite projection on the MSS $|\psi_2^2\rangle$ is responsible for the nontrivial action of the Hamiltonian.

The PDS subspace is a remarkable class of states. On the one hand, from a classical perspective, destructive interference is considered an absence of field, which explains the absence of a generated dipole moment. On the other hand, fluctuations in the electric field operator are usually invoked to explain the excitation of an atom in the absence of a field expectation value, as illustrated by the emblematic single-mode Fock states. Perfectly dark states are transverse to these characteristics since they possess nonzero fluctuations ($\langle\Delta E^2\rangle=2$, see Appendix F.2), an energy proportional to their photon number N, and yet they do not excite the atom. In other words, they go beyond the classical interpretation of destructive interference, for which the fields simply cancel out.

Naturally, a coherent state in only one of the two modes does not provide any collective feature: $H\left|\alpha,0\right\rangle\left|g\right\rangle=g\alpha\left|\alpha,0\right\rangle\left|e\right\rangle$. In the collective basis, it decomposes as

$$|\alpha,0\rangle=e^{-|\alpha|^2/2}\sum_{N=0}^{\infty}\sum_{n=0}^{N}\frac{(-1)^{N-n}\alpha^N}{\sqrt{2^N n!(N-n)!}}\left|\psi_n^N\right\rangle, \tag{6.14}$$

which is a combination of modes of various transition rates, averaging out as the transition rate of a single coherent mode. The situation is equivalent to that of two atoms with a single one excited, $|eg\rangle$, which decomposes equally on the superradiant $[|+\rangle=(|eg\rangle+|ge\rangle)/\sqrt{2}]$ and subradiant $[|-\rangle=(|eg\rangle-|ge\rangle)/\sqrt{2}]$ states as $|eg\rangle=(|+\rangle+|-\rangle)/\sqrt{2}$. Therefore, its radiation averages into the single-atom one.

6.4 Revisiting the double-slit experiment

A key experiment in evidencing the wave nature of light is the Young slit experiment or, equivalently, the Mach-Zehnder interferometer. The fundamental result is that both classical and single-photon coherent sources produce the same fringe pattern, despite the very different natures of these fields, and despite the latter source is composed of a single quantum of energy. To revisit this experiment using the collective basis, one can

consider, in the far field limit, two equal-weight light modes, as previously. Without loss of generality, we assume that the waves with wave vectors $\mathbf{k}_1$ and $\mathbf{k}_2$, with $|\mathbf{k}_1| = |\mathbf{k}_2| = k$, reach the two slits with the same phase. Then, kr_1 and kr_2 are the phases acquired by the respective fields when propagating from slits 1 and 2, respectively, until the detection point (see Fig. 15).

For modes in coherent states, the field on the detector writes

$$\left|e^{ikr_1}\alpha, e^{ikr_2}\alpha\right\rangle = e^{-|\alpha|^2}\sum_{N=0}^{\infty}\sqrt{\frac{2^N}{N!}}\left(e^{ikr_2}\alpha\right)^N\left|\chi^N\left(\delta\phi\right)\right\rangle, \tag{6.15}$$

whereas for single-photon states

$$\left|S\left(\delta\phi\right)\right\rangle = \cos\left(\delta\phi/2\right)\left|\psi_1^1\right\rangle - i\sin\left(\delta\phi/2\right)\left|\psi_0^1\right\rangle, \tag{6.16}$$

where $\delta\phi = k(r_1 - r_2)$ represents the phase difference due to the distinct light paths until the detector. In Eq. (6.15), we have defined the phase-dependent state

$$\left|\chi^N\left(\delta\phi\right)\right\rangle = \sqrt{\frac{N!}{2^N}}\sum_{m=0}^{N}\frac{e^{-im\delta\phi}}{\sqrt{m!\left(N-m\right)!}}\left|m, N-m\right\rangle, \tag{6.17}$$

which corresponds to a MSS when the two modes are in phase, $\left|\chi^N\left(2l\pi\right)\right\rangle = \left|\psi_N^N\right\rangle$, and to a PDS when in opposite phases, $\left|\chi^N\left((2l+1)\pi\right)\right\rangle = \left|\psi_0^N\right\rangle$, with $l = 0, \pm1, \pm2, ...$ The single-photon state $\left|S\left(\delta\phi\right)\right\rangle$, which decomposes as a sum of PDS or MSS only [see Eq. (6.16)], presents the same feature. Therefore, the decomposition in PDSs and MSSs straightforwardly explains why single-photon sources and classical fields exhibit the same fringe pattern, for a ground state atom. The particular case of the slits actually points toward a more general result: states of light composed of PDSs and MSSs only exhibit the same interference patterns as those derived from linear optics or, equivalently, for high-photon-number coherent states.

6.5 Mach-Zehnder interferometer (MZI)

To pursue the discussion on the detection of light states of different natures, let us now consider the MZI setup with two input fields which are either classical fields, with Rabi frequencies $\Omega_a = \Omega$ and $\Omega_b = e^{i\theta}\Omega$, or quantum fields which belong to the PDS subspace, or to the MSS subspace. The latter can be written in terms of creation operators as $f\left(a^\dagger + e^{i\theta}b^\dagger\right)\left|0,0\right\rangle$ (see Appendix F.1). For classical (quantum) fields, $\theta = 0$ corresponds to the case of constructive interference (MSSs only), and $\theta = \pi$ to destructive interference (PDSs only). For either kind of state, the output intensity is (see Appendix C)

$$I_{\text{out}}^{\pm} = I_{\text{in}}\left(1 \pm \cos\theta\sin\varphi\right), \tag{6.18}$$

where $+/-$ refers to the arm a/b, I_{in} is the intensity of the input field and φ the relative phase shift between the two arms of the interferometer. Eq. (6.18) shows that classical and quantum fields exhibit the same fringe pattern through MZI as the phase φ is varied. Differently, state $|\Upsilon\rangle$ has a projection on both MSS and PDS subspaces and it leads to the following output in the MZI:

$$\left(I^{\pm}_{\text{out}}\right)_{|\Upsilon\rangle} = \frac{1}{4}\left(2 \mp \sin\varphi\right). \tag{6.19}$$

This fringe pattern is qualitatively different from the one obtained for classical fields, and for pure PDSs or MSSs, since the intensity does not cancel. Its minimum is $\left(I^{\pm}_{\text{out}}\right)_{|\Upsilon\rangle}(\varphi = \pm\pi/2) = 1/4$, with a visibility

$$V_{|\Upsilon\rangle} = \frac{I_{\max} - I_{\min}}{I_{\max} + I_{\min}} = \frac{1}{2}, \tag{6.20}$$

which is half the value of 1 obtained for classical states and PDS-only or MSS-only. This finite minimum of the intensity can be interpreted in terms of the Hong-Ou-Mandel effect [51, 154], where the projection of $|\Upsilon\rangle$ on the two-indistinguishable-photon state $|1,1\rangle_{ab}$ automatically leads to a nonzero intensity in the MZI.

According to our predictions, PDSs and MSSs provide the same signatures as classical fields through interferometric setups, despite their quantum nature – the states which compose the PDS and MSS basis are photon-number states. Combined with the fact that the "classical" state $|\alpha,\alpha\rangle$ (or $|\alpha,-\alpha\rangle$) decomposes as MSSs (or PDSs) only, this shows that the collective basis offers a natural frame for the concept of interference. Independently of the (classical or quantum) nature of the light, MSSs and arbitrary combinations of them correspond to constructive interference, whereas PDSs result in destructive interference. While for the other states, such as $|\Upsilon\rangle$, more elements from the collective basis are necessary to properly assess their coupling to matter.

Our collective basis (6.6) reveals a broad family of "intermediate" states, which are neither perfectly dark nor maximally superradiant ($\left|\psi^N_n\right\rangle$ for $n \neq 0, N$). By injecting such states in the MZI, one obtains interference patterns which cannot be described by classical theory. For instance, considering the input (entangled) state $|\psi^2_1\rangle = 1/\sqrt{2}\,(|0,2\rangle - |2,0\rangle)$, the output in arm a is $I_{\text{out}} = 1$, independently of the relative phase φ of the MZI (see Appendix F.4). In this case, the fringes have completely disappeared, and the visibility is zero. In Fig. 16, we plot the output intensity in arm a as a function of the phase φ, which highlights the qualitative difference between the different states of light considered. Note that while the PDS considered here is a combination of two out-of-phase coherent (classical) fields, any PDS will provide the same interference pattern, whether classical or quantum. Differently, states $|\psi^2_1\rangle$ and $|\Upsilon\rangle$ present patterns that are different from those obtained with classical states, where the intensity cancels. In this sense, the reduction of visibility here stems from the quantum nature of the field.

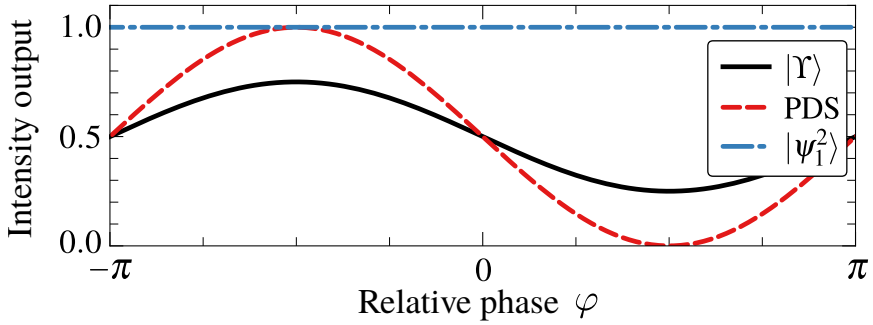

Figure 16 – Light intensity in the output mode A of a MZI as a function of the relative phase φ and for different initial states: $|\Upsilon\rangle$, given by Eq. (6.13), and the PDS, $|\alpha, -\alpha\rangle$ (with $\alpha = 1/\sqrt{2}$), both with total average number of photon equal to 1, and the state $|\psi_1^2\rangle = (1/\sqrt{2})(|0,2\rangle - |2,0\rangle)$ which has exactly two photons, for comparison. Note that the fringes obtained for the PDS state considered here are the same as those obtained for any PDS.

Inspired by the collective basis, let us now introduce a protocol to identify the nature of the light field. As a slight alteration of these setups, we now consider an atom in the excited state $|e\rangle$ to locally probe the field. In this case, two classical fields with the same amplitude, but with opposite phase, do not act on the atom since the classical Hamiltonian simply cancels. Alternatively, a quantum field with a small average number of photons, even in a superposition of PDSs, does exchange energy with the atom. This can be easily demonstrated using the evolution operator $U(t) = e^{-iHt}$, with H given by Eq. (6.1), and by noticing that any superposition of PDSs can be written as $f(a^\dagger - b^\dagger)\,|0,0\rangle$ (see Appendix F.1). Using the commutation relation $[H, (a^\dagger - b^\dagger)] = 0$, one obtains

$$U(t) f(a^\dagger - b^\dagger)\,|0,0\rangle\,|e\rangle = f(a^\dagger - b^\dagger) U(t)\,|0,0\rangle\,|e\rangle\,, \tag{6.21}$$

which, in general, is nonzero. Hence, PDSs exchange energy with an atom in the excited state, just as the two-mode vacuum state does. Thus, the slit experiment combined with a two-level emitter as a probe appears as a new tool to probe the nature of the probe field. This makes field-field correlations appropriate tools to probe the quantum nature of light, instead of the usual intensity-intensity correlations [51, 154]. From a fundamental point of view, this difference between few- (quantum) and many-photon (classical) fields stems from the difference between classical and quantum vacuum. In essence, it is related to the non-commutation relation between a and $a^\dagger$, which implies that the addition and then the subtraction of a photon differs completely from the subtraction followed by the addition of a photon [164, 165].

The similarities between the "true" vacuum state $|0,0\rangle$ and PDSs raises the question of whether it is possible to distinguish the two, since neither a ground-state nor an excited-state atom can differentiate them. However, it is sufficient to observe that a change in the balance between the two modes (not achievable in free space, where the atom-field coupling g is very small) would immediately change the nature of the mode (provided it

is not the vacuum state), giving the new mode a nonzero projection onto bright states. For example, in a two-mode cavity, taking into account the transverse shape of the modes means that a transverse displacement of the emitter would allow for the atom to radiate, as long as the two cavities are not in the vacuum state. In particular, such an experiment could help investigate the existence of a "dark-like energy", since PDSs have an energy proportional to their number of photons (in addition to the energy of the true vacuum state), yet no coupling to the matter. Note that the discussion on the coupling of an atom with a field which locally cancels is reminiscent of the finite momentum diffusion for an atom at the crossing of two lasers, where the fields interfere destructively. The existence of heating is, in that case, related to the spatial gradient of the field, rather than to its quantum fluctuations [166, 167].

6.6 Generalization to M modes

Let us now discuss how our approach generalizes to an arbitrary number of light modes. For M modes equally coupled to the atom, the interaction Hamiltonian reads:

$$H_M = g\sum_{j=1}^{M}(a_j\sigma^+ + a_j^\dagger\sigma^-), \tag{6.22}$$

with a_j ($a_j^\dagger$) the annihilation (creation) operator for the $j-$th light mode. Then, the following generalized coupling relation can be derived (see Appendix F.5):

$$H_M \left|\psi^N_{n_1,n_2,\ldots,n_M}\right\rangle |g\rangle = g\sqrt{Mn_1}\left|\psi^{N-1}_{n_1-1,n_2,\ldots,n_M}\right\rangle |e\rangle\,, \tag{6.23}$$

where we have defined the collective M-mode basis

$$\left|\psi^N_{n_1,n_2,\ldots,n_M}\right\rangle = \prod_{j=1}^{M}\frac{1}{\sqrt{n_j!}}\left(\sum_{k=1}^{M}O_{jk}a_k^\dagger\right)^{n_j}|0,0,\ldots,0\rangle\,, \tag{6.24}$$

for the subspace of $\sum_{k=1}^{M}n_k = N$ photons. In Eq.(6.24), we define $\mathbf{O}$ the orthogonal matrix of dimension $M\times M$, with M even, whose elements in the first row are $O_{1k} = 1/\sqrt{M}$, while the elements in the second row satisfy the rule $O_{2k} = (-1)^{k-1}/\sqrt{M}$ (see Appendix F.5). Consequently, we identify the MSSs as

$$\left|\psi^N_{N,0,\ldots,0}\right\rangle = \frac{1}{\sqrt{N!M^N}}\left(\sum_{m=1}^{M}a_m^\dagger\right)^N|0,0,\ldots,0\rangle\,, \tag{6.25}$$

associated with the largest transition rate $g\sqrt{MN}$. The anti-symmetric PDSs read

$$\left|\psi^N_{0,N,\ldots,0}\right\rangle = \frac{1}{\sqrt{N!M^N}}\left(\sum_{m=1}^{M}(-1)^{m-1}a_m^\dagger\right)^N|0,0,\ldots,0\rangle\,. \tag{6.26}$$

As for the two-mode case, we are now able to expand the M-mode in-phase coherent state in terms of MSSs only:

$$|\alpha, \alpha, \ldots, \alpha\rangle = e^{-M|\alpha|^2/2} \sum_{N=0}^{\infty} \sqrt{\frac{M^N}{N!}} \alpha^N \left|\psi^N_{N,0,\ldots,0}\right\rangle, \tag{6.27}$$

which leads to the coupling relation $H_M|\alpha, \alpha, ..., \alpha\rangle|g\rangle = gM\alpha|\alpha, \alpha, ..., \alpha\rangle|e\rangle$. Therefore, the exchange of energy between the atom and the modes in coherent states is M times faster than the case of a single cavity mode. Finally, the M-mode coherent state corresponding to destructive interference decomposes in the PDS subspace only:

$$|\alpha, -\alpha, \ldots, \alpha, -\alpha\rangle = e^{-M|\alpha|^2/2} \sum_{N=0}^{\infty} \sqrt{\frac{M^N}{N!}} \alpha^N \left|\psi^N_{0,N,\ldots,0}\right\rangle, \tag{6.28}$$

implying immediately the dark state condition $H_M \left|\alpha, -\alpha, \ldots, \alpha, -\alpha\right\rangle \left|g\right\rangle = 0$.

Considering the more general case of M modes, one can now identify that the single mode case ($M = 1$) presents a unique PDS, namely, the vacuum state $|0\rangle$. This case may sound trivial since there is no photon to excite the atom, yet its interest lies in its unicity: any other state excites the atom. The multimode case is fundamentally different since it possesses an infinite family of dark states, with arbitrarily high photon numbers, yet which do not couple to the emitter in the ground state. This scenario is analogous to the case of two-level atoms, where the single-atom (spontaneous) emission always occurs, whereas the emission from a couple of atoms is suppressed in their dark state $|-\rangle = 1/\sqrt{2}(|e, g\rangle - |g, e\rangle)$. In this context, the collective basis is the natural frame to understand why single-mode Fock states couple to matter (since they do not belong to the PDS subspace), whereas two-mode PDSs states with quantum fluctuations do not. Alternatively, dark states can be produced using single emitters with a multilevel structure [168], in particular in Electromagnetically Induced Transparency [169].

6.7 Detection scheme

The two-mode or M-mode light-matter interaction discussed in the present work suggests an implementation in setups where the electromagnetic environment is reduced to a few modes. Examples are optical cavities coupled to a two-level atom [170, 171], trapped ions where a single emitter can be coupled to its two vibrational modes [12, 172], or superconducting circuits [173]. We point out that an important example of the present discussion is the case of two coherent states with the same photon number but opposite phases; these light modes possess nonzero quantum fluctuations, but do not couple to the emitter. A crossed detection of the atom dynamics (for example, from its fluorescence) coupled to a detection of the statistics of the cavity modes, would allow unambiguous measurement of the features discussed in this work. Note that the cavity's finite finesse

(and thus nonzero cavity decay rate) and the atom's spontaneous emission (atomic decay rate) are not expected to affect these features, since they are purely diagonal terms.

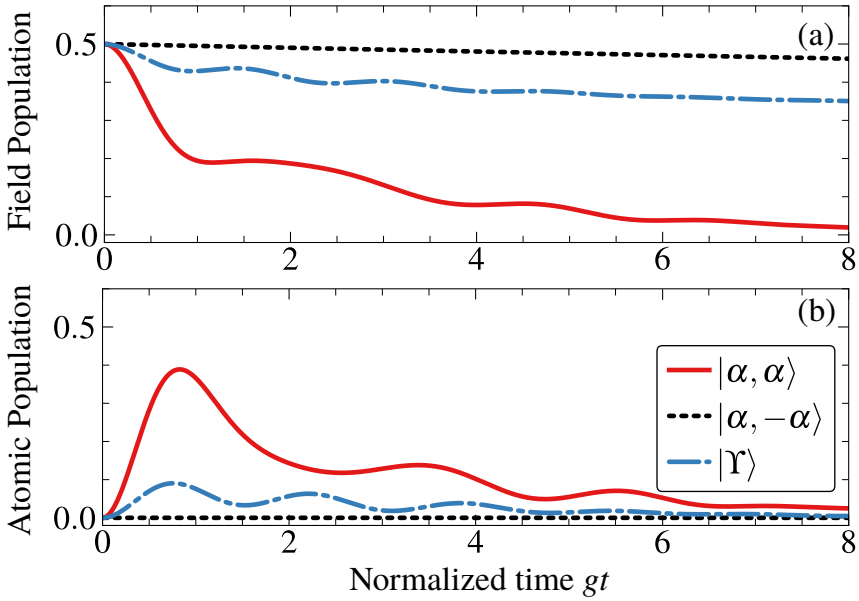

Figure 17 – (a) Field population $\langle a^\dagger a\rangle$ in modes A (same as in mode B) and (b) population of the excited state $\langle\sigma_{ee}\rangle$ as a function of the normalized time gt. The initial states considered are $|\alpha,\alpha\rangle|g\rangle$ (solid red curve), $|\alpha,-\alpha\rangle|g\rangle$ (dashed black curve) and $|\Upsilon\rangle|g\rangle$ (blue dash-dotted curve). Parameters used: $g_a = g_b = g$, $\kappa_a = \kappa_b = g/100$, $\gamma = g$, and $\alpha = 1/\sqrt{2}$.

We study the dynamics of the atom coupled to two cavity modes using a quantum master equation, which takes into account the atom and mode dissipation:

$$\dot{\rho} = -i\left[H,\rho\right] + L_{atom}\left(\rho\right) + L_a\left(\rho\right) + L_b\left(\rho\right), \tag{6.29}$$

with

$$L_{atom}\left(\rho\right) = \left(\gamma/2\right)\left(2\sigma_-\rho\sigma_+ - \sigma_+\sigma_-\rho - \rho\sigma_+\sigma_-\right) \tag{6.30}$$

and

$$L_\beta\left(\rho\right) = \left(\kappa_\beta/2\right)\left(2\beta^\dagger\rho\beta - \beta^\dagger\beta\rho - \rho\beta^\dagger\beta\right), \tag{6.31}$$

with $\beta = a, b$, and where γ and κ_β are the atomic and field decay rates, respectively. This master equation is the standard one employed to study atom-cavity dynamics and is valid under the Rotating Wave Approximation (RWA), where the atom-field coupling energy is much smaller than the free energy of the modes and of the atom, and Born and Markov approximations [51].

Considering an intermediate ($g \sim \kappa, \gamma$) or strong ($g \gg \kappa, \gamma$) atom-field coupling, the results predicted in this work could be observed by monitoring the modes and atomic populations, see Fig. 17. Starting with the atom in the ground state $|g\rangle$, state $|\alpha,\alpha\rangle$ exchanges energy with the atom while the state $|\alpha,-\alpha\rangle$ does not. On the other hand, state $|\Upsilon\rangle$ excites the atom despite its zero average electric field, and electric field fluctuations

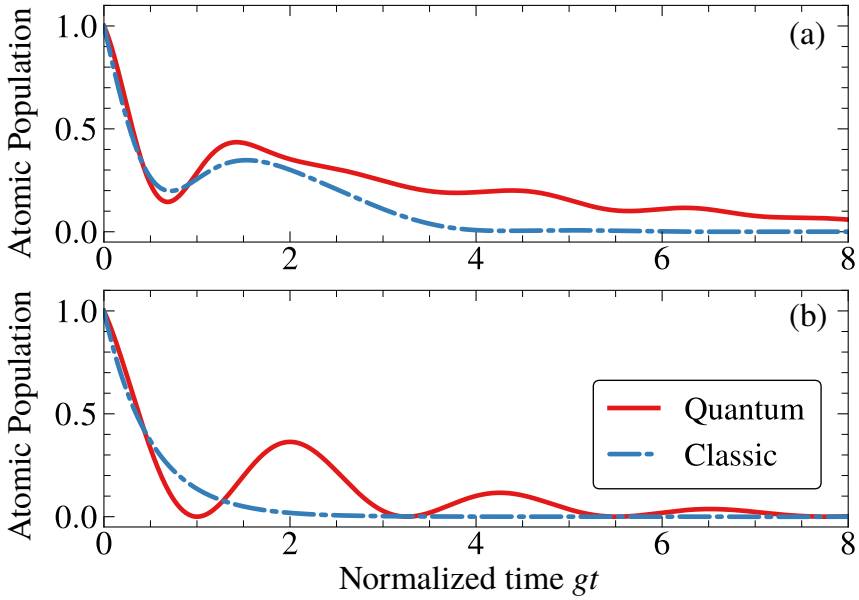

Figure 18 – Excited state population $\langle\sigma_{ee}\rangle$ as a function of the parametrized time gt considering the semi-classical (dashed blue line) and the quantum approaches (solid red line) and the atom initially in the excited state. In the panel (a) both fields are in the constructive interference scenario, *i.e.*, in-phase classical fields with initial amplitude (collective mode) $\alpha_c(0) = \sqrt{2}\alpha$ and $|\alpha, \alpha\rangle$ for the quantum approach. Oppositely, in the figure (b), the fields concern the destructive interference case, *i.e.*, out-of-phase classical fields with initial amplitude (collective mode) $\alpha_c(0) = 0$ and $|\alpha, -\alpha\rangle$ for the quantum description. Parameters: $\alpha = 1/\sqrt{2}$, $g_a = g_b = g$, $\kappa_a = \kappa_b = g/100$, and $\gamma = g$.

equal to those of the $|\alpha, -\alpha\rangle$ states. Thus, by monitoring the excited atomic state population one could distinguish the states considered here, see Fig. 17(a). One could also observe the atom-field coupling/non-coupling by monitoring the cavity mode emission, since the atom acts as an extra source of decay for the cavity modes (that is, for the states which couples to the atom), with an effective decay rate $\kappa_{eff} = g^2/2\gamma$ [174, 175]. In Fig. 17(a) we plot the average number of photons in the cavity mode A (which is the same as in mode B), which shows that the cavity emission depends on the mode state, as expected. In particular, the state $|\alpha, -\alpha\rangle$ remains completely unaffected by the presence of the atom.

Let us now discuss further how the interference experiment presented in Sec. 6.5 allows one to distinguish PDSs from classical fields, provided a two-level detector in the excited state is used. In Fig. 18, considering an atom initially in the excited state $|e\rangle$, we present the evolution of the excited state population for different field states, described by either a quantum model, derived from Eq. (6.29), or a semi-classical one. The latter is obtained by deriving from Eq. (6.29) the equations of motion for the atomic and the cavity field operators. Then, the expected value for the collective operator of the radiation field $c = (a + b)/\sqrt{2}$ is replaced by time-dependent complex amplitude $\alpha_c(t)$ (see Appendix F.6 for details). The panels (a) and (b) in Fig. 18 describe, respectively, in-phase ($|\alpha, \alpha\rangle$ and $\alpha_c(0) = \sqrt{2}\alpha$, for quantum and semi-classical models, respectively) and out-of-phase

($|\alpha, -\alpha\rangle$ and $\alpha_c(0) = 0$, for quantum and semi-classical models, respectively) fields, and they exhibit a qualitative difference between the two approaches. One observes that the semi-classical model predicts a monotonic decay, while the quantum one predicts an oscillating decay: this shows that a quantum and a classical field can be distinguished with this protocol.

6.8 Application: Controlled-Phase Gate

One can take advantage of the bright and dark states of the cavity modes for quantum information processing. To illustrate this point, let us now present how to implement a controlled phase gate on atomic states. On the one hand, since the dark states do not interact with the atom, they do not introduce any phase on the atomic state. On the other hand, the bright states do interact with the atom, so they modify the atomic state.

Our protocol requires a three-level atom in a Λ configuration (with two ground states $|g_1\rangle$ and $|g_2\rangle$, and an excited state $|e\rangle$) interacting with both cavity modes of frequency ω_c. We assume that only the transition $|g_1\rangle \leftrightarrow |e\rangle$ (with transition frequency ω_0) is coupled to the cavity modes. To avoid transfer of atomic population to the unstable excited state, the atom-modes interaction is detuned from the atomic transition: $\omega_c = \omega_0 + \Delta$, In the limit of large detuning ($|\Delta| \gg g$), the excited state will be marginally excited, and one can assume the atomic state to be restricted to the ground state subspace $\{|g_1\rangle, |g_2\rangle\}$. An effective Hamiltonian can then be derived from Eq. (6.1) [176]:

$$H_{\text{eff}} \simeq \frac{g^2}{\Delta}\left(a^\dagger + b^\dagger\right)(a+b)\,|g_1\rangle\langle g_1|\,. \tag{6.32}$$

For simplicity, we consider single-excitation bright and dark states ($|\psi_1^1\rangle$ and $|\psi_0^1\rangle$, respectively). The evolved states are

$$e^{-iH_{\text{eff}}t}\,|g_2\rangle\left|\psi_0^1\right\rangle = |g_2\rangle\left|\psi_0^1\right\rangle, \tag{6.33}$$

$$e^{-iH_{\text{eff}}t}\,|g_1\rangle\left|\psi_0^1\right\rangle = |g_1\rangle\left|\psi_0^1\right\rangle, \tag{6.34}$$

$$e^{-iH_{\text{eff}}t}\,|g_2\rangle\left|\psi_1^1\right\rangle = |g_2\rangle\left|\psi_1^1\right\rangle, \tag{6.35}$$

$$e^{-iH_{\text{eff}}t}\,|g_1\rangle\left|\psi_1^1\right\rangle = e^{-i\xi}\,|g_1\rangle\left|\psi_1^1\right\rangle, \tag{6.36}$$

where we have introduced $\xi = 2g^2/\Delta t$. Adjusting the interaction time t one is able to adjust the phase ξ, thus realizing a Controlled-Phase gate. Combined with single qubit operations (see Appendix F.7), one can implement other more complex gates such as the C-Not gate, eventually achieving universal quantum processing.

6.9 Conclusion

In conclusion, we have discussed how a description of multimode light in terms of maximally superradiant or perfectly dark collective states offers a natural interpretation for constructive and destructive interference. Remarkably, this Dicke-like bosonic basis applies to classical and non-classical states of light, thus going beyond the simple classical approach of average fields. Differently from the classical approach, where no assumption on the matter is necessary to describe the sum of electromagnetic fields, we have shown that interference are intimately related to the light-matter coupling properties from a quantum perspective, since bright and dark states stem from this coupling. One can interpret this as a manifestation of the measurement problem in quantum mechanics, where an observable expectation value also depends on the features of the measuring apparatus [177, 178]. Within this framework, we have revisited the double-slit and MZI experiments to provide an explanation of the similarities and differences expected in these interference setups, when employing quantum or classical light fields.

Moreover, our approach allowed us to identify a necessary and sufficient condition for an atom in its ground state to couple to a light field. While the common wisdom, present in many textbooks, suggests that the coupling of the emitter to light states with zero average electric field is due to the quantum fluctuations of the field, we have shown that this explanation fails for multimode field states. Indeed, the true condition for this coupling is a finite projection out of the PDS subspace. Oppositely, a light state that only decomposes on PDSs does not couple to the atom, despite its fluctuations. These PDSs with nonzero energy thus give rise to a kind of "dark energy", which cannot be detected through usual techniques, that is, they are transparent to the atom.

Our results could be observed in a cavity QED setup (using optical cavities or, equivalently, trapped ions or circuit QED), by monitoring the excited atomic population. On the one hand, a ground state atom is excited only when the initial mode state has a projection out of the PDS subspace. On the other hand, for a PDS-only light state, one could detect the presence of a non-trivial field only using some twists. In a cavity QED setup, these states could be probed by unbalancing the coupling between the modes and the two-level atom, since the PDS nature of a light state is related to a specific set of couplings between the atom and the modes. Our work could thus bring a new understanding of interference effects in general, especially for quantum light fields, since it provides a toolbox to identify, for example, light fields with finite fluctuations yet protected from decoherence through the emitters. This could help the engineering of light-matter interactions and their applications, for instance, in quantum gates and quantum memories for quantum information science [14, 179, 180].

Conclusion

In this master dissertation, we have approached three different topics. In the first topic, we applied the quantum adiabatic brachistochrone method to optimize two types of adiabatic evolutions, the adiabatic quantum search algorithm and the charging process of a quantum battery. Concerning the adiabatic quantum search, we showed that the imposing constraints to the interpolation function can increase the total dynamics time, thus reducing the quadratic speedup over the classical search algorithm. Also, we use a Legendre transformation in the Lagrangian to find the Hamiltonian of the quantum adiabatic brachistochrone, by which we firstly find the non-constrained quantum adiabatic brachistochrone for the adiabatic Grover algorithm. We showed that the non-constrained brachistochrone is qualitative equal to the linear constrained brachristochrone to execute the algorithm. In the quantum battery, in collaboration with Prof. Dapeng Hu's research group, we fully characterize the transmon superconducting three-level quantum battery. We demonstrated that the quadratic constrained brachistochrone with the unstable charging protocol can enhance the ergotropy injection in the artificial atom. The characterization is then concluded with the experiment and theoretical description of the self-discharging process of the battery, which has a non-Ohmic behavior.

The second topic is a study about the D-Wave quantum annealer. We firstly presented its engineering and experimental setup, further we investigated the techniques to formulate QUBO and Ising algorithms and then we solved the traveling salesman problem on the D-Wave quantum computer. This study was published on the *Revista Brasileira de Ensino de Física* [53]. To give a classical alternative to this quantum process and also to have a method for comparing classical and quantum solutions, we described the simulated annealing, which is an algorithm that simulates an approximated slow and smooth cooling process of a thermodynamics system to solve optimization problems. Using the traveling salesman problem, we showed that the simulated annealing can indeed find good solutions, with less than five percent of error in relation to the optimal one for instances with 100 cities, while the present day quantum annealer can not handle with tours containing more than 10 cities. Thus, our analysis corroborate to the literature that states that there is still no evidence of quantum speed up over classical computers using annealers.

In the third topic, we introduced a quantum interpretation of classical interference. We showed that describing light-matter interaction using quantum fluctuations leads to inaccurate predictions. Our new treatment has an unambiguous approach to describe light-matter interaction based on super- and sub-radiance and it can be applied to classical and non-classical states of light. The classical approach does not make any assumption regarding the measurement apparatus for detecting interference phenomena, while we

showed that taking into consideration the light-matter coupling is fundamental to correctly describe interference behavior in classical and non-classical light.

Moreover, throughout the development of this work, we find some relevant questions that might have interesting answers:

1) Generalization of the ladder-like quantum battery. We know that the charging Hamiltonian for a qudit have analytical solutions, which may also enable analytical solutions for describing the self-discharging behavior. A comparison between the total dynamics time between the new charging protocols will lead to new experiments concerning this kind of device. Systems like the one presented in Ref. [181] will find applications of the study we proposed here.

2) Single photons generation (SPG) is a important task for quantum information and communication [182]. In the Refs. [4, 183] the authors experimentally showed that it is possible to generate single photons by using the Λ-STIRAP technique. The quantum system used for SPG is a three-level atom with one branch driven by a laser and the other coupled to a cavity mode. The application of the QAB to this system can yield more efficient technologies for SPG.

3) A Quantum memory is a system that stores and retrieves a quantum state. This kind of system can be created by coupling two macro-atoms via an optical resonator, then one can transfer a magnon in one macro-atom to the other, using adiabatic dark-state transfer [184, 185], which can be accelerated with the QAB.

4) The quantum adiabatic brachistochrone method was recently generalized to open quantum systems [41] and it was successfully tested for small systems, such as the three-level battery and Deutsch-Jozsa algorithm. However, there are analytical solutions of the energy gap (as required for finding analytical motion equations) in just few cases. It will be interesting to develop an efficient numerical method, exact or approximated, for applying this method for larger systems, which will have applications to the NISQ adiabatic quantum computing and technology.

5) Approximated quantum adiabatic brachistochrone. Since the task of finding the energy gap is not generally achieved analytically for the QAB, approximated techniques may be helpful. For example, it is possible to find the eigenvalues of the adiabatic Grover algorithm, but if not, we could solve the dynamics for a set of small N to fit the Gap as a function of N. Therefore, for this case we will approximately find the motion equations. The gain will concern computational resources, since when the energy gap is not available, one has to diagonalize the system in every time interval for solving the motion equations of the QAB.

6) Some methods for speed up adiabatic dynamics make use of an additional Hamiltonian for increasing the energy gap during time evolutions [91]. Then the total Hamiltonian reads $H(t) = q_0(t)H_0 + q_{\text{sc}}(t)H_{\text{sc}} + q_1(t)H_1$ where 'sc' stands for shortcut and $q_{\text{sc}}(0) = q_{\text{sc}}(\tau) = 0$. In this scheme, the QAB method is still to be tested.

Bibliography

[1] C.-K. Hu, J. Qiu, P. J. P. Souza, J. Yuan, Y. Zhou, L. Zhang, J. Chu, X. Pan, L. Hu, J. Li, Y. Xu, Y. Zhong, S. Liu, F. Yan, D. Tan, R. Bachelard, C. J. Villas-Boas, A. C. Santos, and D. Yu, "Optimal charging of a superconducting quantum battery," *arXiv:2108.04298 [quant-ph]*, Aug. 2021. arXiv: 2108.04298.

[2] F. Campaioli, F. A. Pollock, and S. Vinjanampathy, "Quantum batteries," in *Thermodynamics in the Quantum Regime*, pp. 207–225, Springer, 2018.

[3] S. Boixo, T. Albash, F. M. Spedalieri, N. Chancellor, and D. A. Lidar, "Experimental signature of programmable quantum annealing," *Nature Communications*, vol. 4, p. 2067, June 2013.

[4] A. Kuhn, M. Hennrich, and G. Rempe, "Deterministic Single-Photon Source for Distributed Quantum Networking," *Physical Review Letters*, vol. 89, p. 067901, July 2002.

[5] F. Carollo, F. M. Gambetta, K. Brandner, J. P. Garrahan, and I. Lesanovsky, "Nonequilibrium quantum many-body rydberg atom engine," *Physical Review Letters*, vol. 124, no. 17, p. 170602, 2020.

[6] F. Carollo, K. Brandner, and I. Lesanovsky, "Nonequilibrium many-body quantum engine driven by time-translation symmetry breaking," *Physical Review Letters*, vol. 125, no. 24, p. 240602, 2020.

[7] R. P. Feynman, "Simulating physics with computers," *International journal of theoretical physics*, vol. 21, no. 6, pp. 467–488, 1982.

[8] P. Benioff, "The computer as a physical system: A microscopic quantum mechanical hamiltonian model of computers as represented by turing machines," *Journal of Statistical Physics*, vol. 22, no. 5, pp. 563–591, 1980.

[9] J. Preskill, "Quantum computing in the nisq era and beyond," *Quantum*, vol. 2, p. 79, 2018.

[10] S. Boixo, S. V. Isakov, V. N. Smelyanskiy, R. Babbush, N. Ding, Z. Jiang, M. J. Bremner, J. M. Martinis, and H. Neven, "Characterizing quantum supremacy in near-term devices," *Nature Physics*, vol. 14, no. 6, pp. 595–600, 2018.

[11] Y. Ding and A. Javadi-Abhari, "Quantum and post-moore's law computing," *IEEE Internet Computing*, vol. 26, no. 1, pp. 5–6, 2022.

[12] D. Leibfried, R. Blatt, C. Monroe, and D. Wineland, "Quantum dynamics of single trapped ions," *Rev. Mod. Phys.*, vol. 75, pp. 281–324, Mar 2003.

[13] D. Loss and D. P. DiVincenzo, "Quantum computation with quantum dots," *Physical Review A*, vol. 57, no. 1, p. 120, 1998.

[14] S. Haroche, "Nobel lecture: Controlling photons in a box and exploring the quantum to classical boundary," *Rev. Mod. Phys.*, vol. 85, pp. 1083–1102, Jul 2013.

[15] M. Kjaergaard, M. E. Schwartz, J. Braumüller, P. Krantz, J. I.-J. Wang, S. Gustavsson, and W. D. Oliver, "Superconducting qubits: Current state of play," *Annual Review of Condensed Matter Physics*, vol. 11, pp. 369–395, 2020.

[16] P. Krantz, M. Kjaergaard, F. Yan, T. P. Orlando, S. Gustavsson, and W. D. Oliver, "A quantum engineer's guide to superconducting qubits," *Applied Physics Reviews*, vol. 6, no. 2, p. 021318, 2019.

[17] F. Arute, K. Arya, R. Babbush, D. Bacon, J. C. Bardin, R. Barends, R. Biswas, S. Boixo, F. G. Brandao, D. A. Buell, *et al.*, "Quantum supremacy using a programmable superconducting processor," *Nature*, vol. 574, no. 7779, pp. 505–510, 2019.

[18] A. C. Santos, B. Çakmak, S. Campbell, and N. T. Zinner, "Stable adiabatic quantum batteries," *Physical Review E*, vol. 100, p. 032107, Sept. 2019.

[19] C.-K. Hu, A. C. Santos, J.-M. Cui, Y.-F. Huang, D. O. Soares-Pinto, M. S. Sarandy, C.-F. Li, and G.-C. Guo, "Quantum thermodynamics in adiabatic open systems and its trapped-ion experimental realization," *npj Quantum Information*, vol. 6, pp. 1–11, Aug. 2020.

[20] D. Boccaletti and G. Pucacco, "The Theory of Adiabatic Invariants," in *Theory of Orbits: Perturbative and Geometrical Methods* (D. Boccaletti and G. Pucacco, eds.), Astronomy and Astrophysics Library, pp. 179–233, Berlin, Heidelberg: Springer, 1999.

[21] M. Born and V. Fock, "Beweis des Adiabatensatzes," *Zeitschrift für Physik*, vol. 51, pp. 165–180, Mar. 1928.

[22] T. Kato, "On the Adiabatic Theorem of Quantum Mechanics," *Journal of the Physical Society of Japan*, vol. 5, pp. 435–439, Nov. 1950.

[23] Z. Bian, F. Chudak, R. Israel, B. Lackey, W. G. Macready, and A. Roy, "Discrete optimization using quantum annealing on sparse Ising models," *Frontiers in Physics*, vol. 2, 2014. Publisher: Frontiers.

[24] "Digitized adiabatic quantum computing with a superconducting circuit | Nature."

[25] O. Abah and E. Lutz, "Energy efficient quantum machines," *EPL (Europhysics Letters)*, vol. 118, p. 40005, May 2017.

[26] N. V. Vitanov, A. A. Rangelov, B. W. Shore, and K. Bergmann, "Stimulated Raman adiabatic passage in physics, chemistry, and beyond," *Reviews of Modern Physics*, vol. 89, p. 015006, Mar. 2017.

[27] E. Farhi, J. Goldstone, S. Gutmann, J. Lapan, A. Lundgren, and D. Preda, "A Quantum Adiabatic Evolution Algorithm Applied to Random Instances of an NP-Complete Problem," *Science*, vol. 292, pp. 472–475, Apr. 2001.

[28] D. Comparat, "General conditions for quantum adiabatic evolution," *Physical Review A*, vol. 80, p. 012106, July 2009.

[29] M. S. Sarandy, L.-A. Wu, and D. A. Lidar, "Consistency of the Adiabatic Theorem," *Quantum Information Processing*, vol. 3, pp. 331–349, Dec. 2004.

[30] M. H. S. Amin, "Consistency of the adiabatic theorem," *Phys. Rev. Lett.*, vol. 102, p. 220401, Jun 2009.

[31] P. Deift, M. B. Ruskai, and W. Spitzer, "Improved gap estimates for simulating quantum circuits by adiabatic evolution," *Quantum Inf. Process.*, vol. 6, no. 2, pp. 121–125, 2007.

[32] J.-d. Wu, M.-s. Zhao, J.-l. Chen, and Y.-d. Zhang, "Adiabatic condition and quantum geometric potential," *Phys. Rev. A*, vol. 77, p. 062114, Jun 2008.

[33] S. Jansen, M.-B. Ruskai, and R. Seiler, "Bounds for the adiabatic approximation with applications to quantum computation," *J. Math. Phys.*, vol. 48, no. 10, p. 102111, 2007.

[34] D. M. Tong, K. Singh, L. C. Kwek, and C. H. Oh, "Sufficiency criterion for the validity of the adiabatic approximation," *Phys. Rev. Lett.*, vol. 98, p. 150402, Apr 2007.

[35] J.-d. Wu, M.-s. Zhao, J.-l. Chen, and Y.-d. Zhang, "Adiabatic approximation condition," *arXiv preprint arXiv:0706.0264*, 2007.

[36] J. Roland and N. J. Cerf, "Quantum search by local adiabatic evolution," *Physical Review A*, vol. 65, p. 042308, Mar. 2002.

[37] J. Lin, Z. Y. Lai, and X. Li, "Quantum adiabatic algorithm design using reinforcement learning," *Physical Review A*, vol. 101, p. 052327, May 2020.

[38] W. Zheng, Y. Zhang, Y. Dong, J. Xu, Z. Wang, X. Wang, Y. Li, D. Lan, J. Zhao, S. Li, X. Tan, and Y. Yu, "Optimal control of stimulated Raman adiabatic passage in a superconducting qudit," *arXiv:2111.10972 [quant-ph]*, Nov. 2021.

[39] S. Das, R. Kobes, and G. Kunstatter, "Energy and efficiency of adiabatic quantum search algorithms," *Journal of Physics A: Mathematical and General*, vol. 36, no. 11, pp. 2839–2845, 2003.

[40] A. T. Rezakhani, W.-J. Kuo, A. Hamma, D. A. Lidar, and P. Zanardi, "Quantum Adiabatic Brachistochrone," *Physical Review Letters*, vol. 103, p. 080502, Aug. 2009.

[41] A. C. Santos, C. J. Villas-Boas, and R. Bachelard, "Quantum adiabatic brachistochrone for open systems," *Physical Review A*, vol. 103, p. 012206, Jan. 2021.

[42] T. Albash and D. A. Lidar, "Adiabatic quantum computation," *Reviews of Modern Physics*, vol. 90, no. 1, p. 015002, 2018.

[43] N. G. Dickson, M. W. Johnson, M. H. Amin, R. Harris, F. Altomare, A. J. Berkley, P. Bunyk, J. Cai, E. M. Chapple, P. Chavez, F. Cioata, T. Cirip, P. deBuen, M. Drew-Brook, C. Enderud, S. Gildert, F. Hamze, J. P. Hilton, E. Hoskinson, K. Karimi, E. Ladizinsky, N. Ladizinsky, T. Lanting, T. Mahon, R. Neufeld, T. Oh, I. Perminov, C. Petroff, A. Przybysz, C. Rich, P. Spear, A. Tcaciuc, M. C. Thom, E. Tolkacheva, S. Uchaikin, J. Wang, A. B. Wilson, Z. Merali, and G. Rose, "Thermally assisted quantum annealing of a 16-qubit problem," *Nature Communications*, vol. 4, no. 1, p. 1903, 2013.

[44] A. D. King, J. Raymond, T. Lanting, S. V. Isakov, M. Mohseni, G. Poulin-Lamarre, S. Ejtemaee, W. Bernoudy, I. Ozfidan, A. Y. Smirnov, *et al.*, "Scaling advantage over path-integral monte carlo in quantum simulation of geometrically frustrated magnets," *Nature communications*, vol. 12, no. 1, pp. 1–6, 2021.

[45] A. Lucas, "Ising formulations of many np problems," *Frontiers in Physics*, vol. 2, p. 5, 2014.

[46] Y. Ding, X. Chen, L. Lamata, E. Solano, and M. Sanz, "Implementation of a hybrid classical-quantum annealing algorithm for logistic network design," *SN Computer Science*, vol. 2, no. 2, pp. 1–9, 2021.

[47] D-Wave: The Quantum Computing Company, "Getting started with the d-wave system: User manual," Mar 2020.

[48] D. Venturelli, D. Marchand, and G. Rojo, "Job shop scheduling solver based on quantum annealing," in *Proc. of ICAPS-16 Workshop on Constraint Satisfaction Techniques for Planning and Scheduling (COPLAS)*, pp. 25–34, 2016.

[49] C. C. Chang, A. Gambhir, T. S. Humble, and S. Sota, "Quantum annealing for systems of polynomial equations," *Scientific reports*, vol. 9, no. 1, pp. 1–9, 2019.

[50] J. D. Jackson, "Classical electrodynamics," 1999.

[51] M. O. Scully and M. S. Zubairy, *Quantum Optics*. Cambridge University Press, 1997.

[52] C. E. Máximo, P. P. de Souza, C. Ianzano, G. Rempe, R. Bachelard, and C. J. Villas-Boas, "Bright and dark states of light: The quantum origin of classical interference," *arXiv preprint arXiv:2112.05512*, 2021.

[53] P. J. P. Souza, T. M. Mendonça, E. V. B. d. Oliveira, C. J. Villas-Boas, P. J. P. Souza, T. M. Mendonça, E. V. B. d. Oliveira, and C. J. Villas-Boas, "Computação Quântica Adiabática: Do Teorema Adiabático ao Computador da D-Wave," *Revista Brasileira de Ensino de Física*, vol. 43, 2021.

[54] P. J. de Souza, "The thermodynamics of the travelling salesman problem," *arXiv preprint arXiv:2104.03922*, 2021.

[55] J. R. Mohallem and J. R. Mohallem, "Two helpful developments towards better understanding of adiabatic invariance in classical mechanics," *Revista Brasileira de Ensino de Física*, vol. 41, no. 2, 2019.

[56] G. F. L. Ferreira, "Adiabatic invariant generated by slow variation of a generalized coordinate," *Revista Brasileira de Ensino de Física*, vol. 26, pp. 415–417, Dec. 2004.

[57] A. Ambainis and O. Regev, "An Elementary Proof of the Quantum Adiabatic Theorem," *arXiv e-prints*, pp. quant–ph/0411152, Nov 2004.

[58] T. Kato, "On the adiabatic theorem of quantum mechanics," *Journal of the Physical Society of Japan*, vol. 5, no. 6, pp. 435–439, 1950.

[59] M. V. Berry, "Quantal phase factors accompanying adiabatic changes," *Proceedings of the Royal Society of London. A. Mathematical and Physical Sciences*, vol. 392, no. 1802, pp. 45–57, 1984.

[60] C. S. Kahane, "Generalizations of the Riemann-Lebesgue and Cantor-Lebesgue lemmas," *Czechoslovak Mathematical Journal*, vol. 30, no. 1, pp. 108–117, 1980.

[61] D. M. Tong, K. Singh, L. C. Kwek, and C. H. Oh, "Sufficiency Criterion for the Validity of the Adiabatic Approximation," *Physical Review Letters*, vol. 98, p. 150402, Apr. 2007.

[62] M. d. I. Herrera, "Galileo, Bernoulli, Leibniz and Newton around the brachistochrone problem," *Revista Mexicana de Física*, vol. 40, pp. 459–475, Jan. 1993.

[63] H. H. Goldstine, *A History of the Calculus of Variations from the 17th through the 19th Century*. Springer Science & Business Media, Dec. 2012.

[64] N. A. Lemos, *Mecânica Analítica*. Editora Livraria da Fisica, 2007.

[65] I. M. Gelfand, S. V. Fomin, and R. A. Silverman, *Calculus of Variations*. Courier Corporation, Jan. 2000.

[66] P. Benioff, "The computer as a physical system: A microscopic quantum mechanical hamiltonian model of computers as represented by turing machines," *Journal of statistical physics*, vol. 22, no. 5, pp. 563–591, 1980.

[67] R. P. Feynman, "Simulating physics with computers," *Int. J. Theor. Phys*, vol. 21, no. 6/7, 1982.

[68] Y. Manin, "Computable and uncomputable," *Sovetskoye Radio, Moscow*, vol. 128, 1980.

[69] M. A. Nielsen and I. Chuang, *Quantum computation and quantum information*. American Association of Physics Teachers, 2002.

[70] J.-H. Bae, P. M. Alsing, D. Ahn, and W. A. Miller, "Quantum circuit optimization using quantum karnaugh map," *Sci. Rep.*, vol. 10, no. 1, pp. 1–8, 2020.

[71] L. Gyongyosi, "Quantum state optimization and computational pathway evaluation for gate-model quantum computers," *Sci. Rep.*, vol. 10, no. 1, p. 4543, 2020.

[72] L. Gyongyosi and S. Imre, "Circuit depth reduction for gate-model quantum computers," *Scientific Reports*, vol. 10, no. 1, p. 11229, 2020.

[73] J. I. Cirac and P. Zoller, "A scalable quantum computer with ions in an array of microtraps," *Nature*, vol. 404, no. 6778, pp. 579–581, 2000.

[74] S. Takeda and A. Furusawa, "Toward large-scale fault-tolerant universal photonic quantum computing," *APL Photonics*, vol. 4, no. 6, p. 060902, 2019.

[75] J. Alicea, Y. Oreg, G. Refael, F. Von Oppen, and M. P. Fisher, "Non-abelian statistics and topological quantum information processing in 1d wire networks," *Nature Physics*, vol. 7, no. 5, pp. 412–417, 2011.

[76] P. W. Shor, "Algorithms for quantum computation: discrete logarithms and factoring," in *Proceedings 35th annual symposium on foundations of computer science*, pp. 124–134, Ieee, 1994.

[77] L. K. Grover, "Quantum mechanics helps in searching for a needle in a haystack," *Physical review letters*, vol. 79, no. 2, p. 325, 1997.

[78] T. Albash and D. A. Lidar, "Adiabatic quantum computation," *Reviews of Modern Physics*, vol. 90, p. 015002, Jan. 2018.

[79] E. Farhi, J. Goldstone, S. Gutmann, and M. Sipser, "Quantum Computation by Adiabatic Evolution," *arXiv:quant-ph/0001106*, 2000.

[80] D. Aharonov, W. van Dam, J. Kempe, Z. Landau, S. Lloyd, and O. Regev, "Adiabatic quantum computation is equivalent to standard quantum computation," in *45th Annual IEEE Symposium on Foundations of Computer Science*, pp. 42–51, Oct 2004.

[81] M. Born and V. Fock, "Beweis des adiabatensatzes," *Zeitschrift für Physik A Hadrons and Nuclei*, vol. 51, no. 3, p. 165, 1928.

[82] S. Boixo, T. F. Rønnow, S. V. Isakov, Z. Wang, D. Wecker, D. A. Lidar, J. M. Martinis, and M. Troyer, "Evidence for quantum annealing with more than one hundred qubits," *Nature Physics*, vol. 10, pp. 218–224, Mar. 2014.

[83] A. D. King, J. Raymond, T. Lanting, S. V. Isakov, M. Mohseni, G. Poulin-Lamarre, S. Ejtemaee, W. Bernoudy, I. Ozfidan, A. Y. Smirnov, M. Reis, F. Altomare, M. Babcock, C. Baron, A. J. Berkley, K. Boothby, P. I. Bunyk, H. Christiani, C. Enderud, B. Evert, R. Harris, E. Hoskinson, S. Huang, K. Jooya, A. Khodabandelou, N. Ladizinsky, R. Li, P. A. Lott, A. J. R. MacDonald, D. Marsden, G. Marsden, T. Medina, R. Molavi, R. Neufeld, M. Norouzpour, T. Oh, I. Pavlov, I. Perminov, T. Prescott, C. Rich, Y. Sato, B. Sheldan, G. Sterling, L. J. Swenson, N. Tsai, M. H. Volkmann, J. D. Whittaker, W. Wilkinson, J. Yao, H. Neven, J. P. Hilton, E. Ladizinsky, M. W. Johnson, and M. H. Amin, "Scaling advantage over path-integral Monte Carlo in quantum simulation of geometrically frustrated magnets," *Nature Communications*, vol. 12, no. 1, p. 1113, 2021.

[84] E. Farhi and S. Gutmann, "Analog analogue of a digital quantum computation," *Physical Review A*, vol. 57, pp. 2403–2406, Apr. 1998.

[85] I. B. Coulamy, "Adiabatic dynamics and shortcuts to adiabaticity in many-body systems," 2018.

[86] A. Mitra, A. Ghosh, R. Das, A. Patel, and A. Kumar, "Experimental implementation of local adiabatic evolution algorithms by an nmr quantum information processor," *Journal of Magnetic Resonance*, vol. 177, no. 2, pp. 285–298, 2005.

[87] I. Hen, "Realizable quantum adiabatic search," *EPL (Europhysics Letters)*, vol. 118, no. 3, p. 30003, 2017.

[88] A. Rezakhani, W.-J. Kuo, A. Hamma, D. Lidar, and P. Zanardi, "Quantum adiabatic brachistochrone," *Physical review letters*, vol. 103, no. 8, p. 080502, 2009.

[89] K. Takahashi, "Hamiltonian Engineering for Adiabatic Quantum Computation: Lessons from Shortcuts to Adiabaticity," *Journal of the Physical Society of Japan*, vol. 88, p. 061002, Mar. 2019. Publisher: The Physical Society of Japan.

[90] P. Virtanen, R. Gommers, T. E. Oliphant, M. Haberland, T. Reddy, D. Cournapeau, E. Burovski, P. Peterson, W. Weckesser, J. Bright, S. J. van der Walt, M. Brett, J. Wilson, K. J. Millman, N. Mayorov, A. R. J. Nelson, E. Jones, R. Kern, E. Larson, C. J. Carey, İ. Polat, Y. Feng, E. W. Moore, J. VanderPlas, D. Laxalde, J. Perktold, R. Cimrman, I. Henriksen, E. A. Quintero, C. R. Harris, A. M. Archibald, A. H. Ribeiro, F. Pedregosa, P. van Mulbregt, and SciPy 1.0 Contributors, "SciPy 1.0: Fundamental Algorithms for Scientific Computing in Python," *Nature Methods*, vol. 17, pp. 261–272, 2020.

[91] I. B. Coulamy, A. C. Santos, I. Hen, and M. S. Sarandy, "Energetic Cost of Superadiabatic Quantum Computation," *Frontiers in ICT*, vol. 3, 2016.

[92] M. Kieferová and N. Wiebe, "On the power of coherently controlled quantum adiabatic evolutions," *New Journal of Physics*, vol. 16, no. 12, p. 123034, 2014.

[93] Y. Zheng, S. Campbell, G. De Chiara, and D. Poletti, "Cost of counterdiabatic driving and work output," *Physical Review A*, vol. 94, no. 4, p. 042132, 2016.

[94] G. Wendin, "Quantum information processing with superconducting circuits: a review," *Reports on Progress in Physics*, vol. 80, no. 10, p. 106001, 2017.

[95] V. Giovannetti, S. Lloyd, and L. Maccone, "Advances in quantum metrology," *Nature Photonics*, vol. 5, no. 4, pp. 222–229, 2011.

[96] R. Schnabel, N. Mavalvala, D. E. McClelland, and P. K. Lam, "Quantum metrology for gravitational wave astronomy," *Nature Communications*, vol. 1, no. 1, p. 121, 2010.

[97] J. Yin, Y.-H. Li, S.-K. Liao, M. Yang, Y. Cao, L. Zhang, J.-G. Ren, W.-Q. Cai, W.-Y. Liu, S.-L. Li, R. Shu, Y.-M. Huang, L. Deng, L. Li, Q. Zhang, N.-L. Liu, Y.-A. Chen, C.-Y. Lu, X.-B. Wang, F. Xu, J.-Y. Wang, C.-Z. Peng, A. K. Ekert, and J.-W. Pan, "Entanglement-based secure quantum cryptography over 1,120 kilometres," *Nature*, vol. 582, pp. 501–505, June 2020.

[98] R. P. Feynman, "Simulating Physics with Computers," in *Feynman and Computation*, CRC Press, 2002.

[99] B. Çakmak, "Ergotropy from coherences in an open quantum system," *Physical Review E*, vol. 102, no. 4, p. 042111, 2020.

[100] A. C. Santos, "Quantum advantage of two-level batteries in the self-discharging process," *Physical Review E*, vol. 103, no. 4, p. 042118, 2021.

[101] A. C. Santos, A. Saguia, and M. S. Sarandy, "Stable and charge-switchable quantum batteries," *Physical Review E*, vol. 101, no. 6, p. 062114, 2020.

[102] A. E. Allahverdyan, R. Balian, and T. M. Nieuwenhuizen, "Maximal work extraction from finite quantum systems," *Europhysics Letters*, vol. 67, p. 565, Aug. 2004. Publisher: IOP Publishing.

[103] H.-P. Breuer and F. Petruccione, *The Theory of Open Quantum Systems*. Oxford: Oxford University Press, 2007.

[104] H. Goldstein, C. Poole, and J. Safko, "Classical mechanics," 2002.

[105] J. R. Banga, "Optimization in computational systems biology," *BMC systems biology*, vol. 2, no. 1, p. 47, 2008.

[106] H. A. Taha, *Operations research: an introduction*. Pearson Education India, 2013.

[107] T. Benoist, F. Gardi, A. Jeanjean, and B. Estellon, "Randomized local search for real-life inventory routing," *Transportation Science*, vol. 45, no. 3, pp. 381–398, 2011.

[108] D. L. Applegate, R. E. Bixby, V. Chvatal, and W. J. Cook, *The traveling salesman problem: a computational study*. Princeton university press, 2006.

[109] J. A. Carlson, A. Jaffe, and A. Wiles, *The millennium prize problems*. Citeseer, 2006.

[110] F. R. Cardoso, D. Y. Akamatsu, V. L. Campo Junior, E. I. Duzzioni, A. Jaramillo, and C. J. Villas-Boas, "Detailed account of complexity for implementation of circuit-based quantum algorithms," *Frontiers in Physics*, p. 582, 2021.

[111] "Material suplementar códigos." https://github.com/PauloJPS/QuantumAnnealing. Accessed: 18/01/2021.

[112] "Ms windows nt kernel description." https://aws.amazon.com/pt/braket/, 2022. Accessed: 2022-01-11.

[113] P. J. Van Laarhoven and E. H. Aarts, "Simulated annealing," in *Simulated annealing: Theory and applications*, pp. 7–15, Springer, 1987.

[114] J. De Vicente, J. Lanchares, and R. Hermida, "Placement by thermodynamic simulated annealing," *Physics Letters A*, vol. 317, no. 5-6, pp. 415–423, 2003.

[115] D. Aharonov, W. Van Dam, J. Kempe, Z. Landau, S. Lloyd, and O. Regev, "Adiabatic quantum computation is equivalent to standard quantum computation," *SIAM review*, vol. 50, no. 4, pp. 755–787, 2008.

[116] B. Apolloni, C. Carvalho, and D. de Falco, "Quantum stochastic optimization," *Stochastic Processes and their Applications*, vol. 33, pp. 233–244, Dec. 1989.

[117] A. Das and B. K. Chakrabarti, *Quantum annealing and related optimization methods*, vol. 679. Springer Science & Business Media, 2005.

[118] S. Morita and H. Nishimori, "Mathematical foundation of quantum annealing," *Journal of Mathematical Physics*, vol. 49, no. 12, p. 125210, 2008.

[119] D. Drung, C. Abmann, J. Beyer, A. Kirste, M. Peters, F. Ruede, and T. Schurig, "Highly sensitive and easy-to-use squid sensors," *IEEE Transactions on Applied Superconductivity*, vol. 17, no. 2, pp. 699–704, 2007.

[120] R. Harris, J. Johansson, A. Berkley, M. Johnson, T. Lanting, S. Han, P. Bunyk, E. Ladizinsky, T. Oh, I. Perminov, *et al.*, "Experimental demonstration of a robust and scalable flux qubit," *Physical Review B*, vol. 81, no. 13, p. 134510, 2010.

[121] R. Jaklevic, J. Lambe, A. Silver, and J. Mercereau, "Quantum interference effects in josephson tunneling," *Physical Review Letters*, vol. 12, no. 7, p. 159, 1964.

[122] R. Harris, T. Lanting, A. Berkley, J. Johansson, M. Johnson, P. Bunyk, E. Ladizinsky, N. Ladizinsky, T. Oh, and S. Han, "Compound josephson-junction coupler for flux qubits with minimal crosstalk," *Physical Review B*, vol. 80, no. 5, p. 052506, 2009.

[123] V. Choi, "Minor-embedding in adiabatic quantum computation: I. the parameter setting problem," *Quantum Information Processing*, vol. 7, no. 5, pp. 193–209, 2008.

[124] M. S. Könz, W. Lechner, H. G. Katzgraber, and M. Troyer, "Embedding Overhead Scaling of Optimization Problems in Quantum Annealing," *PRX Quantum*, vol. 2, p. 040322, Nov. 2021. Publisher: American Physical Society.

[125] M. Ohzeki, A. Miki, M. J. Miyama, and M. Terabe, "Control of automated guided vehicles without collision by quantum annealer and digital devices," *arXiv preprint arXiv:1812.01532*, 2018.

[126] R. H. Warren, "Solving the traveling salesman problem on a quantum annealer," *SN Applied Sciences*, vol. 2, no. 1, p. 75, 2020.

[127] M. Herrero-Collantes and J. C. Garcia-Escartin, "Quantum random number generators," *Reviews of Modern Physics*, vol. 89, no. 1, p. 015004, 2017.

[128] "D-wave power consumption." https://www.dwavesys.com/sites/default/files/14-1005A_D_wp_Computational_Power_Consumption_and_Speedup.pdf. Acessado: 5/10/2020.

[129] "Dwave leap." https://cloud.dwavesys.com/leap/login/?next=/leap/. Accessed: 2022-01-11.

[130] R. Matai, S. P. Singh, and M. L. Mittal, "Traveling salesman problem: an overview of applications, formulations, and solution approaches," *Traveling salesman problem, theory and applications*, vol. 1, 2010.

[131] M. Held and R. M. Karp, "A dynamic programming approach to sequencing problems," *Journal of the Society for Industrial and Applied mathematics*, vol. 10, no. 1, pp. 196–210, 1962.

[132] D. L. Applegate, R. E. Bixby, V. Chvátal, W. Cook, D. G. Espinoza, M. Goycoolea, and K. Helsgaun, "Certification of an optimal tsp tour through 85,900 cities," *Operations Research Letters*, vol. 37, no. 1, pp. 11–15, 2009.

[133] C. Rego, D. Gamboa, F. Glover, and C. Osterman, "Traveling salesman problem heuristics: Leading methods, implementations and latest advances," *European Journal of Operational Research*, vol. 211, no. 3, pp. 427–441, 2011.

[134] D. J. Moylett, N. Linden, and A. Montanaro, "Quantum speedup of the traveling-salesman problem for bounded-degree graphs," *Physical Review A*, vol. 95, no. 3, p. 032323, 2017.

[135] C. Papalitsas, T. Andronikos, K. Giannakis, G. Theocharopoulou, and S. Fanarioti, "A qubo model for the traveling salesman problem with time windows," *Algorithms*, vol. 12, no. 11, p. 224, 2019.

[136] Y. Usami and M. Kitaoka, "Traveling salesman problem and statistical physics," *International Journal of Modern Physics B*, vol. 11, no. 13, pp. 1519–1544, 1997.

[137] J. H. Holland *et al.*, *Adaptation in natural and artificial systems: an introductory analysis with applications to biology, control, and artificial intelligence*. MIT press, 1992.

[138] E. Goldbarg, M. Goldbarg, and H. Luna, *Otimização Combinatória e Metaheurísticas: Algoritmos e Apliacações*. Elsevier Brasil, 2017.

[139] R. Rubinstein, "The cross-entropy method for combinatorial and continuous optimization," *Methodology and computing in applied probability*, vol. 1, no. 2, pp. 127–190, 1999.

[140] D. Delahaye, S. Chaimatanan, and M. Mongeau, "Simulated annealing: From basics to applications," in *Handbook of Metaheuristics*, pp. 1–35, Springer, 2019.

[141] S. Kirkpatrick, C. D. Gelatt, and M. P. Vecchi, "Optimization by simulated annealing," *science*, vol. 220, no. 4598, pp. 671–680, 1983.

[142] V. Černỳ, "Thermodynamical approach to the traveling salesman problem: An efficient simulation algorithm," *Journal of optimization theory and applications*, vol. 45, no. 1, pp. 41–51, 1985.

[143] D. Henderson, S. H. Jacobson, and A. W. Johnson, "The theory and practice of simulated annealing," in *Handbook of metaheuristics*, pp. 287–319, Springer, 2003.

[144] D. Bertsimas, J. Tsitsiklis, *et al.*, "Simulated annealing," *Statistical science*, vol. 8, no. 1, pp. 10–15, 1993.

[145] R. Chibante, *Simulated annealing: theory with applications*. BoD–Books on Demand, 2010.

[146] T. Tomé and M. J. de Oliveira, *Dinâmica estocástica e irreversibilidade*, ch. 5, pp. 88–89. Edusp, 2001.

[147] L. Onsager, "Reciprocal relations in irreversible processes. i.," *Physical review*, vol. 37, no. 4, p. 405, 1931.

[148] M. J. de Oliveira, *Dinâmica Estocástica e Irreversibilidade Vol. 35*. EdUSP, 2001.

[149] V. L. Líbero, "De ising a metropolis," *Revista Brasileira de Ensino de Física*, vol. 22, no. 3, pp. 346–352, 2000.

[150] K. Binder, D. M. Ceperley, J.-P. Hansen, M. Kalos, D. Landau, D. Levesque, H. Mueller-Krumbhaar, D. Stauffer, and J.-J. Weis, *Monte Carlo methods in statistical physics*, vol. 7. Springer Science & Business Media, 2012.

[151] T. Tomé, *Dinâmica Estocástica e Irreversibilidade Vol. 35*. Edusp, 2001.

[152] J. Deng, L. Chen, H. Chen, and M. Chen, "A reliable solver of regular-grid travelling salesman problems: double threshold accepting for schedule planning optimisation with unified pattern of normalised threshold values," *The International Journal of Advanced Manufacturing Technology*, vol. 21, no. 12, pp. 985–994, 2003.

[153] R. J. Glauber, "The quantum theory of optical coherence," *Physical Review*, vol. 130, no. 6, p. 2529, 1963.

[154] L. Mandel and E. Wolf, *Optical Coherence and Quantum Optics*. Cambridge University Press, 1995.

[155] W. P. Schleich, *Quantum Optics in Phase Space*. Wiley-VCH, New York, 2001.

[156] D. F. Walls and G. J. Milburn, *Quantum optics*. Springer Science & Business Media, 2007.

[157] R. J. Glauber, "Coherent and incoherent states of the radiation field," *Phys. Rev.*, vol. 131, pp. 2766–2788, Sep 1963.

[158] C. E. Máximo, T. B. B. ao, R. Bachelard, G. D. de Moraes Neto, M. A. de Ponte, and M. H. Y. Moussa, "Quantum atomic lithography via cross-cavity optical stern–gerlach setup," *J. Opt. Soc. Am. B*, vol. 31, pp. 2480–2484, Oct 2014.

[159] C. E. Máximo, R. Bachelard, G. D. de Moraes Neto, and M. H. Y. Moussa, "Entanglement detection via atomic deflection," *J. Opt. Soc. Am. B*, vol. 34, pp. 2452–2458, Dec 2017.

[160] R. H. Dicke, "Coherence in spontaneous radiation processes," *Phys. Rev.*, vol. 93, pp. 99–110, Jan 1954.

[161] M. Delanty, S. Rebic, and J. Twamley, "Superradiance of harmonic oscillators," 2011.

[162] E. Jaynes and F. Cummings, "Comparison of quantum and semiclassical radiation theories with application to the beam maser," *Proceedings of the IEEE*, vol. 51, no. 1, pp. 89–109, 1963.

[163] M. Gross and S. Haroche, "Superradiance: An essay on the theory of collective spontaneous emission," *Physics Reports*, vol. 93, pp. 301–396, Dec. 1982.

[164] A. Zavatta, S. Viciani, and M. Bellini, "Quantum-to-classical transition with single-photon-added coherent states of light," *Science*, vol. 306, no. 5696, pp. 660–662, 2004.

[165] V. Parigi, A. Zavatta, M. Kim, and M. Bellini, "Probing quantum commutation rules by addition and subtraction of single photons to/from a light field," *Science*, vol. 317, no. 5846, pp. 1890–1893, 2007.

[166] C. Cohen-Tannoudji, "Atomic motion in laser light," in *Fundamental Systems in Quantum Optics* (J. Dalibard, J. M. Raimond, and J. Zinn-Justin, eds.), p. 1, Elsevier Science Publisher, 1992. Les Houches, Session LIII, 1990.

[167] K. Murr, P. Maunz, P. W. H. Pinkse, T. Puppe, I. Schuster, D. Vitali, and G. Rempe, "Momentum diffusion for coupled atom-cavity oscillators," *Phys. Rev. A*, vol. 74, p. 043412, Oct 2006.

[168] A. Piñeiro Orioli and A. M. Rey, "Dark states of multilevel fermionic atoms in doubly filled optical lattices," *Phys. Rev. Lett.*, vol. 123, p. 223601, Nov 2019.

[169] M. Fleischhauer, A. Imamoglu, and J. P. Marangos, "Electromagnetically induced transparency: Optics in coherent media," *Rev. Mod. Phys.*, vol. 77, pp. 633–673, Jul 2005.

[170] C. Hamsen, K. N. Tolazzi, T. Wilk, and G. Rempe, "Strong coupling between photons of two light fields mediated by one atom," *Nature Physics*, vol. 14, no. 9, pp. 885–889, 2018.

[171] M. Brekenfeld, D. Niemietz, J. D. Christesen, and G. Rempe, "A quantum network node with crossed optical fibre cavities," *Nature Physics*, pp. 647–651, 2020.

[172] A. Mokhberi, M. Hennrich, and F. Schmidt-Kaler, "Chapter four - trapped rydberg ions: A new platform for quantum information processing," vol. 69 of *Advances In Atomic, Molecular, and Optical Physics*, pp. 233–306, Academic Press, 2020.

[173] A. Blais, A. L. Grimsmo, S. M. Girvin, and A. Wallraff, "Circuit quantum electrodynamics," *Rev. Mod. Phys.*, vol. 93, p. 025005, May 2021.

[174] F. O. Prado, E. I. Duzzioni, M. H. Y. Moussa, N. de Almeida, and C. J. Villas-Bôas, "Nonadiabatic coherent evolution of two-level systems under spontaneous decay," *Physical review letters*, vol. 102, no. 7, p. 073008, 2009.

[175] F. Prado, N. de Almeida, E. Duzzioni, M. Moussa, and C. Villas-Boas, "Decoherence-free evolution of time-dependent superposition states of two-level systems and thermal effects," *Physical Review A*, vol. 84, no. 1, p. 012112, 2011.

[176] F. O. Prado, N. G. de Almeida, M. H. Y. Moussa, and C. J. Villas-Bôas, "Bilinear and quadratic hamiltonians in two-mode cavity quantum electrodynamics," *Phys. Rev. A*, vol. 73, p. 043803, Apr 2006.

[177] M. Srinivas and E. Davies, "Photon counting probabilities in quantum optics," *Optica Acta: International Journal of Optics*, vol. 28, no. 7, pp. 981–996, 1981.

[178] A. V. Dodonov, S. S. Mizrahi, and V. V. Dodonov, "Microscopic models of quantum-jump superoperators," *Phys. Rev. A*, vol. 72, p. 023816, Aug 2005.

[179] A. Reiserer and G. Rempe, "Cavity-based quantum networks with single atoms and optical photons," *Rev. Mod. Phys.*, vol. 87, pp. 1379–1418, Dec 2015.

[180] A. Blais, A. L. Grimsmo, S. M. Girvin, and A. Wallraff, "Circuit quantum electrodynamics," *Rev. Mod. Phys.*, vol. 93, p. 025005, May 2021.

[181] K. Zhang, H. Li, P. Zhang, J. Yuan, J. Chen, W. Ren, Z. Wang, C. Song, D.-W. Wang, H. Wang, *et al.*, "Synthesizing five-body interaction in a superconducting quantum circuit," *arXiv preprint arXiv:2109.00964*, 2021.

[182] Y. Arakawa and M. J. Holmes, "Progress in quantum-dot single photon sources for quantum information technologies: A broad spectrum overview," *Applied Physics Reviews*, vol. 7, p. 021309, June 2020.

[183] G. S. Vasilev, D. Ljunggren, and A. Kuhn, "Single photons made-to-measure," *New Journal of Physics*, vol. 12, p. 063024, June 2010.

[184] H. P. Specht, C. Nölleke, A. Reiserer, M. Uphoff, E. Figueroa, S. Ritter, and G. Rempe, "A single-atom quantum memory," *Nature*, vol. 473, pp. 190–193, May 2011.

[185] X. Maître, E. Hagley, G. Nogues, C. Wunderlich, P. Goy, M. Brune, J. M. Raimond, and S. Haroche, "Quantum Memory with a Single Photon in a Cavity," *Physical Review Letters*, vol. 79, pp. 769–772, July 1997.

[186] C. A. Brasil, F. F. Fanchini, and R. d. J. Napolitano, "A simple derivation of the Lindblad equation," *Revista Brasileira de Ensino de Física*, vol. 35, pp. 01–09, Mar. 2013.

APPENDIX A – Second derivative test

The solution of the Euler-Lagrange equations give us functions that *extremises* the functional. However, we can not say if the solution is a local minimum, a local maximum or a saddle point. For getting this information it is necessary to apply the second derivative test. We have to evaluate the equation

$$\begin{aligned}\frac{\mathrm{d}^2\xi}{\mathrm{d}\epsilon^2} &= \int_a^b \frac{\mathrm{d}}{\mathrm{d}\epsilon}\left(\frac{\partial f}{\partial q}\frac{\mathrm{d}\bar{q}}{\mathrm{d}\epsilon}+\frac{\partial f}{\partial q'}\frac{\mathrm{d}\bar{q}'}{\mathrm{d}\epsilon}\right)\mathrm{d}s \\ &= \int_a^b \left[\frac{\mathrm{d}\bar{q}}{\mathrm{d}\epsilon}\frac{\mathrm{d}}{\mathrm{d}\epsilon}\left(\frac{\partial f}{\partial q}\right)+\frac{\partial f}{\partial q}\frac{\mathrm{d}^2\bar{q}}{\mathrm{d}\epsilon^2}+\frac{\mathrm{d}\bar{q}'}{\mathrm{d}\epsilon}\frac{\mathrm{d}}{\mathrm{d}\epsilon}\left(\frac{\partial f}{\partial q'}\right)+\frac{\partial f}{\partial q'}\frac{\mathrm{d}^2\bar{q}'}{\mathrm{d}\epsilon^2}\right]\mathrm{d}s \\ &= \int_a^b \left[\eta\frac{\mathrm{d}}{\mathrm{d}\epsilon}\left(\frac{\partial f}{\partial q}\right)+\eta'\frac{\mathrm{d}}{\mathrm{d}\epsilon}\left(\frac{\partial f}{\partial q'}\right)\right]\mathrm{d}s\ ,\end{aligned} \tag{A.1}$$

where we used that $\mathrm{d}^2\bar{q}/\mathrm{d}\epsilon^2 = \mathrm{d}^2\bar{q}'/\mathrm{d}\epsilon^2 = 0$, due to the definition. Now, applying the chain rule,

$$\begin{aligned}\frac{\mathrm{d}^2\xi}{\mathrm{d}\epsilon^2} &= \int_a^b \left[\frac{\mathrm{d}\bar{q}}{\mathrm{d}\epsilon}\frac{\mathrm{d}}{\mathrm{d}\epsilon}\left(\frac{\partial f}{\partial \bar{q}}\right)+\frac{\mathrm{d}\bar{q}'}{\mathrm{d}\epsilon}\frac{\mathrm{d}}{\mathrm{d}\epsilon}\left(\frac{\partial f}{\partial \bar{q}'}\right)\right]\mathrm{d}s\ , \\ &= \int_a^b \left[\eta\frac{\mathrm{d}}{\mathrm{d}\epsilon}\left(\frac{\partial f}{\partial \bar{q}}\right)+\eta'\frac{\mathrm{d}}{\mathrm{d}\epsilon}\left(\frac{\partial f}{\partial \bar{q}'}\right)\right]\mathrm{d}s\ , \\ &= \int_a^b \left[\eta\left(\frac{\partial^2 f}{\partial \bar{q}^2}\frac{\mathrm{d}\bar{q}}{\mathrm{d}\epsilon}+\frac{\partial^2 f}{\partial \bar{q}\partial \bar{q}'}\frac{\mathrm{d}\bar{q}'}{\mathrm{d}\epsilon}\right)+\eta'\left(\frac{\partial^2 f}{\partial \bar{q}'^2}\frac{\mathrm{d}\bar{q}'}{\mathrm{d}\epsilon}+\frac{\partial^2 f}{\partial \bar{q}'\partial \bar{q}}\frac{\mathrm{d}\bar{q}}{\mathrm{d}\epsilon}\right)\right]\mathrm{d}s\ , \\ &= \int_a^b \left[\eta\left(\frac{\partial^2 f}{\partial \bar{q}^2}\eta+\frac{\partial^2 f}{\partial \bar{q}\partial \bar{q}'}\eta'\right)+\eta'\left(\frac{\partial^2 f}{\partial \bar{q}'^2}\eta+\frac{\partial^2 f}{\partial \bar{q}'\partial \bar{q}}\eta'\right)\right]\mathrm{d}s\ , \\ &= \int_a^b \left[\frac{\partial^2 f}{\partial \bar{q}^2}\eta^2+2\eta\eta'\frac{\partial^2 f}{\partial \bar{q}\partial \bar{q}'}+\eta'^2\frac{\partial^2 f}{\partial \bar{q}'^2}+\right]\mathrm{d}s\ .\end{aligned} \tag{A.2}$$

Evaluating the equation when $\epsilon = 0$ we find

$$\left.\frac{\mathrm{d}^2\xi}{\mathrm{d}\epsilon^2}\right|_{\epsilon=0} = \int_a^b \left[\frac{\partial^2 f}{\partial q^2}\eta^2+2\eta\eta'\frac{\partial^2 f}{\partial q\partial q'}+\eta'^2\frac{\partial^2 f}{\partial q'^2}+\right]\mathrm{d}s\ . \tag{A.3}$$

An important difference that appears in the second derivative of the functional is the persistent dependency on η. In this case, it is necessary to evaluate $\mathrm{d}^2\xi/\mathrm{d}\epsilon^2|_{\epsilon=0}$ for every function in the set of functions that satisfy the boundary conditions of the problem. Thus, calculating the second derivative test is a task that is possible to do analytically for few cases.

The meaning of the functional value fallows the idea of the second derivative test in multi-variable calculus. For understanding it better, we can use a Taylor's expansion for functionals

$$A[q(s)+\epsilon\eta(s)] = A[q(s)] + \left.\frac{\mathrm{d}A[q(s)]}{\mathrm{d}\epsilon}\right|_{\epsilon=0} + \frac{1}{2!}\left.\frac{\mathrm{d}^2A[q(s)+\epsilon\eta]}{\mathrm{d}\epsilon^2}\right|_{\epsilon=0} + \cdots \ . \tag{A.4}$$

Since we q is a extremum of $A[q(s)]$, we can write

$$A[q(s)+\epsilon\eta(s)] - A[q(s)] \approx \frac{1}{2!}\left.\frac{\mathrm{d}^2A[q(s)+\epsilon\eta]}{\mathrm{d}\epsilon^2}\right|_{\epsilon=0} \ . \tag{A.5}$$

Then

- if $\mathrm{d}^2_\epsilon\xi > 0$, q and q' are, at least, a local minimum of f ,
- if $\mathrm{d}^2_\epsilon\xi < 0$, q and q' are, at least, a local maximum of f ,
- if $\mathrm{d}^2_\epsilon\xi = 0$, q and q' are a saddle 'point' of f ,

where $\mathrm{d}^2_\epsilon\xi = (\mathrm{d}^2\xi/\mathrm{d}\epsilon^2)_{\epsilon=0}$.

APPENDIX B – Beltrami Identity

We will now prove the Beltrami identity that is a relation useful when there is no explicit time dependence in the functional. Let us take the Euler-Lagrange equations

$$\frac{\mathrm{d}}{\mathrm{d}t}\frac{\partial \mathcal{L}}{\partial \dot{q}} - \frac{\partial \mathcal{L}}{\partial q} = 0 \ . \tag{B.1}$$

We can multiply it by $\dot{q}$,

$$\dot{q}\frac{\mathrm{d}}{\mathrm{d}t}\frac{\partial \mathcal{L}}{\partial \dot{q}} - \dot{q}\frac{\partial \mathcal{L}}{\partial q} = 0 \tag{B.2}$$

The chain rule states that

$$\frac{\mathrm{d}\mathcal{L}}{\mathrm{d}t} = \frac{\partial \mathcal{L}}{\partial q}\dot{q} + \frac{\partial \mathcal{L}}{\partial \dot{q}}\ddot{q} + \frac{\partial \mathcal{L}}{\partial t} \ , \tag{B.3}$$

and we can write

$$\dot{q}\frac{\partial \mathcal{L}}{\partial q} = \frac{\mathrm{d}\mathcal{L}}{\mathrm{d}t} - \frac{\partial \mathcal{L}}{\partial \dot{q}}\ddot{q} - \frac{\partial \mathcal{L}}{\partial t} \ , \tag{B.4}$$

Now, substituting Eq. (B.4) in Eq. (B.2), we get

$$\dot{q}\frac{\mathrm{d}}{\mathrm{d}t}\frac{\partial \mathcal{L}}{\partial \dot{q}} = \frac{\mathrm{d}\mathcal{L}}{\mathrm{d}t} - \frac{\partial \mathcal{L}}{\partial \dot{q}}\ddot{q} - \frac{\partial \mathcal{L}}{\partial t} \ , \tag{B.5}$$

but we can express the left-handed size of this equation as

$$\frac{\mathrm{d}}{\mathrm{d}t}\left(\frac{\partial \mathcal{L}}{\partial \dot{q}}\dot{q}\right) = \dot{q}\frac{\mathrm{d}}{\mathrm{d}t}\frac{\partial \mathcal{L}}{\partial \dot{q}} + \frac{\partial \mathcal{L}}{\partial \dot{q}}\ddot{q} \ . \tag{B.6}$$

Therefore, the Euler-Lagrange equation becomes

$$\begin{aligned} \frac{\mathrm{d}}{\mathrm{d}t}\left(\frac{\partial \mathcal{L}}{\partial \dot{q}}\dot{q}\right) - \frac{\partial \mathcal{L}}{\partial \dot{q}}\ddot{q} &= \frac{\mathrm{d}\mathcal{L}}{\mathrm{d}t} - \frac{\partial \mathcal{L}}{\partial \dot{q}}\ddot{q} - \frac{\partial \mathcal{L}}{\partial t} \\ \frac{\mathrm{d}}{\mathrm{d}t}\left(\frac{\partial \mathcal{L}}{\partial \dot{q}}\dot{q}\right) &= \frac{\mathrm{d}\mathcal{L}}{\mathrm{d}t} - \frac{\partial \mathcal{L}}{\partial t} \\ \frac{\mathrm{d}}{\mathrm{d}t}\left(\mathcal{L} - \frac{\partial \mathcal{L}}{\partial \dot{q}}\dot{q}\right) &= \frac{\partial \mathcal{L}}{\partial t} \ . \end{aligned} \tag{B.7}$$

This a form to express the Euler-Lagrange equation. However, if $\mathcal{L}$ is not explicit time dependent, *i.e* $\mathcal{L} = \mathcal{L}(q(t), \dot{q}(t))$ the motion equation becomes

$$\begin{aligned} \frac{\mathrm{d}}{\mathrm{d}t}\left(\mathcal{L} - \frac{\partial \mathcal{L}}{\partial \dot{q}}\dot{q}\right) &= 0 \\ \therefore \quad \mathcal{L} - \dot{q}\frac{\partial \mathcal{L}}{\partial \dot{q}} &= C \ , \end{aligned} \tag{B.8}$$

which is the Beltrami identity and C is a constant that depends on the initial conditions.

APPENDIX C – Equivalent squared Lagrangian

In the Quantum Adiabatic Brachistochrone section 2.3, we used an equivalent Lagrangian defined as $\mathcal{L}' = \mathcal{L}^2$. But, in which conditions this will lead to the equivalents motion equations? When considering the Euler-Lagrange equation to $\mathcal{L}'$ we have,

$$\begin{aligned} \frac{\mathrm{d}}{\mathrm{d}t}\frac{\partial \mathcal{L}^2}{\partial \dot{q}} - \frac{\partial \mathcal{L}^2}{\partial q} &= 0 \\ \frac{\mathrm{d}}{\mathrm{d}t} 2\mathcal{L}\frac{\partial \mathcal{L}}{\partial \dot{q}} - 2\mathcal{L}\frac{\partial \mathcal{L}}{\partial q} &= 0 \\ 2\mathcal{L}\left(\frac{\mathrm{d}}{\mathrm{d}t}\frac{\partial \mathcal{L}}{\partial \dot{q}} - \frac{\partial \mathcal{L}}{\partial q}\right) + 2\frac{\partial \mathcal{L}}{\partial \dot{q}}\frac{\mathrm{d}\mathcal{L}}{\mathrm{d}t} &= 0 \ . \end{aligned} \tag{C.1}$$

Therefore, if $\mathrm{d}\mathcal{L}/\mathrm{d}t = 0$ we have a necessary and sufficient condition to $\mathcal{L}'$ has an equivalent motion equation of $\mathcal{L}$.

In this thesis, the all the Lagrangians that we use has the form

$$\mathcal{L} = \sum_i \dot{q}_i^2 f_i(q_0, q_1) + \dot{q}_0 \dot{q}_1 g(q_0, q_1) \ , \tag{C.2}$$

where q_0 and q_1 are functions of a parametrized time s. A Legendre transform action of $\mathcal{L}$ with respect to $\dot{q}_i$ yields

$$\mathcal{H}(q_0, q_1, p_0, p_1) = \sum_i \dot{q}_i p_i - \mathcal{L} \ . \tag{C.3}$$

The new canonical variables read

$$\begin{aligned} p_0 &= \frac{\partial \mathcal{L}}{\partial \dot{q}_i} = 2\dot{q}_0 f_0(q_0, q_1) + \dot{q}_1 g(q_0, q_1) \ , \\ p_1 &= \frac{\partial \mathcal{L}}{\partial \dot{q}_i} = 2\dot{q}_1 f_1(q_0, q_1) + \dot{q}_0 g(q_0, q_1) \ . \end{aligned} \tag{C.4}$$

The Hamiltonian then becomes

$$\begin{aligned} \mathcal{H} &= \sum_i \dot{q}_i p_i - \mathcal{L} \\ &= q_0' \left[2\dot{q}_0 f_0(q_0, q_1) + \dot{q}_1 g(q_0, q_1)\right] + \dot{q}_1 \left[2\dot{q}_1 f_1(q_0, q_1) + \dot{q}_0 g(q_0, q_1)\right] - \mathcal{L} \\ &= 2\mathcal{L} - \mathcal{L} \\ &= \mathcal{L} \ . \end{aligned} \tag{C.5}$$

We find that the Hamiltonian is not explicitly time-dependent, thus $\mathrm{d}H/\mathrm{d}t = 0$. Since we proved that the Lagrangian is equal to the Hamiltonian we will have

$$\frac{\mathrm{d}\mathcal{L}}{\mathrm{d}t} = 0 \ . \tag{C.6}$$

Therefore, the squared Lagrangian do not changes the length of the curve yielded by the Euler-Lagrange equations.

APPENDIX D – Frobenious norm identity

In this appendix we will prove an identity concerning the Frobenious norm, which will help us will the physical interpretation of the procedure to change the norm in the Lagrangian of the quantum adiabatic brachistochrone.

The Frobenious norm of an operator A reads

$$F_A = ||A^\dagger A|| = \mathrm{Tr}\left[A^\dagger A\right] \ . \tag{D.1}$$

Equivalently, considering $C_{ik} = (A^\dagger A)_{ik} = \sum_j a^*_{i,j} a_{j,k}$, we can expand the trace as

$$\begin{aligned}
\mathrm{Tr}\left[A^\dagger A\right] &= \sum_i \sum_{j,k} \langle i| \, c_{jk} \, |j\rangle \, \langle k| \, |i\rangle \\
&= \sum_i \sum_{j,k} c_{jk} \delta_{ij} \delta_{ki} \\
&= \sum_{i,j} c_{i,j} \delta_{i,j} \\
&= \sum_i c_{i,i} \\
&= \sum_{i,j} a^*_{i,j} a_{j,i} \ .
\end{aligned} \tag{D.2}$$

Therefore, for a hermitian matrix A,

$$\mathrm{Tr}\left[A^\dagger A\right] = \sum_{i,j} |a_{i,j}|^2 \ . \tag{D.3}$$

APPENDIX E – Lindblad equation

In this Master's thesis we talk about quantum open-systems in two situations, one regarding the self-discharging process of a three-level quantum battery and the other in the simulations of quantum optics dynamics in decaying in the atom and in the cavity. Therefore, for giving self-consistency for this thesis, we will derive the Lindblad equation used to describe these phenomenon.

The method we will use fallows the reference [186]. The derivation starts with the Lioville-von Newumann equation in which we will perform a Markovian approximation to find the Born-Markov master equation. Finally, we will introduce a Jaynes-Commings-like interaction and thereafter we will trace out the degrees of freedom of the bath.

The system we have interest in is composed by main system, an infinite bath and a interaction Hamiltonian,

$$H(s) = H_s + H_b + \alpha H_{sb} \ , \tag{E.1}$$

where $H_s = H_s \otimes I$ is the Hamiltonian of the main system, $H_b = I \otimes H_b$ is the Hamiltonian of the bath and $H_{sb} = H_s \otimes H_b$ is the interaction between the bath and the system and α is the intensity of this former interaction. The motion equation for the global density operator ρ_{bs} is given by the Liouville-von Neuman equation, which is a generalization of the Heisenberg equation for composed systems,

$$\frac{\mathrm{d}\rho_{bs}}{\mathrm{d}t} = -\frac{i}{\hbar}\left[H_s + H_b + \alpha H_{sb}, \rho_{bs}\right] \ . \tag{E.2}$$

Further, we can write the Hamiltonian in the interaction picture, therefore

$$H_I(t) = e^{i(H_s+H_b)t/\hbar} H_{sb} e^{-i(H_s+H_b)t/\hbar} \quad \text{and} \quad \rho(t) = e^{i(H_s+H_b)t/\hbar} \rho_{sb} e^{-i(H_s+H_b)t/\hbar} \ . \tag{E.3}$$

The motion equation for the density operator in the interaction picture reads

$$\frac{\mathrm{d}\rho(t)}{\mathrm{d}t} = -\frac{i\alpha}{\hbar}\left[H_I(t), \rho(t)\right] \ , \tag{E.4}$$

and its integration leads to

$$\rho(t) = \rho(0) - \frac{i\alpha}{\hbar}\int_0^t \left[H_I(t), \rho(t)\right] \mathrm{d}t \ . \tag{E.5}$$

We can make a recursive procedure by substituting Eq. (E.5) in Eq. (E.4)

$$\frac{\mathrm{d}\rho(t)}{\mathrm{d}t} = -\frac{i\alpha}{\hbar}\left[H_I(t), \rho(0)\right] - \frac{\alpha}{\hbar^2}\left[H_I(t), \int_0^t \left[H_i(t'), \rho(t')\right] \mathrm{d}t'\right] \ . \tag{E.6}$$

This is the Born approximation and we will stop in the second order. Further, always it is possible to manage the initial conditions of the problem for the first term after de equality to be zero. Also, we want the density operator of the system, thus we will trace the bath out

$$\frac{\mathrm{d}\rho_s(t)}{\mathrm{d}t} = -\frac{\alpha}{\hbar^2}\mathrm{Tr}_b\left\{\left[H_I(t), \int_0^t [H_i(t'), \rho(t')]\,\mathrm{d}t'\right]\right\} . \tag{E.7}$$

Now, we can make three approximations: consider $\rho(t) = \rho_s(t) \otimes \rho_b$, $\rho(t) = \rho(t')$ and $t \to \infty$. In the first approximation we consider that the bath is not affected by the system and that the bath does not evolves in time. The variable changing in ρ does not affect the Born approximation, since $\rho(t) - \rho(t')$ is also in the second order in α. The third consideration is the Markov approximation and in it we consider that the correlation time is very short, in other words we consider that the system has a short memory. The motion equation for the density operator of the system is now the Born-Markov equation and it is expressed as

$$\frac{\mathrm{d}\rho_s(t)}{\mathrm{d}t} = -\frac{1}{\hbar^2}\int_0^\infty \mathrm{Tr}_b\left\{[H_I(t), [H_i(t'), \rho(t)]]\right\}\mathrm{d}t' , \tag{E.8}$$

where we set $\alpha = 1$ because we are now evaluating just the interaction and its magnitude will not change its behavior.

Furthermore, to calculate the commutator we will set the interaction Hamiltonian to have Jaynes-Cummings-like form. Hence,

$$H_{sb} = \hbar\left(S^\dagger B + S B^\dagger\right) , \tag{E.9}$$

where the operator S acts in the main system and the operator B acts in the bath. In addition we are considering that the system operator does not evolves in time, which means that the interaction will the bath does to chances the structure of the system, thus

$$[S, H_S] = 0 . \tag{E.10}$$

The Hamiltonian of the bath is then given by

$$H_b = \hbar\sum_k \omega_k a^\dagger a , \tag{E.11}$$

where ω_k is the frequency of the mode k, a and $a^\dagger$ are the annihilator and creator operators, respectively. The bath operator is then

$$B = \sum_k g_k^* a_k , \tag{E.12}$$

where g_k are complex coefficients that gives the coupling strange. For finding B in the interaction picture we can use the Baker-Campbell-Hausdorff relation

$$\begin{aligned} B(t) &= e^{iH_b t/\hbar} B e^{-iH_b t/\hbar} \\ &= B + \left[\frac{iH_b t}{\hbar}, B\right] + \frac{1}{2!}\left[\frac{iH_b t}{\hbar}, \left[\frac{iH_b t}{\hbar}, B\right]\right] + \cdots \\ &= B + \sum_{k,z} i\omega_k g_z^* t \left[a_k^\dagger a_k, a_z\right] + \frac{1}{2!}\sum_{k,z} i\omega_k g_z^* t \left[\frac{iH_b t}{\hbar}, \left[a_k^\dagger a_k, a_z\right]\right] + \cdots \\ &= B - \sum_k i\omega_k g_k^* t a_k + \frac{1}{2!}\sum_k \omega_k^2 g_k^* t^2 \left[a_k^\dagger a_k, a_k\right] + \cdots \\ &= \sum_k g_k^* a_k e^{-i\omega_k t} \ , \end{aligned} \tag{E.13}$$

where we use that $[\mathbf{N}, a] = -a$.

Now we can evaluate the commutators. The first one is

$$[H(t), [H(t'), \rho_b \otimes \rho_s(t)]] = \hbar\left[SB^\dagger(t), [H(t'), \rho_b \otimes \rho_s(t)]\right] + \hbar\left[S^\dagger B(t), [H(t'), \rho_b \otimes \rho_s(t)]\right] \tag{E.14}$$

After the expansions we find that the first term in the right-hand side of the equation is

$$\begin{aligned} \left[SB^\dagger(t), [H(t'), \rho_b \otimes \rho_s(t)]\right] &= \hbar^2 SS\rho_s(t)B^\dagger(t)B^\dagger(t')\rho_b + \hbar^2 SS^\dagger\rho_s(t)B^\dagger(t)B(t')\rho_b \\ &- \hbar^2 S\rho_s(t)SB^\dagger(t)\rho_b B^\dagger(t') - \hbar^2 S\rho_s(t)S^\dagger B^\dagger(t)\rho_b B(t') \\ &- \hbar^2 S\rho_s(t)SB^\dagger(t')\rho_b B^\dagger(t) - \hbar^2 S^\dagger\rho_s(t)SB(t')\rho_b B^\dagger(t) \\ &+ \hbar^2 \rho_s(t)SS\rho_b B^\dagger(t')B^\dagger(t) + \hbar^2\rho_s(t)S^\dagger S\rho_b B(t')B^\dagger(t) \ . \end{aligned} \tag{E.15}$$

The other term is

$$\begin{aligned} \left[S^\dagger B(t), [H(t'), \rho_b \otimes \rho_s(t)]\right] &= \hbar^2 S^\dagger S\rho_s(t)B(t)B^\dagger(t')\rho_b + \hbar^2 S^\dagger S^\dagger\rho_s(t)BB^\dagger(t')\rho_b \\ &- \hbar^2 S^\dagger\rho_s(t)SB\rho_b B^\dagger(t') - \hbar^2 S^\dagger\rho_s(t)S^\dagger B(t)\rho_b B(t') \\ &- \hbar^2 S\rho_s(t)S^\dagger B^\dagger(t')\rho_b B(t) - \hbar^2 S^\dagger\rho_s(t)S^\dagger B(t')\rho_b B^\dagger(t) \\ &+ \hbar^2 \rho_s(t)SS^\dagger B^\dagger(t')\rho_b B(t) - \hbar^2\rho_s(t)S^\dagger S^\dagger\rho_b B(t')B^\dagger(t) \ . \end{aligned} \tag{E.16}$$

For the traces, we can first note that

$$\mathrm{Tr}_b\left[B(t)B(t')\rho_b\right] = \mathrm{Tr}_b\left[B^\dagger(t)B^\dagger(t')\rho_b\right] = 0, \forall\ t \text{ and } t' \ . \tag{E.17}$$

Also, using the cyclic property of the trace we can reduce our terms to

$$\begin{aligned} \mathrm{Tr}_b\left\{[H(t), [H(t'), \rho_b \otimes \rho_s(t)]]\right\} &= \hbar^2\left[SS^\dagger\rho_s(t) - S^\dagger\rho_s(t)S\right]\mathrm{Tr}\left[B^\dagger(t)B(t')\rho_b\right] \\ &+ \hbar^2\left[\rho_s(t)SS^\dagger - S\rho_s(t)S\dagger\right]\mathrm{Tr}\left[B(t')B^\dagger(t)\rho_b\right] \\ &+ \hbar^2\left[S^\dagger S\rho_s(t) - S\rho_s(t)S^\dagger\right]\mathrm{Tr}\left[B(t)B^\dagger(t')\rho_b\right] \\ &+ \hbar^2\left[\rho_s(t)S^\dagger S - S^\dagger\rho_s(t)S\right]\mathrm{Tr}\left[B^\dagger(t')B(t)\rho_b\right] \ . \end{aligned} \tag{E.18}$$

For simplifying the notation we can define the functions

$$F(t) = \int_0^t \mathrm{d}t' \mathrm{Tr}_b \left\{ B(t)B^\dagger(t')\rho_b \right\}, \quad G(t) = \int_0^t \mathrm{d}t' \mathrm{Tr}_b \left\{ B^\dagger(t')B^\dagger(t)\rho_b \right\} \ . \tag{E.19}$$

If we consider the vacuum to be initial state of the bath we get

$$\begin{aligned} \mathrm{Tr}_b \left\{ B(t)B^\dagger(t')\rho_b \right\} &= \sum_b \langle b| \, B(t)B^\dagger(t') \, |0,0,\cdots\rangle \, \langle \cdots,0,0| \, |b\rangle \\ &= \sum_b \langle \cdots,0,0|b\rangle \, \langle b| \, B(t)B^\dagger(t') \, |0,0,\cdots\rangle \\ &= \langle \cdots,0,0| \left[\sum_b |b\rangle \, \langle b| \right] B(t)B^\dagger(t') \, |0,0,\cdots\rangle \\ &= \langle \cdots,0,0| \, B(t)B^\dagger(t') \, |0,0,\cdots\rangle \ . \end{aligned} \tag{E.20}$$

Now, we can expand the bath operators

$$\begin{aligned} \mathrm{Tr}_b \left\{ B(t)B^\dagger(t')\rho_b \right\} &= \langle \cdots,0,0| \left[\sum_k g_k^* a_k e^{i\omega_k t} \sum_z g_z a_z^\dagger e^{-i\omega_z t'} \right] |0,0,\cdots\rangle \\ &= \sum_{k,z} e^{i\omega_k t - i\omega_z t'} g_z g_k^* \, \langle \cdots,0,0| \, a_k a_z^\dagger \, |0,0,\cdots\rangle \\ &= \sum_{k,z} e^{i\omega_k t - i\omega_z t'} g_z g_k^* \, \langle \cdots,0,0| \, (\delta_{kz} + a_k^\dagger a_z) \, |0,0,\cdots\rangle \\ &= \sum_k |g_z|^2 e^{-i\omega_z(t-t')} \ . \end{aligned} \tag{E.21}$$

For the trace in $G(t)$ we have

$$\begin{aligned} \mathrm{Tr}_b \left\{ B(t')^\dagger B(t)\rho_b \right\} &= \langle \cdots,0,0| \left[\sum_k g_k a_k^\dagger e^{-i\omega_k t'} \sum_z g_z^* a_z e^{i\omega_z t} \right] |0,0,\cdots\rangle \\ &= \sum_{k,z} e^{-i\omega_k t + i\omega_z t'} g_z^* g_k \, \langle \cdots,0,0| \, a_k^\dagger a_z \, |0,0,\cdots\rangle \\ &= 0 \end{aligned} \tag{E.22}$$

Therefore

$$F(t) = \sum_k |g_k|^2 \int_0^t \mathrm{d}t' e^{-i\omega_k(t-t')}, \quad G(t) = 0 \ . \tag{E.23}$$

Again, we can use the Markov approximation in F

$$F(t) = \sum_k |g_k|^2 \int_0^t \mathrm{d}t' e^{-\omega_k(t-t')} \approx \sum_k |g_k|^2 \int_0^\infty \mathrm{d}t' e^{-\omega_k(t-t')} \equiv \frac{\gamma}{2} \ , \tag{E.24}$$

where γ is a real constant. The differential equation for the density matrix of the system is then

$$\frac{\mathrm{d}}{\mathrm{d}t}\rho_s(t) = \gamma \left[S\rho_s(t)S^\dagger - \frac{1}{2} \left\{ S^\dagger S, \rho_s(t) \right\} \right] . \tag{E.25}$$

Note that the lest term is an anti-commutator. Finally, in the lest act we will return to the Schrödinger picture. For this, let us consider $\rho_s(t) = e^{iH_s t/\hbar}\rho_s e^{-iH_s t/\hbar}$, then the left-handed

size of the equation is

$$\begin{aligned}\frac{\mathrm{d}}{\mathrm{d}t}e^{iH_st/\hbar}\rho_s e^{-iH_st/\hbar} &= \frac{iH_s}{\hbar}e^{iH_st/\hbar}\rho_s e^{-iH_st/\hbar} - e^{iH_st/\hbar}\rho_s e^{-iH_st/\hbar}\frac{iH_s}{\hbar} + e^{iH_st/\hbar}\frac{\mathrm{d}\rho_s}{\mathrm{d}t}e^{-iH_st/\hbar} \\ &= e^{iH_st/\hbar}\left\{\frac{\mathrm{d}\rho_s}{\mathrm{d}t} + \frac{i}{\hbar}\left[H_s,\rho\right]\right\}e^{-iH_st/\hbar} \ .\end{aligned} \tag{E.26}$$

The right-handed side of the equation is

$$\gamma\left[S\rho_s(t)S^\dagger - \frac{1}{2}\left\{S^\dagger S,\rho_s(t)\right\}\right] = \gamma e^{iH_bt/\hbar}\left[S\rho_s S^\dagger - \frac{1}{2}\left\{S^\dagger S,\rho_s\right\}\right]e^{-iH_bt/\hbar} \ . \tag{E.27}$$

Therefore, the Lindblad equation for more than one bath is generalized to

$$\frac{\mathrm{d}}{\mathrm{d}t}\rho_s = -\frac{1}{\hbar}\left[H_s,\rho_s\right] + \sum_i \gamma_i\left[\mathcal{L}_i\rho_s(t)\mathcal{L}^\dagger - \frac{1}{2}\left\{\mathcal{L}^\dagger\mathcal{L},\rho_s(t)\right\}\right] \ . \tag{E.28}$$

where $\mathcal{L}$ is the system operator, just like S, and is known as Lindbladian.

The Lindblad equation is a generalization of the Schrödinger equation, since it can describe decoherence, dissipation and quantum measurements process and, when the bath is ignored, we find the von Neumann equation. Although this equation can be applied to a wide range of system, the approximations we did to derive it dictates the regime of validity of this equation. This equation is valid when the bath-system interaction is markovian, when the bath has infinity degrees of freedom and when γ is small comparing to $[H_s,\rho_s]$. The master equation was derived, but it has some differences concerning quantum mechanics for closed system. For instance, for non unitary evolutions appears the concept of super-operators, which increases the dimension of the system. In the following we will describe a method for solving this equation while we show these differences. In order to write the operators in using matrices, let us we define

$$\mathcal{L}(A)[\rho] = A\rho, \quad \mathcal{R}(A)[\rho] = \rho A, \quad , \tag{E.29}$$

where we have the left- and right-multiplication super-operators, respectively. With this two super-operators we can represent all terms in the Lindblad equation, such as the commutator

$$[H,\rho] = \mathcal{L}(H)[\rho] - \mathcal{R}(H)[\rho] \ . \tag{E.30}$$

Now, we have to flatten the density operator by performing the transformation

$$\rho = \sum_{ij}\rho_{ij}\left|i\right\rangle\left\langle j\right| \to \varrho = \sum_{ij}\rho_{ij}\left|i\right\rangle\otimes\left|j\right\rangle \ , \tag{E.31}$$

which means that now we have an vector and the new space of the system operator has the dimension $\mathcal{D}^2\times\mathcal{D}^2$. For illustrating this for a system initially with dimension $\mathcal{D}$, let us evaluate the action of $\mathcal{L}$ in ϱ,

$$\begin{aligned}\mathcal{L}(A)[\varrho] &= \sum_{ij}\rho_{ij}(A\left|i\right\rangle)\otimes\left|b\right\rangle \\ &= \sum_{ij}\rho_{ij}(A\otimes I)\left|i\right\rangle\otimes\left|b\right\rangle \ ,\end{aligned} \tag{E.32}$$

where I is the identity matrix of dimension D. Further, the right-multiplication superoperator action is

$$\begin{aligned} \mathcal{R}(A)[\varrho] &= \left[\mathcal{R}(A^\dagger)[\varrho]\right]^\dagger \\ &= (I \otimes A^\dagger)\varrho \ . \end{aligned} \tag{E.33}$$

With this, it is possible to derive the matrix elements of the problem and solve it, using numerical or analytic approaches.

APPENDIX F – Quantum optics

F.1 Derivation of the two-mode collective basis

Considering the two-mode Fock basis $\{|m, N-m\rangle\}$ for the operators a and b, where N is the total number of photons in both modes, our goal is to find a collective basis of states

$$\left|\psi_n^N\right\rangle = \sum_{m=0}^{N} C_{n,m}^N \left|m, N-m\right\rangle, \tag{F.1}$$

which fulfill the following relation:

$$H\left|g\right\rangle \left|\psi_n^N\right\rangle = g\eta \left|e\right\rangle \left|\psi_{n'}^{N-1}\right\rangle. \tag{F.2}$$

with $0 \leq n' \leq N-1$. Eq. (F.2) describes the process of a single-photon absorption by the atom from any of the modes, where η represents a coupling factor, to be determined in the next steps. In this context, three classes of collective states are of general interest when considering two modes: Perfectly Dark states (PDS) ($\eta = 0$), Maximally Superradiant (MSR) States ($\eta = \eta_{\max}$ as large as possible), and the intermediate states ($0 < \eta < \eta_{\max}$). For $\eta = 0$, the exchange of photons never happens between atom and modes.

In order to find the complete set $\left\{\left|\psi_n^N\right\rangle\right\}$, let us define the symmetric and antisymmetric collective operators, respectively:

$$c \equiv \frac{1}{\sqrt{2}}(a+b), \qquad d \equiv \frac{1}{\sqrt{2}}(-a+b). \tag{F.3}$$

One can straightforwardly verify that the transformation (F.3) corresponds to orthogonal operators, preserves the canonical commutation relations, and conserves the total number of photons:

$$c^\dagger c + d^\dagger d = a^\dagger a + b^\dagger b. \tag{F.4}$$

In the space of these new operators, note that the Jaynes-Cummings Hamiltonian H turns into

$$H = \sqrt{2}\hbar g c\sigma^+ + \text{H.c}, \tag{F.5}$$

where only the collective mode c couples to the atom. The multiplicative factor $\sqrt{2}$ serves as a reminder that, despite the simplicity of Eq.(F.5), we are still dealing with a two-mode configuration.

Finally, we prove that operators c and d share the same vacuum state as the previous operators a and b:

$$\begin{pmatrix} c \\ d \end{pmatrix} |0,0\rangle = \frac{1}{\sqrt{2}} \begin{pmatrix} a+b \\ -a+b \end{pmatrix} |0,0\rangle = \begin{pmatrix} 0 \\ 0 \end{pmatrix}. \tag{F.6}$$

Therefore, the vacuum state is unique ($|0,0\rangle_{c,d} = |0,0\rangle_{a,b}$) and all elements of the new collective basis can be built from it:

$$\left|\psi_n^N\right\rangle \equiv |n, N-n\rangle_{c,d}\,, \tag{F.7}$$

$$= \frac{\left(c^\dagger\right)^n \left(d^\dagger\right)^{N-n}}{\sqrt{n!\,(N-n)!}}\,|0,0\rangle\,, \tag{F.8}$$

$$= \frac{\left(a^\dagger + b^\dagger\right)^n \left(-a^\dagger + b^\dagger\right)^{N-n}}{\sqrt{2^N n!\,(N-n)!}}\,|0,0\rangle\,, \tag{F.9}$$

with $0 \leq n \leq N$. Using the binomial expansion for operators, we can finally obtain the probability amplitudes (6.7) given in the main text. Although the new basis $\left|\psi_n^N\right\rangle = |n, N-n\rangle_{c,d}$ still requires two modes, the transformed Hamiltonian (F.5) does not depend on the operator d. As a result, the condition (F.2) can be easily calculated from (F.7):

$$H\,|g\rangle\left|\psi_n^N\right\rangle = g\sqrt{2n}\,|e\rangle\left|\psi_{n-1}^{N-1}\right\rangle, \tag{F.10}$$

$$H\,|g\rangle\,|n\rangle_c = g\sqrt{2n}\,|e\rangle\,|n-1\rangle_c\,, \tag{F.11}$$

with the whole description concentrated only in the symmetric mode $|n\rangle_c$. Finally, we are able to recognize the MSSs ($n = N$) and PDSs ($n = 0$) discussed in the main text.

F.2 $\langle E\rangle$ and $\langle \Delta E\rangle$ in the two-mode collective basis

The expectation value of the total electric field operator E, for an arbitrary element of the collective basis, can now be calculated by using the symmetric operators only:

$$\langle E\rangle = \left\langle\psi_n^N\right|(a+b) + \left(a^\dagger + b^\dagger\right)\left|\psi_n^N\right\rangle, \tag{F.12}$$

$$= \sqrt{2}\,\langle n, N-n|\,c + c^\dagger\,|n, N-n\rangle_{c,d}\,, \tag{F.13}$$

$$= 0. \tag{F.14}$$

This property is not surprising since $\left|\psi_n^N\right\rangle$ are states with perfectly defined photon numbers, like Fock states for single modes. Similarly, we can calculate the second moment,

$$\left\langle E^2\right\rangle = \left\langle\psi_n^N\right|\left[(a+b) + \left(a^\dagger + b^\dagger\right)\right]^2\left|\psi_n^N\right\rangle, \tag{F.15}$$

$$= 2\,\langle n, N-n|\left(c + c^\dagger\right)^2|n, N-n\rangle_{c,d}\,, \tag{F.16}$$

$$= 2\,(2n+1)\,, \tag{F.17}$$

which is precisely the two-mode variance $\langle \Delta E\rangle^2 = 2\,(2n+1)$ of the total electric field operator. The generalization of this procedure allows us to obtain straightforwardly $\langle E\rangle$ and $\langle \Delta E\rangle$ for any state expanded in terms of the two-mode collective basis.

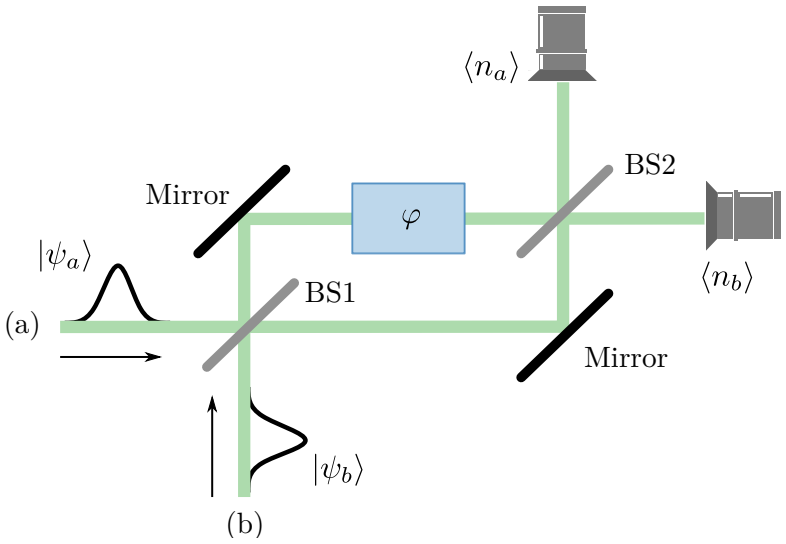

Figure 19 – Mach-Zehnder interferometer. BS1 and BS2 are 50/50 symmetrical beam splitters. Fields that go through mode "B" acquire an adjustable phase φ.

F.3 Classical and quantum interference - Mach-Zehnder Interferometer

We here discuss the output from a Mach-Zehnder interferometer (MZI) when PDSs, MSSs, or superpositions of them, are the input states, see Fig. 19. In particular, we show how MSSs and PDSs yield fringe patterns which do not depend on whether "classical" high-photon-number coherent states, or "quantum" number states, are interacting with a ground-state atom. Yet other states, such as the $|\Upsilon\rangle$, present clearly different fringes as compared to any classical state.

We consider a MZI with two symmetric 50/50 beam splitters (BS), where the transmission t and reflection r coefficients transforms the input modes according to the rule

$$a \rightarrow ta + irb = \frac{a + ib}{\sqrt{2}}, \tag{F.18}$$

$$b \rightarrow tb + ira = \frac{b + ia}{\sqrt{2}}. \tag{F.19}$$

Interference of classical fields – Firstly we consider classical fields as inputs, with Rabi frequencies $\Omega_A = \Omega$ and $\Omega_B = e^{i\theta}\Omega$. Constructive (destructive) interference is obtained by setting $\theta = 0$ ($\theta = \pi$). After crossing the first BS, we obtain the following transformed fields $\Omega_A \rightarrow \Omega'_A$ and $\Omega_B \rightarrow \Omega'_B$:

$$\Omega'_A = \Omega\frac{1 - ie^{i\theta}}{\sqrt{2}}, \tag{F.20}$$

$$\Omega'_B = \Omega\frac{e^{i\theta} - i}{\sqrt{2}}. \tag{F.21}$$

Then, the field Ω'_B acquires a phase shift φ, turning into $\Omega'_B e^{i\varphi}$. Finally, both fields cross the second BS, transforming Ω'_A (Ω'_B) into Ω''_A (Ω''_B) such that

$$\Omega''_{\binom{A}{B}} = -i\Omega e^{i\varphi/2}\left[\sin\left(\frac{\varphi}{2}\right) \pm e^{i\theta}\cos\left(\frac{\varphi}{2}\right)\right], \tag{F.22}$$

Eq.(F.22) leads to Eq.(6.18) of the main text, which is valid for any θ. The special case $\theta = 0$ ($\theta = \pi$) corresponds to constructive (destructive) interference.

Interference of quantum fields – Two-mode states expanded only in terms of PDSs or MSSs can be expressed as a function f of creation operators (see Appendix A):

$$|\Psi\rangle = f\left(a^\dagger + e^{i\theta}b^\dagger\right)|0,0\rangle, \tag{F.23}$$

where $\theta = 0$ for MSSs and $\theta = \pi$ for PDSs. Using the rules (F.18) and (F.19), as applied before to the classical case, we transform twice the combined state of the fields: $|\Psi\rangle \to |\Psi'\rangle \to |\Psi''\rangle$. The result reads:

$$|\Psi'\rangle = f\left[\left(\frac{a^\dagger - ib^\dagger}{\sqrt{2}}\right) + e^{i\theta}\left(\frac{b^\dagger - ia^\dagger}{\sqrt{2}}\right)\right]|0,0\rangle, \tag{F.24}$$

$$\begin{aligned}|\Psi''\rangle = f\Big\{&-ie^{i\varphi/2}\left[e^{i\theta}\cos\left(\frac{\varphi}{2}\right) + \sin\left(\frac{\varphi}{2}\right)\right]a^\dagger \\ &-ie^{i\varphi/2}\left[\cos\left(\frac{\varphi}{2}\right) - e^{i\theta}\sin\left(\frac{\varphi}{2}\right)\right]b^\dagger\Big\}|0,0\rangle.\end{aligned} \tag{F.25}$$

The sequence of states above generates exactly the same fringe pattern predicted for classical fields, see Eq.(6.18). We can thus conclude that, when the input of the MZI are two out-of-phase classical fields, or two out-of-phase phase coherent fields, or any quantum field by with projection only on PDSs or only on MSSs, the interference pattern will always be the same. Hence, there is no way to distinguish classical from quantum fields in these families.

When quantum states have a projection on both PDSs and MSSs, as it happens with state $|\Upsilon\rangle$ (see Eq. (6.13)), the interference pattern is clearly distinguishable from the one obtained from classical fields. Indeed, if state $|\Upsilon\rangle$ is injected in the MZI, the output state

$$\begin{aligned}|\Upsilon''\rangle = &\frac{e^{i\varphi}}{\sqrt{2}}\sin\left(\frac{\varphi}{2}\right)\cos\left(\frac{\varphi}{2}\right)(|2,0\rangle - |0,2\rangle) \\ &+\frac{ie^{i\varphi/2}}{2}\left[\cos\left(\frac{\varphi}{2}\right) - \sin\left(\frac{\varphi}{2}\right)\right]|1,0\rangle \\ &-\frac{ie^{i\varphi/2}}{2}\left[\cos\left(\frac{\varphi}{2}\right) + \sin\left(\frac{\varphi}{2}\right)\right]|0,1\rangle \\ &+\frac{1}{2}\left(|0,0\rangle + e^{i\varphi}\cos\varphi\,|1,1\rangle\right)\end{aligned} \tag{F.26}$$

generates the average numbers of photons

$$\left\langle n_{\binom{A}{B}}\right\rangle_{|\Upsilon\rangle} = \frac{1}{4}(2 \mp \sin\varphi). \tag{F.27}$$

This fringe pattern is qualitatively similar to the case of out-of-phase coherent states (see Fig.16),

$$\left\langle n_{\binom{A}{B}} \right\rangle_{|\alpha,-\alpha\rangle} = |\alpha|^2 (1 \mp \sin\varphi) . \tag{F.28}$$

However, if we measure only one of the outputs, in mode A for instance, we observe an interesting difference. For $|\alpha|^2 = 1/2$ and $\varphi = \pi/2$, classical or coherent fields predicts zero intensity $\langle n_A \rangle_{|\alpha,-\alpha\rangle} = 0$, while we obtain $\langle n_A \rangle_{|\Upsilon\rangle} = 1/4$ for the quantum state $|\Upsilon\rangle$. Thus, measuring the intensity rather than intensity-intensity correlations is sufficient to distinguish the quantum and classical fields discussed above. The explanation for this difference can be found on the decomposition on dark and superradiant states, by observing that $|\Upsilon\rangle$ always has a finite projection on a MSS.

F.4 General output for a MZI

Let us consider an arbitrary state of the collective basis,

$$\left|\psi_n^N\right\rangle = \frac{\left(b^\dagger + a^\dagger\right)^n \left(b^\dagger - a^\dagger\right)^{N-n}}{\sqrt{2^N n!\,(N-n)!}} |0,0\rangle \tag{F.29}$$

as the input for the MZI. After the BS1, the light field acquires the phase shift φ, turning into

$$\left|\psi_n'^N\right\rangle = \frac{\left(a^\dagger + b^\dagger e^{i\varphi}\right)^n \left(b^\dagger e^{i\varphi} - a^\dagger\right)^{N-n}}{e^{i(2n-N)\pi/4}\sqrt{2^N n!\,(N-n)!}} |0,0\rangle . \tag{F.30}$$

The final state after BS2 is then

$$\begin{aligned} \left|\psi_n''^N\right\rangle = & \sqrt{\frac{2^N}{n!\,(N-n)!}} \\ & \times \left[b^\dagger \cos\left(\frac{\varphi+\frac{\pi}{2}}{2}\right) + a^\dagger \cos\left(\frac{\varphi-\frac{\pi}{2}}{2}\right)\right]^n \\ & \times \left[b^\dagger \cos\left(\frac{\varphi-\frac{\pi}{2}}{2}\right) - a^\dagger \cos\left(\frac{\varphi+\frac{\pi}{2}}{2}\right)\right]^{N-n} \\ & \times |0,0\rangle , \end{aligned} \tag{F.31}$$

where we have omitted an irrelevant global phase factor. Note now that the outputs (6.18) can be easily recovered by simply setting $n = 0$ (PDS) or $n = N$ (MSS), accompanied by the suitable value of the phase θ. In particular, the case of the intermediate quantum state $|\psi_1^2\rangle$, discussed in the main text, simplifies to the final state

$$\left|\psi_1''^2\right\rangle = e^{i\varphi}\left[\frac{\cos\varphi}{\sqrt{2}}(|0,2\rangle - |2,0\rangle) + \sin\varphi\,|1,1\rangle\right] . \tag{F.32}$$

It provides the same average number of photons for mode A and B: $\langle n_A \rangle_{|\psi_1^2\rangle} = \langle n_B \rangle_{|\psi_1^2\rangle} = 1$. In other words, no fringe is observed for such a state.

F.5 M-mode collective basis

Considering the ordinary M-mode Fock basis $\{|m_1, m_2, \dots m_M\rangle\}$ for the operators $a_1, a_2, \dots, a_M$, with total number of photons $\sum_{k=1}^{M} m_k = N$, our goal is to find a collective basis of states which fulfill the following relation:

$$H_M \left|\psi^N_{n_1,n_2,\dots,n_M}\right\rangle |g\rangle = g\eta \left|\psi^{N-1}_{n'_1,n'_2,\dots,n'_M}\right\rangle |e\rangle\,, \tag{F.33}$$

with $\sum_{k=1}^{M} n'_k = N-1$. Eq. (F.33) describes the process of a single-photon absorption by the atom from any of the M modes, and η represents a coupling factor.

In order to derive the proper M-mode collective basis, we define the set of collective operators

$$c_j = \sum_{k=1}^{M} O_{jk} a_k, \tag{F.34}$$

where $\mathbf{O}$ is an orthogonal matrix of dimension $M \times M$, with M even, such that all elements of its first row are $O_{1k} = 1/\sqrt{M}$, and the elements of the second row satisfy the rule $O_{2k} = (-1)^{k-1}/\sqrt{M}$. The other rows can be obtained by considering all possible combinations of ± 1 which satisfy the linear independence of the rows. For $M = 4$, for example, a possible orthogonal matrix reads:

$$\frac{1}{2}\begin{pmatrix} 1 & 1 & 1 & 1 \\ 1 & -1 & 1 & -1 \\ 1 & 1 & -1 & -1 \\ 1 & -1 & -1 & 1 \end{pmatrix}, \tag{F.35}$$

In particular, the orthogonality ensures the preservation of the canonical commutation relations $\left[c_j, c_l^\dagger\right] = \delta_{jl}$, and guarantees the conservation of the total number of photons:

$$\sum_{j=1}^{M} c_j^\dagger c_j = \sum_{j=1}^{M} a_j^\dagger a_j. \tag{F.36}$$

Using transformation (F.34), the M-mode Hamiltonian becomes

$$H_M = \sqrt{M}\hbar g c_1 \sigma^+ + \text{H.c.}, \tag{F.37}$$

which recovers the Jaynes-Cummings Hamiltonian, since only the first mode $c_1 = \sum_{k=1}^{M} a_k/\sqrt{M}$ couples to the atom. Moreover, the presence of M modes modifies the atom-light coupling by a factor $\sqrt{M}$.

Just as for two modes, the basis on which the operators c_j act can also be built from the fact that the vacuum state is unique:

$$c_j |0, 0, \dots, 0\rangle = \sum_{k=1}^{M} O_{jk} a_k |0, 0, \dots, 0\rangle = 0. \tag{F.38}$$

Therefore, the elements of the M-mode basis can be expanded as follows:

$$\begin{aligned}\left|\psi^N_{n_1,n_2,\ldots,n_M}\right\rangle &\equiv |n_1,n_2,\ldots,n_M\rangle_c\,,\\ &= \prod_{j=1}^{M}\frac{1}{\sqrt{n_j!}}\left(c_j^\dagger\right)^{n_j}|0,0,\ldots,0\rangle\,,\\ &= \prod_{j=1}^{M}\frac{1}{\sqrt{n_j!}}\left[\sum_{k=1}^{M}O_{jk}a_k^\dagger\right]^{n_j}|0,0,\ldots,0\rangle\,,\end{aligned} \tag{F.39}$$

with $\sum_{k=1}^{M} n_k = N$. As the transformed Hamiltonian (F.37) depends only on the first operator c_1, the condition (F.33) simply reads:

$$\begin{aligned}H_M\left|\psi^N_{n_1,n_2,\ldots,n_M}\right\rangle|g\rangle &= g\sqrt{Mn_1}\left|\psi^{N-1}_{n_1-1,n_2,\ldots,n_M}\right\rangle|e\rangle\,,\\ H_M|n_1\rangle_{c_1}|g\rangle &= g\sqrt{Mn_1}\,|n_1-1\rangle_{c_1}|e\rangle\,,\end{aligned} \tag{F.40}$$

which allows us to easily identify the MSS state ($n_1 = N$) and all PDS states ($n_1 = 0$) of the main text.

Finally, we would like to highlight that there are other matrices which connect different Fock spaces. For example, the matrix

$$\begin{cases}\frac{1}{\sqrt{M}} & j=1,\forall k\\ \frac{1-j}{\sqrt{j(j-1)}} & k=j\geq 2\\ \frac{1}{\sqrt{j(j-1)}} & k<j\\ 0 & k>j\end{cases} \tag{F.41}$$

also satisfies the orthogonality condition and holds for M either odd or even. Yet it does not provide a straightforward expansion of M-mode coherent states in terms of its associated Fock basis.

F.6 Semiclassical Model

By considering the Hamiltonian (F.5), it is possible to derive the dynamical equations for the operators expectation values from the quantum master equation. Defining the atomic decay rate as γ and the cavity dissipation rate as κ (assumed to be the same for both cavity modes), we obtain

$$\langle\dot{c}\rangle = -\kappa\langle c\rangle - ig\sqrt{2}\langle\sigma_{ge}\rangle, \tag{F.42}$$

$$\langle\dot{\sigma}_{ge}\rangle = -\gamma\langle\sigma_{ge}\rangle + ig\sqrt{2}\langle c\sigma_z\rangle, \tag{F.43}$$

$$\langle\dot{\sigma}_z\rangle = -2\gamma\left(1+\langle\sigma_z\rangle\right) + 2ig\sqrt{2}\left(\langle c^\dagger\sigma_{ge}\rangle + \langle c\sigma_{eg}\rangle\right). \tag{F.44}$$

Neglecting quantum correlations, the operators can be factorized, i.e., $\langle c\sigma\rangle = \langle c\rangle\langle\sigma\rangle$, thus describing the classical dynamics. With the definitions $\langle c\rangle = \alpha_c$, the initial conditions are $\alpha_c(0) = 0$ for out-of-phase classical fields and $\alpha_c(0) = \sqrt{2}\alpha$ for in-phase fields.

F.7 Arbitrary Single Qubit Rotations

As mentioned in Section 6.8, bright and dark states of light, together with the atomic states, can be employed to implement the operations required for universal quantum computing. In addition to the Controlled-Phase gate described in Section 6.8, it is necessary to operate arbitrary rotations on the atomic and mode states individually. Regarding the atomic system, such rotations can be implemented using two classical fields driving a Raman transition, to which an effective Hamiltonian is associated with: $H_{\text{at}} = \Omega_{\text{eff}}/2 \left|g_1\right\rangle \left\langle g_2\right| + \text{H.c.}$, with Ω_{eff} the Rabi frequency of the desired transition. On the other hand, arbitrary rotations on the light states (bright and dark states) can be achieved using an auxiliary atom placed in a given position to interact (non-resonantly) with only one of the modes. Focusing on mode A, the effective Hamiltonian (6.32) reduces to $H_A = g^2/\Delta a^\dagger a \left|g_1^2\right\rangle \left\langle g_1^2\right|$, where $\left|g_1^2\right\rangle$ is the ground state of the second atom. This interaction is not able to change the state of the second atom, but it introduces a relative phase in the collective two-mode state only when there is one excitation in mode A, thus allowing us to implement arbitrary rotations involving the bright and dark single excitation states. For instance, starting the modes in the bright state, the evolved state becomes

$$e^{-iH_A t}\left|\psi_1^1\right\rangle\left|g_1^2\right\rangle = e^{-i\theta}\left(\cos(\theta)\left|\psi_1^1\right\rangle - i\sin(\theta)\left|\psi_0^1\right\rangle\right)\left|g_1^2\right\rangle, \tag{F.45}$$

with $\theta = g^2/\Delta t$. This corresponds to the desired rotation from the bright to the dark state.